Design and Assessment of a Super High Speed, Hybrid Hydrofoil/SWATH Crew Boat

By

Vasileios Georgiadis

Bachelor of Science in Mechanical Engineering,
Hellenic Naval Academy, 2006

SUBMITTED TO THE DEPARTMENT OF MECHANICAL ENGINEERING IN PARTIAL FULFILLMENT OF THE REQUIREMENTS FOR THE DEGREES OF

NAVAL ENGINEER AND
MASTER OF SCIENCE IN MECHANICAL ENGINEERING
AT THE
MASSACHUSETTS INSTITUTE OF TECHNOLOGY

JUNE 2014

Signature of Author: Signature redacted
Vasileios Georgiadis
Department of Mechanical Engineering
May 9, 2014

Certified by: Signature redacted
Chryssostomos Chryssostomidis, Director of MIT Sea Grant
Doherty Professor of Ocean Science and Engineering
Professor, Department of Mechanical Engineering
Thesis Supervisor

Certified by: Signature redacted
Stefano Brizzolara, Assistant Director for Research at MIT Sea Grant
Research Scientist, Department of Mechanical Engineering
Thesis Advisor

Accepted by: Signature redacted
David E. Hardt
Chairman, Department Committee on Graduate Studies
Ralph E. and Eloise F. Cross Professor of Mechanical Engineering

THIS PAGE IS INTENTIONALLY LEFT BLANK

Design and Assessment of a Super High Speed, Hybrid hydrofoil/SWATH Crew Boat

By

Vasileios Georgiadis

Submitted to the Department of Mechanical Engineering
on May 9, 2014 in Partial Fulfillment of the
Requirements for the degrees of Naval Engineer and
Master of Science in Mechanical Engineering

Abstract

This thesis presents the preliminary design and assessment of Wavecutter, an innovative super high speed, hybrid hydrofoil/SWATH crew boat. The intended mission of the vessel is the very-fast transportation of crew and cargo, to and from offshore installations. The design builds on Brizzolara's unmanned high speed hybrid SWATH/hydrofoil vessel concept (Brizzolara, 2010), maintaining the dual operating mode: foilborne to reach top speed of 85 knots in moderate sea states and a displacement SWATH to sail in the higher sea states. This vessel is expanding the family of unmanned hybrid SWATH vessels of Brizzolara and Chryssostomidis to include manned vessels (Brizzolara & Chryssostomidis, 2013). The special hydrofoil profile recently optimized and verified by model tests in free-surface cavitation tunnel, has been adopted, to ensure high lift to drag ratios and avoid typical instability phenomena of conventional super-cavitating hydrofoils (Brizzolara, 2013). The surface piercing configuration of the hydrofoils was adopted in order to make the vessel inherently stable, without the use of control mechanisms.

The general design phase was focused on the integration of the manned module, internal arrangements, weight estimation, speed profile determination and engine selection. The hydrofoil design phase limits on resizing the four surface-piercing super-cavitating hydrofoils to keep the vessel even keel at maximum speed. To achieve this, the front foils need to have a larger size than the aft ones, due to the trim moment produced by the turbo-jet thrust force. The feasibility assessment phase in foil borne mode confirmed the static stability of the vessel and good seaworthiness in waves. It is recommended that future work be conducted with CFD simulations in unsteady conditions, to obtain a more accurate understanding of the vessel's dynamic behavior.

Thesis Supervisor: Chryssostomos Chryssostomidis
Title: Director, MIT Sea Grant; Doherty Professor of Ocean Science and Engineering

Acknowledgements

During my studies at MIT, I have benefited greatly from the Mechanical Engineering Department. The 'mens et manus' culture of the department has given me a new perspective, which I will always carry with me in my life. The course infrastructure and faculty expertise of the program has strengthened my engineering skillset. Therefore, I would like to sincerely thank the staff, the professors and my colleagues for this unique experience. I feel privileged to be a member of the MIT engineering school.

I would like to express my sincere appreciation and respect to my advisor, Professor Stefano Brizzolara, for his support throughout my thesis. Observing his advanced engineering intuition, a result of years of hard work, inspired me to become a better engineer myself. His amicable character made working under his guidance enjoyable and seamless.

I would like to express my gratitude to Professor Chrys Chryssostomidis for welcoming me to be part of the greater research community of Sea Grant, and for supervising my thesis research.

I would like to express my gratitude to the Hellenic Navy and the Greek government in general, for sponsoring my studies in MIT. I aim to use the new skillset gained from MIT to advance the Hellenic Navy's capabilities and do my part in helping Greece improve, especially after the recent financial crisis.

But most of all, I would like to thank my wife. Had it not been for her emotional and practical everyday support, I would never have had the stamina and time to study hard and complete my MIT degrees.

Table of Contents

List of Figures

List of Tables

1 Introduction

The state of the art vessels in fast transportation in speed ranges above 70 knots lack seaworthiness and payload capacity. The motivation for this design is to create a better vessel for rapid crew or small goods transportation from harbors to offshore installations.

1.1 Motivation/benchmarking

The need for rapid transportation of industrial personnel between harbor and offshore installation is currently covered by planing hulls and some hydrofoil vessels. The maximum speed reached by planing hulls is in the range of 40-50 knots in almost flat seas, while speed rapidly falls in the 15-18 knots range already, in moderate sea states. Hydrofoil vessels can reach speeds of around 60 knots. However, they use fully submerged foils, which require complex control mechanisms and lack seaworthiness. These type of hydrofoil vessels switch to displacement mode, when encountering heavy weather. For reaching speeds above 70 knots, one must use helicopters or surface effect ships. These vessels have even higher limitations than planing hulls and hydrofoil vessels in terms of seaworthiness. In addition they are very limited in payload capacity.

Some representative transportation vehicles that address this need today are presented in Table 1. The most important attributes of these vessels are crew payload, cargo payload, maximum sustainable speed, endurance and price. An example of operation of a helicopter would be to transfer medical personnel to an oil rig due to a medical emergency. An example for use of a monohull fast crew supplier would be the regular monthly route to perform personnel transfer. A SWATH vessel, as an example, could be used to transport personnel to an offshore wind installation for maintenance. A hydrofoil industrial personnel transportation vessel could not be found; a passenger ferry hydrofoil vessel is listed in the table below for reference.

Table 1: Existing crew transportation vessels

Vehicle	Industrial Personnel Payload (people)	Cargo Payload (tons)	Maximum Sustainable Speed (knots)	Endurance range (nautical miles)	Price/per passenger
Helicopter S-76C++ (Sikorsky)	9	0	155	345	Large
Monohull Fast Crew Supplier 1605 (Damen)	29	Unknown	40	Unknown	Small
SWATH crew boat (Danish Yachts)	24	0	23	500	Medium

Boeing 929-100	243	Unknown	45	Unknown	Medium

1.2 Requirements

Table 2 shows the requirements generated from the vessel's intended mission. Requirements R1, R2 and R3 are based on the rational that Wavecutter should have at least the same capability in these areas as some existing vehicles. Wavecutter is intended to be operated in the higher speed ranges, being a hydrofoil vessel, hence the requirement R4. Requirement R5, endurance, is generated based on the distance of the furthest oil rig from the Gulf of Mexico central harbor, with +50% allowance for future growth in the deep water oil drilling segment of the industry. Requirement R6 is based on sea statistics for the Gulf of Mexico, so that the vessel will be able to operate safely approximately 85% of the time (more information is given in the Appendix, section 6.1).

Table 2: Design Requirements

Requirement ID	Requirement	Goal	Threshold
R1	Passengers	24	20
R2	Cargo (tons)	15	10
R3	Crew	4	6
R4	Maximum speed	85	70
R5	Endurance (n. miles)	600	400
R6	Operational Sea State	4	3

Table 3 presents derived requirements. Derived requirements are requirements generated as a consequence of design requirements, whether directly stated in Table 2 or inferred. D1 is derived from the fact that manned compartments are expected to accommodate people and is based on the average male height of 1.8 m. D2 is a requirement derived from R6, the operational sea state requirement. D3 is decided to account for the needed space for structural support. By assigning this extra space, the present study allows future studies to conduct global structural design of the vessel. Requirement D4 is a consequence of requirements R2, using the density of water (1000 kg/ cu. m.) to calculate the required volume, with an allowance of +50% volume. D8 and D9 are derived from R6, but the vessel is expected to switch to displacement mode when encountering a sea state of 3 and higher.

Table 3: Derived requirements

Requirement ID	Derived requirements	Goal	Threshold
D1	Minimum manned compartment height [m]	2.2	2.0
D2	Minimum distance of lowest point of wing/deck from sea level [m]	2.5	2
D3	Allowance for structural support of manned compartments [m]	0.5 all around	0.35 above compartment, 0.5 below and 0.5 on the sides
D4	Storage space for cargo [m^3]	22.5	15
D8	Displacement mode operational sea state	4	3
D9	Foil borne mode operational sea state	3	2

2 General design

The general design of the vessel is presented in this section. The general design phase starts from the concept design and continues with the integration of the manned module, internal arrangements, weight estimation, speed profile determination and engine selection. At the end of the section a preliminary evacuation plan is demonstrated.

2.1 Concept design

The concept design of the vessel is based on S. Brizzolara's autonomous unmanned hybrid concept design (Brizzolara, 2010, p. 10), shown in Figure 1. The design features a hybrid 20 m long vessel, capable of reaching a maximum speed of 120 knots, intended to carry a payload of 5 MT. The unmanned vessel sails in displacement mode at low speeds, the hydrofoils being kept in vertical position in this mode, as shown on the top right of the figure. Above take-off speed, the vessel switches to foilborne mode, shown in the bottom right of the figure. In foilborne mode, lift is partially provided by the wing shaped deck. Volume is allocated to carry the payload in the front part of the wing, noticed in the left part of the figure.

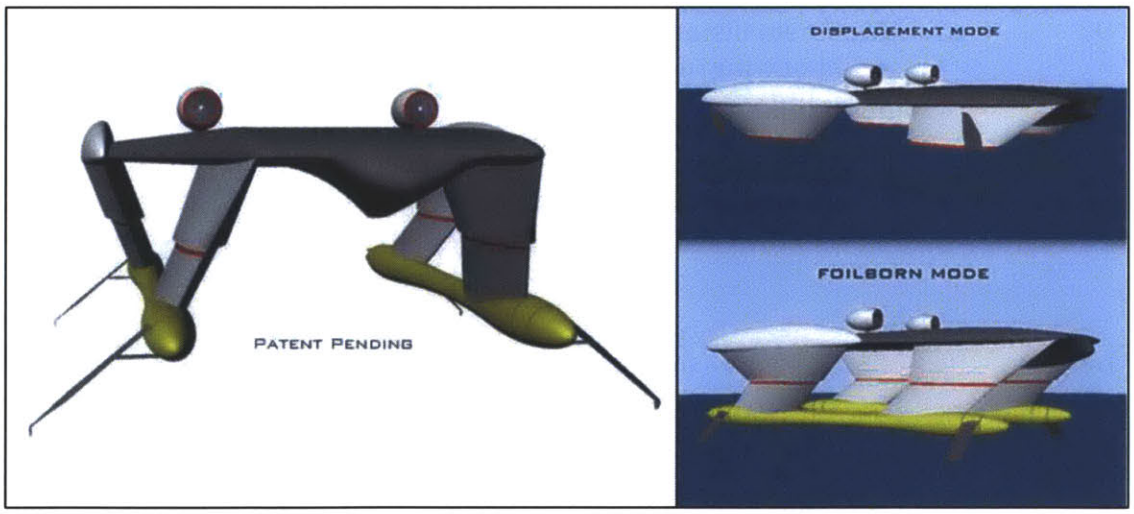

Figure 1: S. Brizzolara's unmanned ASV HYGE-SWATH

The required payload of Wavecutter is significantly different both in weight, weight distribution and type. The very fact that the vessel is intended to be manned generates extra requirements and considerations. Safety is of great concern, which is why a whole section is devoted to an evacuation plan (2.6). The risk of capsizing is also of major concern, which is why stability is the first on the list of feasibility assessments. In addition, seakeeping and dynamic behavior are topics that require more attention than they would in an unmanned vessel, which is the second priority of the feasibility assessment phase of this study.

Figure 2 presents the preferred concept design of Wavecutter. The cylindrical shaped nacelle placed in the middle of the wing deck contains all manned compartments. At this stage of the design, neither the exact size of the compartments or their configuration had been decided upon. The molded diameter of the nacelle represented in Figure 2 is about 5 m. An alternative concept design option is to increase the thickness of the wing deck to 3 m, to be able to incorporate compartments directly inside the wing. This concept was discarded, because it increases the wing's weight significantly, and it would be unlikely that the wing will provide any lift at all with this shape. Other options were also considered, but only the preferred one is shown here.

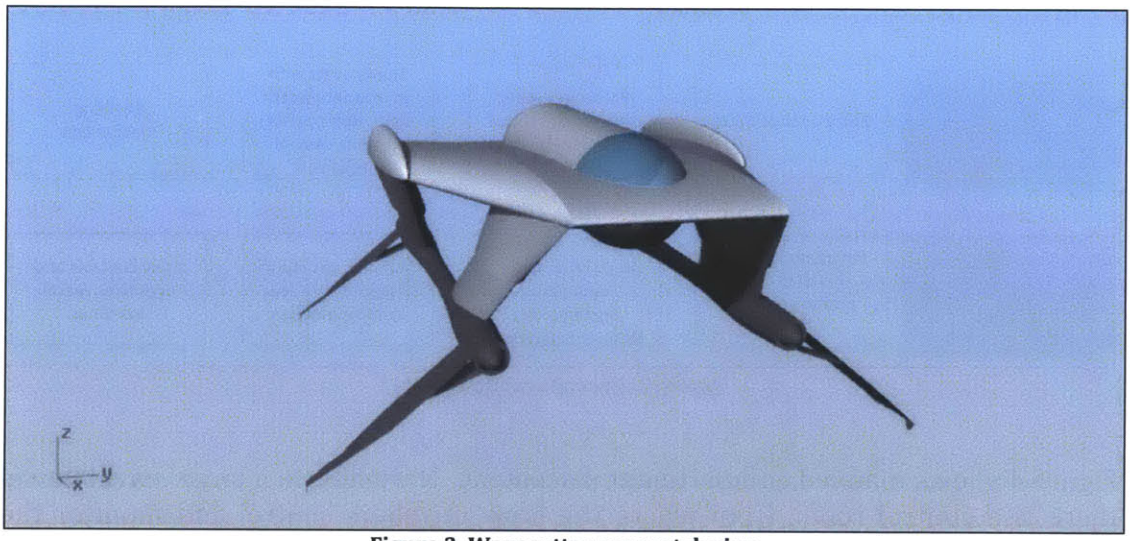

Figure 2: Wavecutter concept design

2.2 Manned compartments design

The basic intended function of this vessel is to transport people, thus the manned compartments were designed in advance. To better understand the problem, this procedure has been mapped in a flowchart, shown in Figure 3. Mapping out the procedure helps infer the vessel's required attributes. The main difficulty in compartment design and general arrangements is the limited available space in this vessel. Unlike conventional vessels, the only spaces here are inside the wing, struts and SWATH hulls. Thus, in this design stage, effort was made to consume minimum space from the available. Another challenge has been the peculiar sensitivity of vessel trim to weight distribution, unlike for a conventional displacement hull.

Manned compartments need to be a continuous space in the vessel. The only part of the vessel that can facilitate this is the wing. This continuous space needs to be shaped to reduce aerodynamic resistance. This study did not focus in optimizing this shape for aerodynamic resistance; a shape similar to an airplane's fuselage was adopted. This continuous space needs to include room for passengers, crew and

cargo. The direct and indirect system requirements derived from the intended procedure are shown in Figure 3.

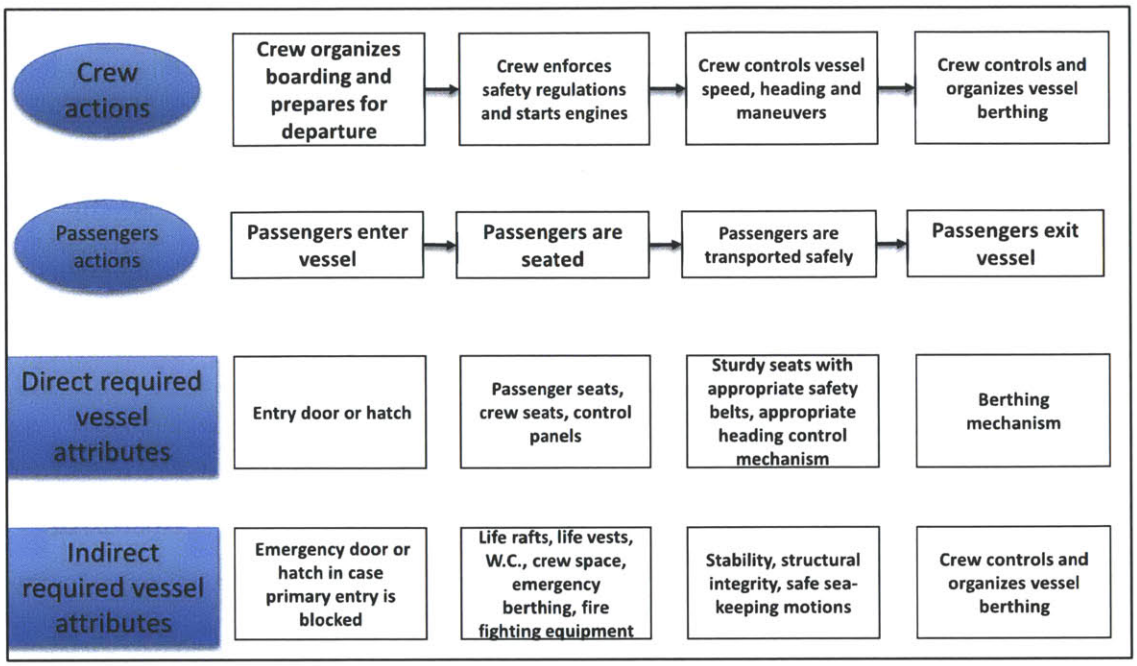

Figure 3: Procedural flow chart

Figure 4 shows manned compartment placement. Normally, in a large naval vessel there is a control room, from where the crew members control and monitor the vessel's systems. There is also a need for a navigation room, from where a visual appreciation of the surroundings will be possible. To keep consumed space low, these two rooms were combined into a common control room, which was placed in the front part of the wing. From the procedural flow chart, there is also a need for crew office space, W.C. and an emergency berthing room. All these spaces are allocated in a common compartment behind the control room compartment. The emergency berthing room will be used in case someone on board, crew member or passenger, has a sudden medical need to rest. This could also serve as a resting place for the crew member who will perform watch duty while berthed at harbor.

The passenger space and control room dimensions were calculated based on the average human standing and sitting 'box' dimensions, with some allowance. These calculations were trivial and are not presented here. It is noticed that there are two hatches in the compartment placement profile drawing. The aft hatch is for normal entry/exit and the forward hatch is intended for emergency entry/exit. The forward hatch includes a portable 'fire-escape' type ladder, not shown in the drawing. The entry space's dimensions have been estimated based on the required cargo capacity of the vessel. The dimensions of the tube which contains the manned compartments has been estimated based on the structural allowance requirement

(D3). The exact dimensions of the manned compartments and the size of their internal components are presented in section 2.5.

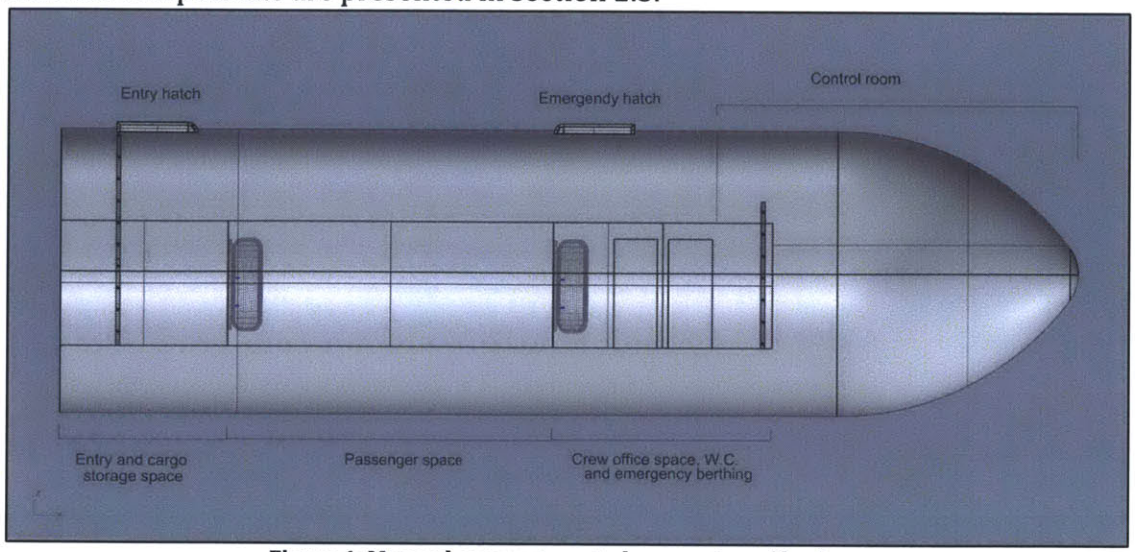

Figure 4: Manned compartment placement-profile view

2.3 Speed profile, propulsion system configuration and engine selection

Adopting the parent vessel's operational profile, Wavecutter operates in two modes, displacement and foilborne. In displacement mode, hydrofoils are folded and buoyancy is provided by the submerged SWATH hulls. In the transition phase, hydrofoils are rotated to be perpendicular to the water level, providing maximum lift for the given speed. As the vessel lifts, hydrofoils rotate further, until they reach a negative dihedral angle of -140^0, or a 40^0 angle from the water level directly above the foils. The two modes along with the transition phase are shown in the three figures below.

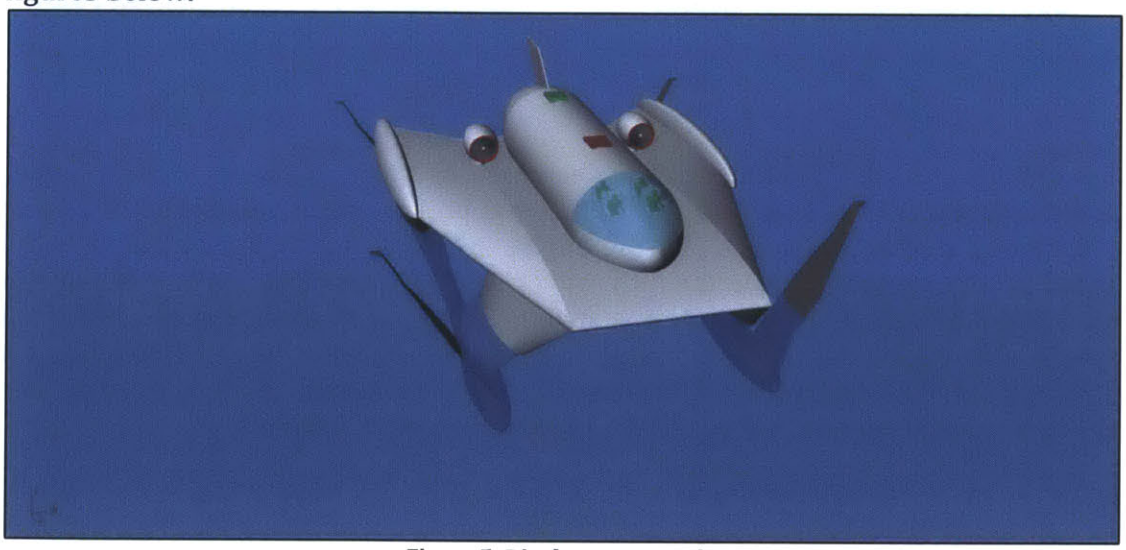

Figure 5: Displacement mode

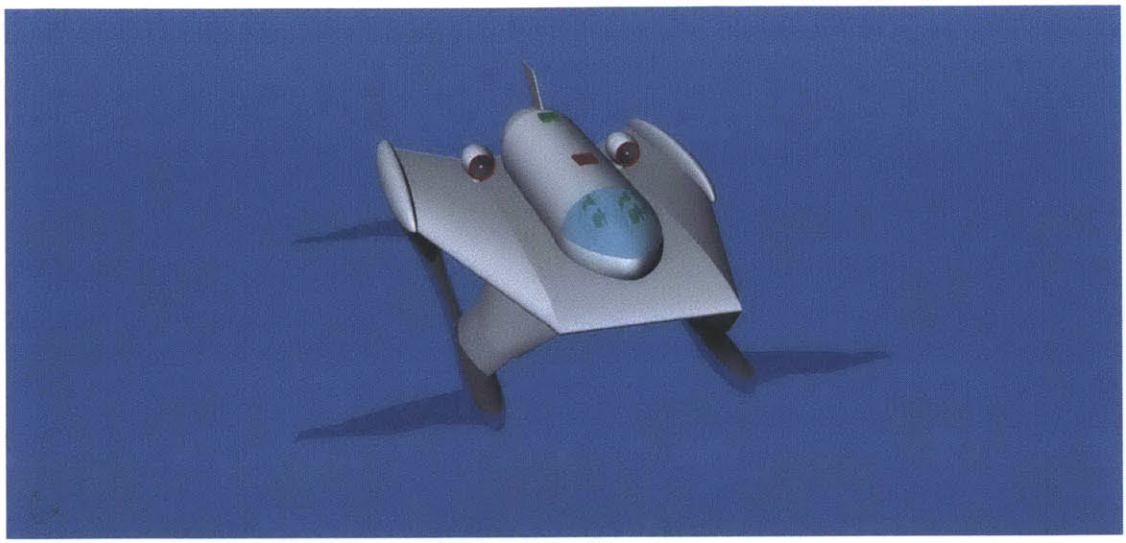

Figure 6: Transition phase

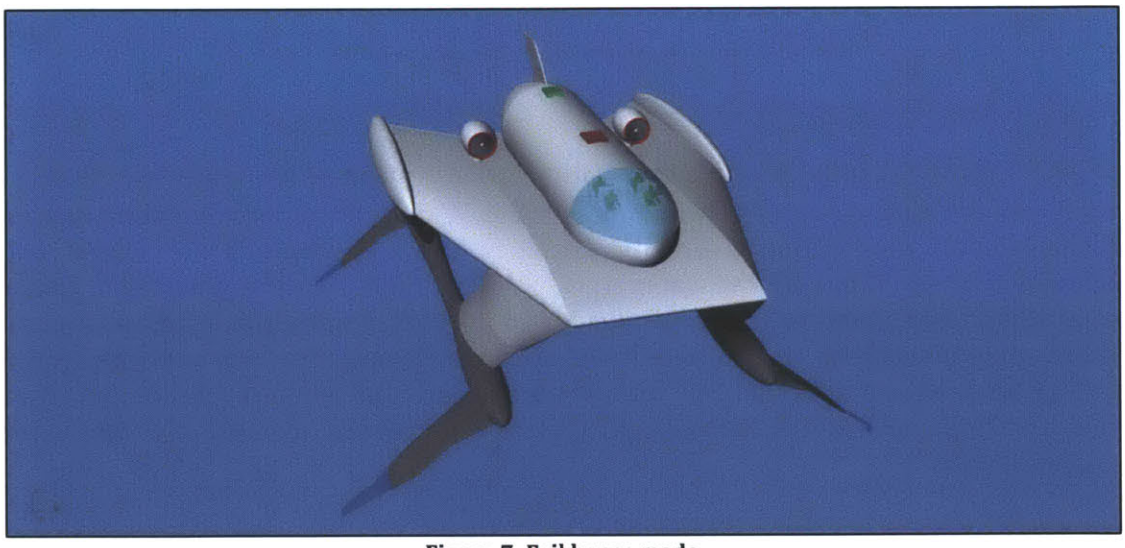

Figure 7: Foil borne mode

The submerged area of the hydrofoils decreases, as speed increases; thus in higher speeds vessel draft is less. The desired speed profile of the vessel before engine selection is shown in Table 4. During engine selection, a change was made in the speed profile, shown in red in the fifth row of Table 4. This change was made due to the limited available space inside the struts: engines with enough power to reach speeds above 17 knots were too large to fit in the available space. However, if a manufacturer is found to make engines of such power small enough to fit in this space, the diesel engines will be able to reach the speed of 27 knots.

Table 4: Vessel speed profile

Mode	Speed range [knots]		Speed range [m/s]	
Displacement	0	17	0.00	8.75
Transitional	17	37	8.75	19.03
Foil borne	37	85	19.03	43.73
Diesel Generators	0	27 (17)	0.00	13.89 (8.75)
Turbo fans	17	85	8.75	43.73

To select a diesel engine, the resistance has been estimated in displacement mode for the speed 17 knots. The resistance in displacement has been found with two approaches. In the first approach, the total resistance is decomposed into the resistance of the SWATH hulls, the struts and the wing's.

$$R_{tot} = R_{hulls} + R_{struts} + R_{wing}$$

Using the ITTC practical guidelines for estimating resistance (F.Campana, 2011), the hulls' and struts' individual resistance is:

$$Re = \frac{Length * Speed}{kinematic\ viscosity}$$

$$C_f = \frac{0.075}{(log_{10}(Re) - 2)^2}$$

$$C_d = C_f * \left(1 + 1.5 * \left(\frac{Dmax}{L}\right)^{1.5} + 7 * \left(\frac{Dmax}{L}\right)^{3}\right)$$

The above is an empirical formula from S. Brizzolara's work (Brizzolara, 2010).

$$R = \frac{1}{2} * \rho * S * C_d * Speed^2$$

Using Oswald's coefficient for wing efficiency (Raymer, 2012, p. 456), the wing resistance is:

$$C_D = C_{D0} + \frac{(C_L)^2}{\pi * e * AR}$$

$$R = \frac{1}{2} * \rho * S * (C_i + C_{d0}) * Speed^2$$

Using these formulas the total resistance in 17 knots is 73 KN.

However, in the above calculations of total resistance, wave resistance is not taken into account. Wave resistance is important for this vessel, because the volumetric Froude number is greater than 1. Specifically the volumetric Froude number is:

$$Fn_v = \frac{V_{ship}}{\sqrt{\nabla^{(\frac{1}{3})} * g}} = 1.127$$

$V_{ship} = 17\ knots$
$\nabla = 245.52\ m^3, total\ diplaced\ volume$

To include wave resistance, an alternative approach is followed, to find the total resistance. This approach is based on S. Brizzolara's total resistance comparison of SWATH hulls with different slenderness ratios and Froude numbers (Brizzolara & Villa, 2010, p. 13).

The total resistance with this approach is:

$$R_t = C_{T\nabla} * \frac{1}{2} * \rho * {V_{ship}}^2 * \nabla^{\frac{2}{3}} = 123\ KN$$

$C_{T\nabla} = 0.08, total\ resistance\ volumetric\ coefficient$

Diesel engine selection is based on the total resistance calculations from the second approach.

$$EHP[KW] = Resistance[KN] * Speed\left[\frac{m}{s}\right]$$

Using typical propulsive, mechanical and electrical efficiency coefficients, the Break Horsepower has been calculated. Break Horsepower divided by 2 gives the required power per engine, and the diesel engine selection is based on this number. The selected engine selected is MTU DQCA (Cummings) rated at 850 KW. These calculations are presented in Table 5.

Table 5: Diesel engine selection for displacement mode

Calculation of needed power of Diesel Generator			
EHP [KW]	1076	Maximum speed with Diesel [m/s]	8.75
SHP [KW]	1435	Propulsive coefficient (P.C.)	0.75
BHP [KW]	1511	Mechanical Efficiency	0.95
Required power of Diesel Engines [KW]	1679	Electrical efficiency	0.9
Number of Engines	2		
Required power per engine {KW]	840		
Engine selected power [KW]	850	Type of Engine selected: DQCA of Cummings (MTU engine)	

In displacement mode, power is transmitted from the diesel engines to the propeller via electricity. Figure 8 shows the propulsion components. The yellow boxes inside the struts represent the diesel engines, and the smaller green boxes the generators. Power is transmitted through cables to the motors in the aft part of the SWATH hulls, colored red, and finally to the propellers.

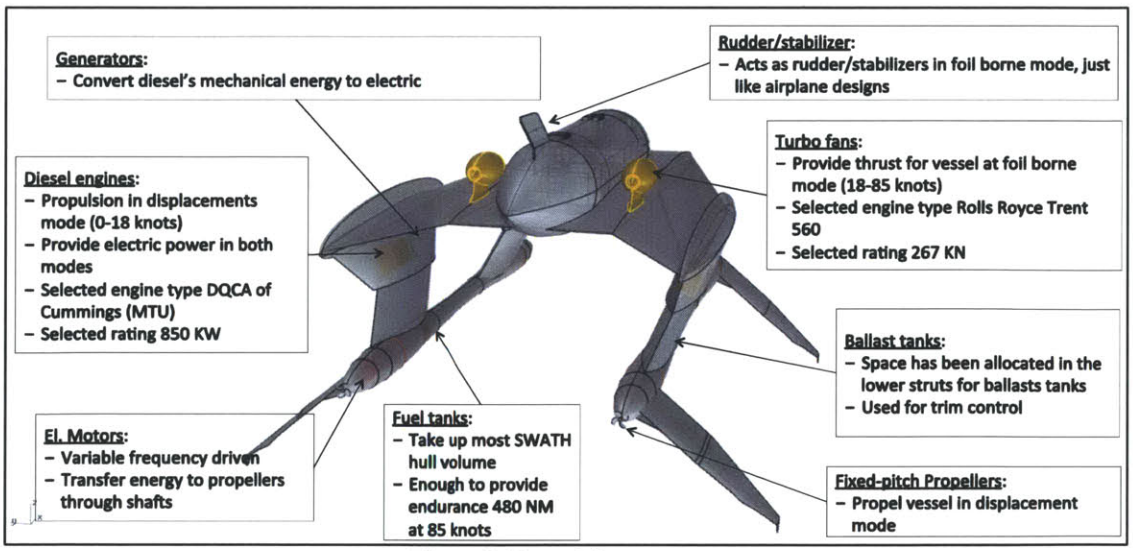

Figure 8: Propulsion system

The engines providing propulsion in foil borne mode are turbofan aircraft engines, located right and left of the manned nacelle on top of the wing. These types of engines are rated in KN. In the initial design loop, the turbofan selection has been based on estimations of water and air drag at maximum speed. In the second design loop (this study accomplished two design loops), these calculations are done with greater detail, relying on experimental data for the calculation of water drag, which is the largest of the two components (air and water drag). The selected engine from the first design loop will not be mentioned here, since the second design loop is more accurate in predicting total drag.

In the initial design loop, drag in water has been calculated using the simple assumption of drag being one fifth of lift for hydrofoils. Lifts for front and aft foils have been found from equilibrium conditions at maximum speed, similar to the process followed in section 3.2.1. The resistance of the foil has been found 443.3 KN. The resistance in air was only a small portion of the resistance in water, 5.1%. The total resistance in the first design loop has been found 466 KN. The resistance in air was:

$$R_{air} = A_{frontal} * C_{D0} * \frac{1}{2} * \rho * Speed^2$$

In the second design loop, water drag resistance at maximum speed is based on the experimental formulas found in the Appendix in section 6.2.1, instead of assuming a fixed ratio between lift and drag for the hydrofoils. Aid drag is calculated from experimental formulas derived from Hoerner for small aspect ratio wings (Hoerner, 1992). A more detailed explanation of the method for calculating air drag at maximum speed is found in the Appendix section 6.3.

The distribution of drag components at maximum speed can be seen in Figure 9. Just as in the first design loop, air drag is a small portion of the total drag. The total drag is 483.43 KN. Adding a non-calm sea allowance of +10%, the total drag is 531.77 KN. Thus, each turbofan engine must provide at least 266 KN.

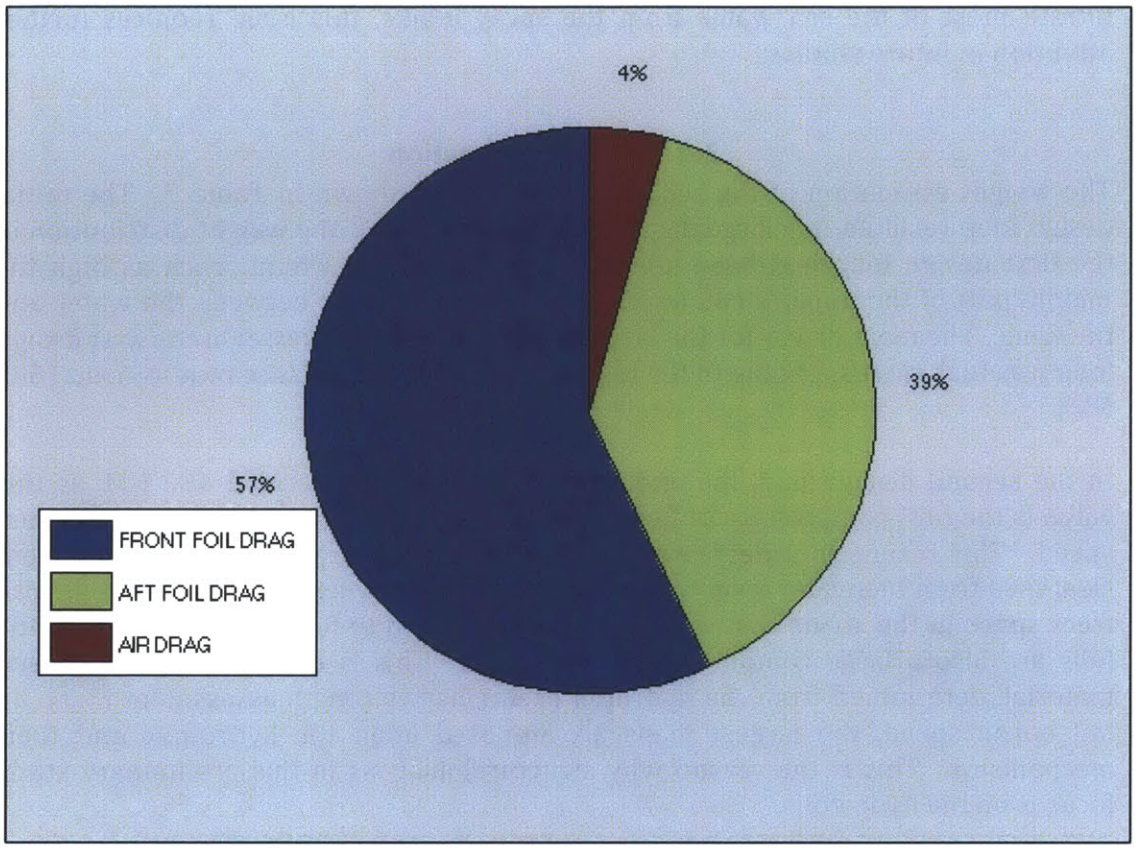

Figure 9: Total drag force distribution at maximum speed in equilibrium condition

The engine database for turbofan selection was the Trent series of Rolls-Royce, because it was the most open source database found. The engine selected is Trent 560, currently used in airplanes Airbus 340-600. The ratings and characteristics of the engine are shown in Table 6.

Table 6: Selected turbofan characteristics

Engine	Trent 560
Entry Into Service	2002
Applications	Airbus A340-600
Static Thrust [KN]	266.89
Basic Engine Weight [kg]	4717.36
Thrust to Weight Ratio	5.76
Length [m]	3.91
Fan Diameter [m]	2.47

A recognized technical risk of this design is the placement or airplane turbo fans close to the sea water surface level. Corrosion problems that may arise due to the salt deposits on the blades may be significant. While technologies do exist that

filtrate most of the sea water from the spray intake, this issue requires further attention in future studies.

2.4 Weight estimation

The weight estimation of the second design loop is shown in Table 7. The initial design loop resulted in a large displacement and draft. If the weight distribution of the first design loop had been adopted, the water level would reach as high the middle part of the upper strut, leaving very little clearance between the water and the wing. The main driver for the large displacement of the vessel in the first design loop was fuel, corresponding to the higher range of the endurance requirement (600 NM).

In the second design loop, the endurance capability was decided 480 NM, as this value is the best compromise of fuel/displacement while maintaining the maximum speed. This results in a decrease in displacement and draft that allows sufficient clearance from the water level to the lower part of the wing. This modification also frees space in the struts that was previously allocated to fuel. Apart from fuel, the foils are also a large component of the weight. This is due to the foil's chosen material, determined from the hydrofoil preliminary strength assessment (3.3). In foil borne speed, the largest loads are imposed upon the hydrofoils and their mechanisms. This is the reason why structural analysis in this preliminary study focuses on the hydrofoils.

Table 7: Weight estimation

Weight component	Weight [t]	Longitudinal position Xg [m]	Vertical position Zg [m]
Hull	7.74	14.72	0.00
Struts	12.77	17.43	3.73
Wing	22.31	18.12	6.53
Permanent Payload	3.00	19.37	6.21
Fore Foils	30.58	27.20	-2.40
Aft Foils	30.58	2.63	-2.40
El.motor+shafts+props	1.20	0.00	0.00
rotating/folding mech. Fore	0.90	27.14	-0.20
rotating/folding mech. Aft	0.90	2.56	-0.20
Batt+inv.	1.00	11.00	4.00
Electr, Aut & Nav Equipm.	1.00	18.12	6.53
Cables + pipes	1.00	19.37	6.21
2 x Turbofans	9.43	14.15	8.14
2 x Diesels + Generators	13.00	8.24	4.45
Allowance	6.77	17.94	1.91
LIGHT SHIP	**142.17**	**15.11**	**1.61**
Mission Payload	17.24	19.37	6.21
Fuel in Hulls	86.11	14.72	0.00
Fuel in Struts	0.00	0.00	0.00
Service Tank	1.00	8.24	4.95
Ballast Tanks	8.00	16.79	1.70
WEIGHT at FULL LOAD	**254.52**	**15.79**	**1.44**

To appreciate the components and their location in the vessel visually, a ghosted profile view is provided in Figure 10. The scale used is 1 m-1 square.

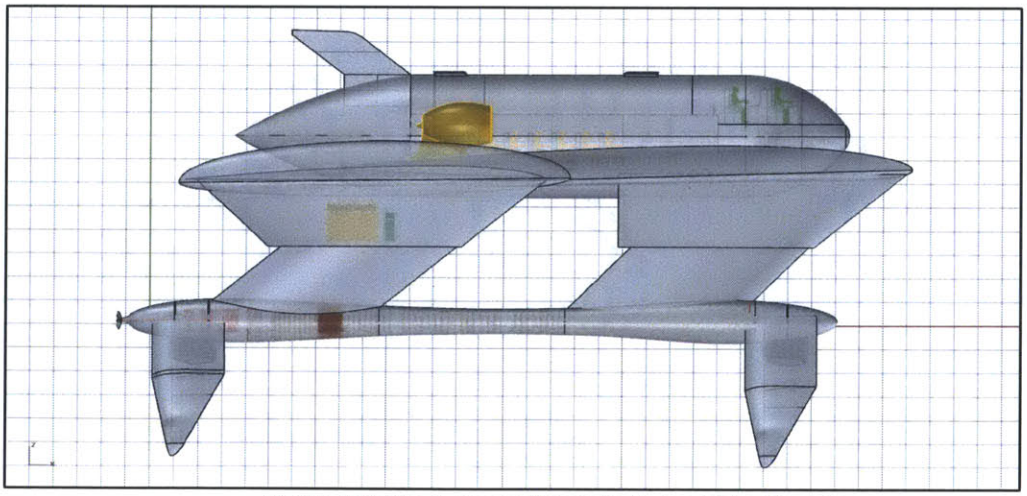

Figure 10: Wireframe profile view for weight estimation

2.5 General arrangements

This section presents the general arrangements of the vessel, with three dimensional outer deck views, profile compartmentation views and two dimensional internal arrangement views.

2.5.1 Three dimensional views

Figures 11 and 12 show the vessel from a forward and backward viewing perspective respectively, in foil borne mode. The normal and emergency hatches can be seen in green and red on the top of the manned nacelle. The control room can be seen through the transparent viewing window in the front of the nacelle. The hydrofoils are partially submerged; the waterline level corresponds to maximum speed. The rudder serves to maneuver and stabilize the vessel in foil born mode.

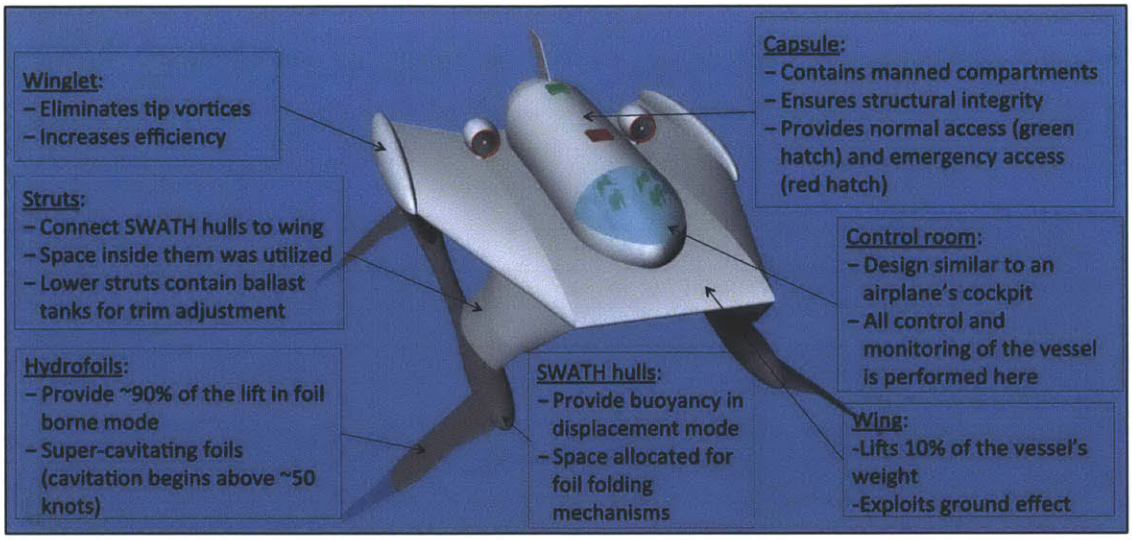

Figure 11: 3-D view from forward position with vessel components explained

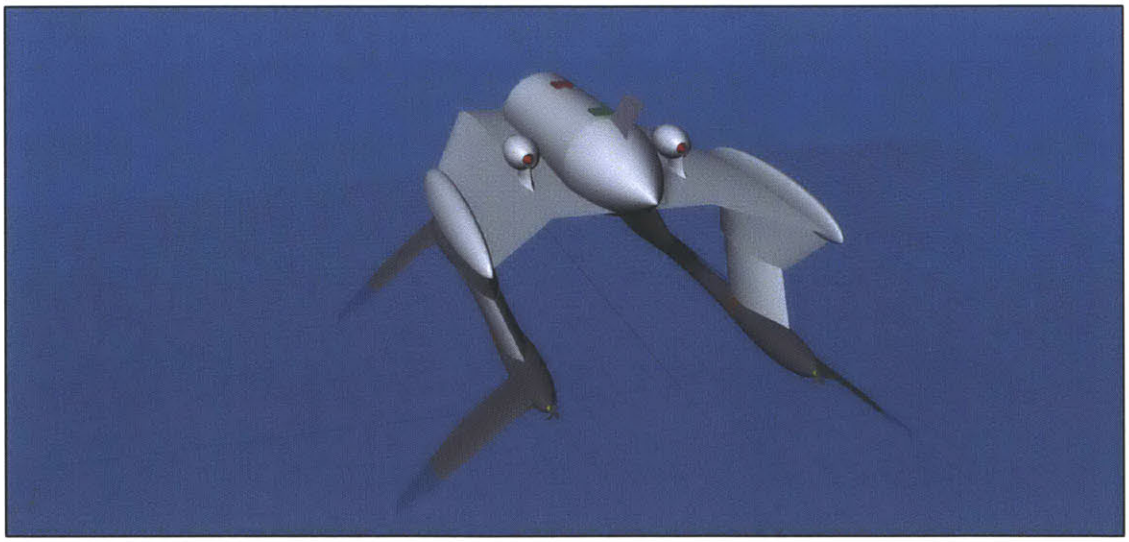

Figure 12: 3-D view from backward position

Figure 13 shows a view of the inside of the manned compartments from a forward perspective. Two ladders are seen in this figure. The aft ladder is for normal access to the vessel and the forward ladder is for control room access by the crew. Figure 14 gives a closer view of the passenger room. The seats should accommodate a strong foundation and professional seat belts for vibration and shock absorption.

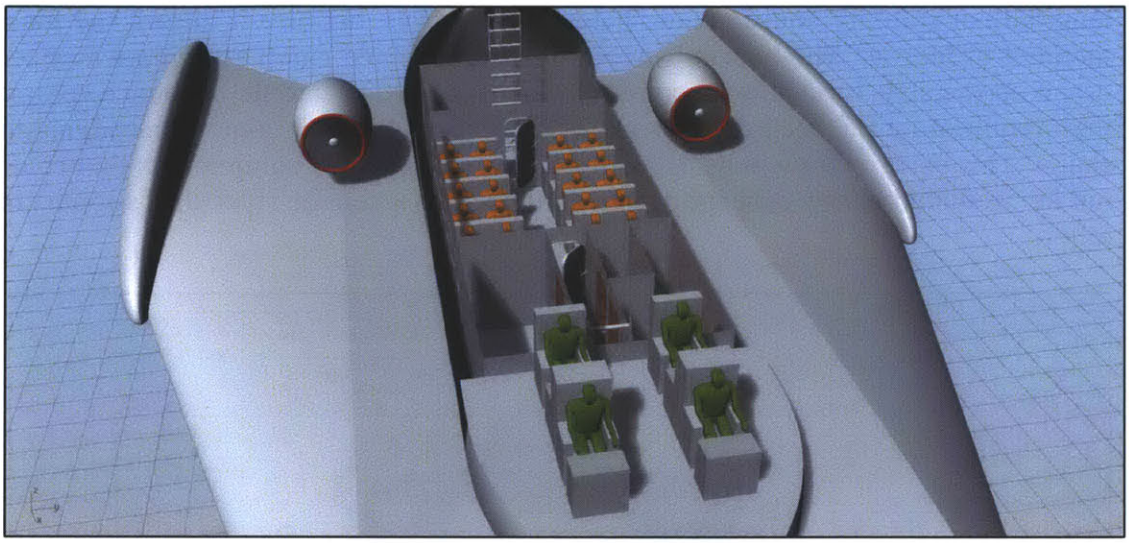

Figure 13: 3-D compartment inside view

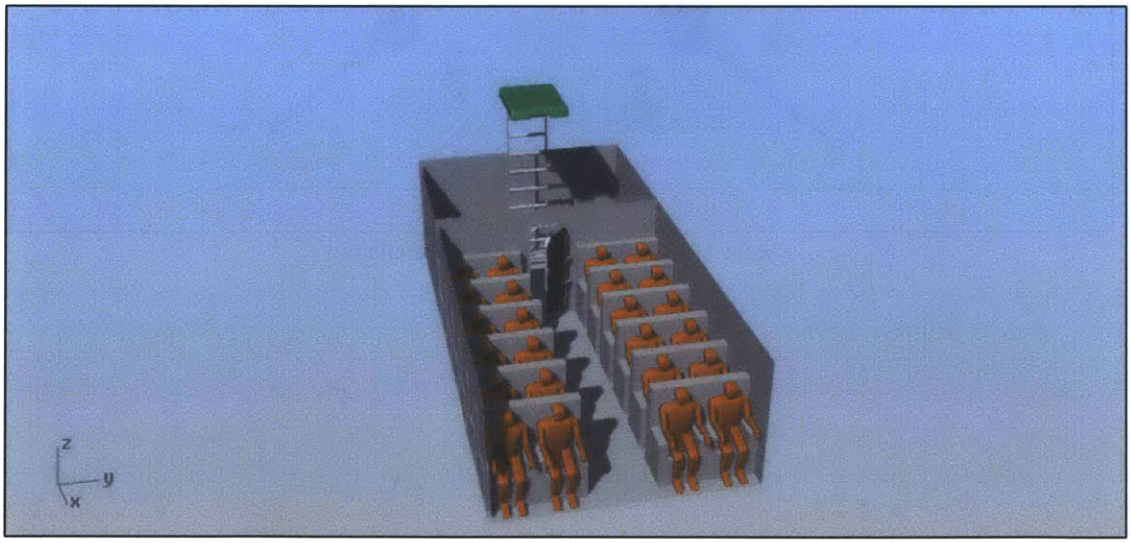

Figure 14: 3-D view of inside of passengers and cargo rooms

2.5.2 Two dimensional drawings

The following three figures are two dimensional drawings, each from a different perspective, and show the vessel's primary dimensions. The waterline level corresponds to the vessel's draft at maximum speed. Important vessel dimensions are seen, such as length overall, length between foils, nacelle size, wing dimensions and others. The longitudinal length between foils plays a major role in the vessel's longitudinal stability and dynamic behavior in waves, because it affects the mass moment of inertia. The nacelle surrounding the manned compartments was sized based on the structural allowance requirement (D3). The nacelle has more volume than required by D3, because it is cylindrically shaped to have a more aerodynamic shape. This extra space will be useful for allocating space for components that could not be predicted in this concept design study, whether that be structural support or other.

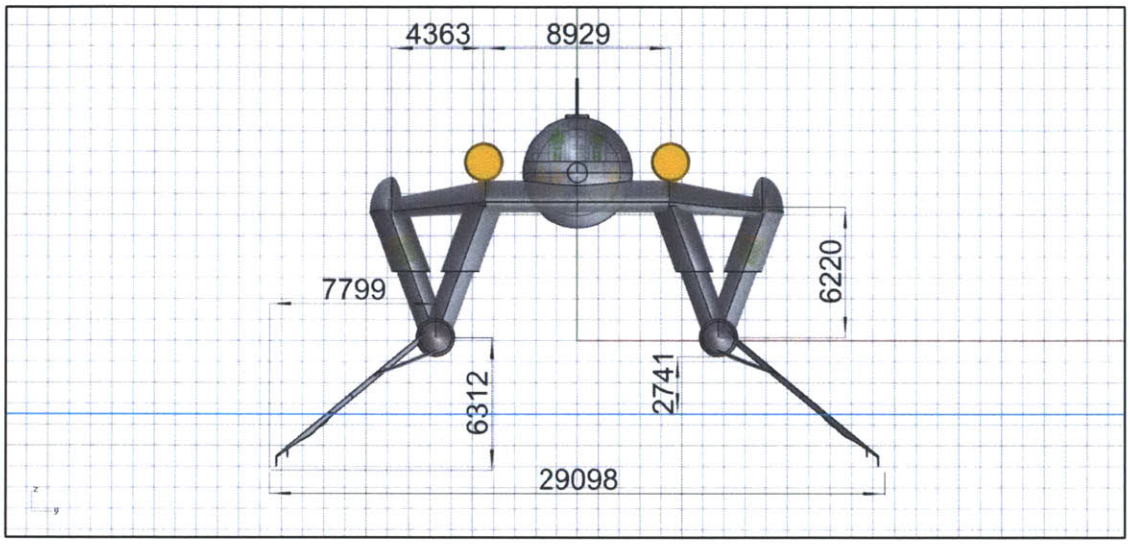

Figure 15: 2-D front view vessel dimensions

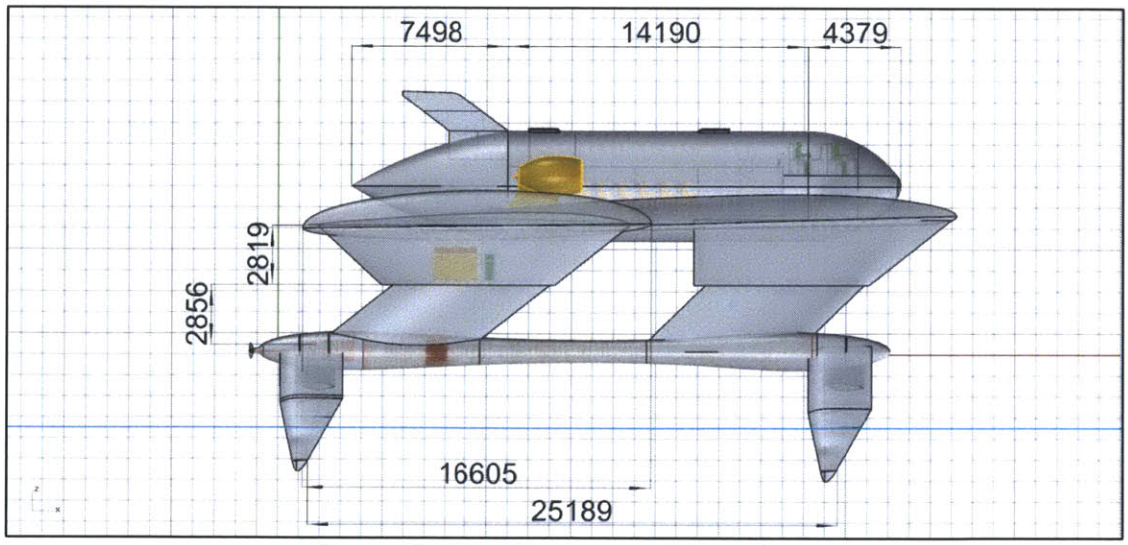

Figure 16: 2-D profile view vessel dimensions

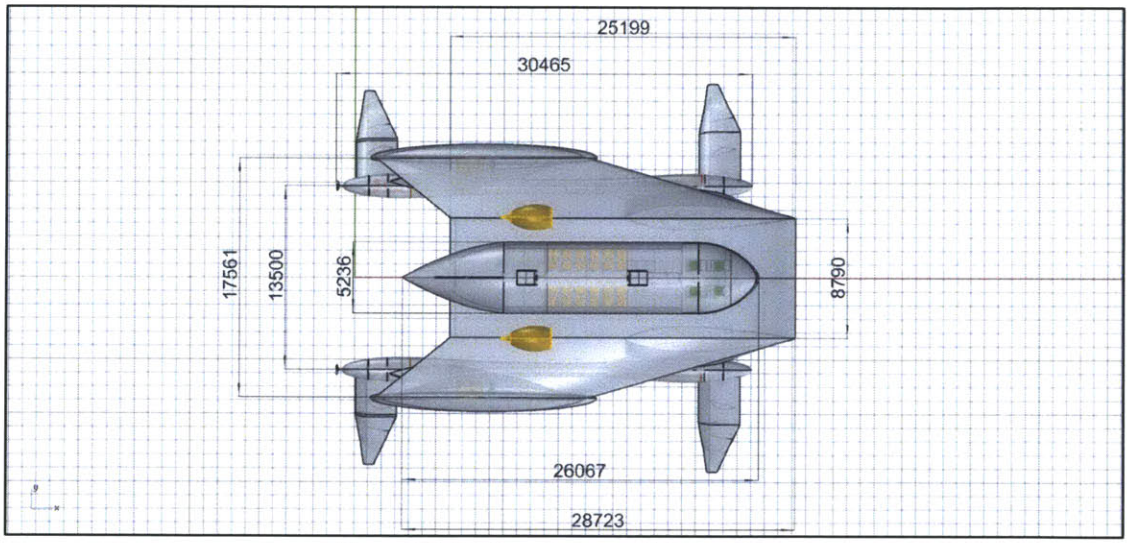

Figure 17: 2-D top view vessel dimensions

Most of the SWATH hulls' space is allocated to fuel, which is due to the endurance requirement (R5). In the forward and aft part of the SWATH hulls some space is allocated to the foil folding mechanisms. A small amount of space is left empty in the forward part of the hulls. In the aft part of the hulls, space is also allocated to the generator, shaft and bearing.

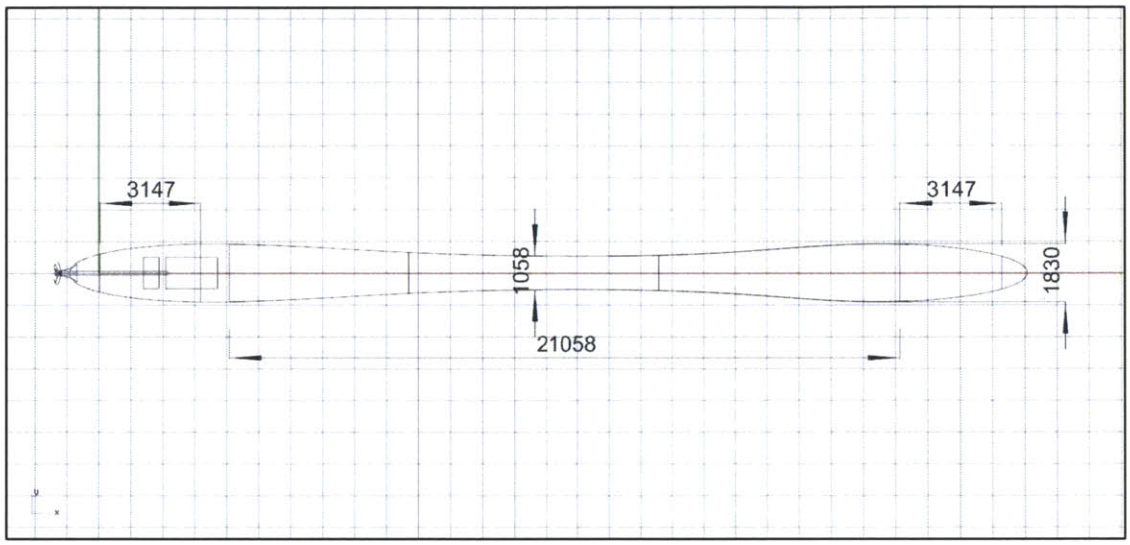

Figure 18: SWATH hulls dimensions 2-D drawing

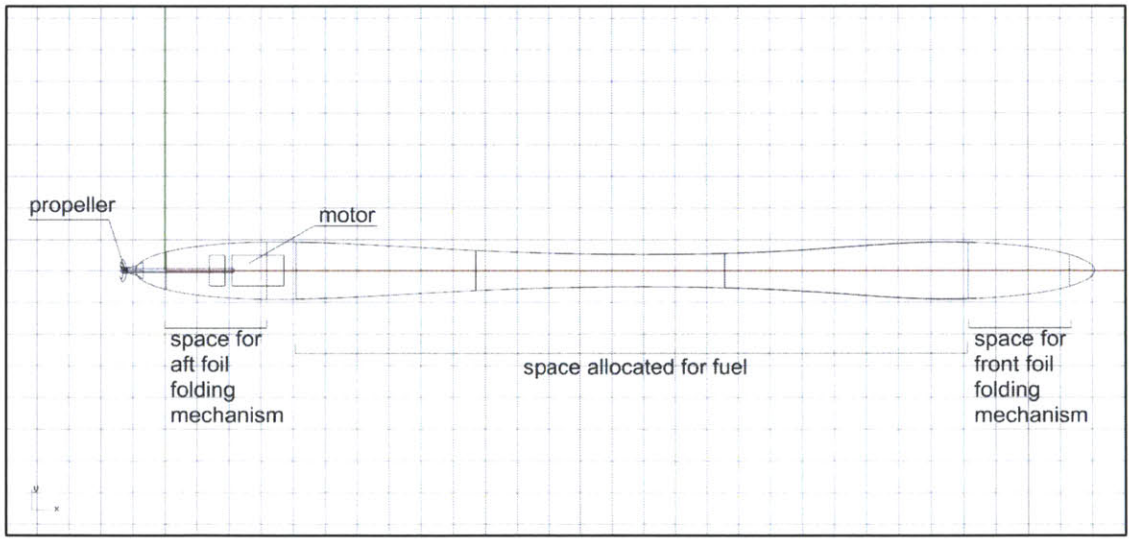

Figure 19: SWATH hulls space allocation 2-D drawing

Ballast tanks are a necessity, especially for this type of vessel, for which trim is highly sensitive to weight distribution. For example, trim changes from the full load to minimum operating conditions. Between different operating conditions, ballast tanks will be used to restore trim, by restoring the weight distribution. Most of the space in the lower struts is allocated as ballast.

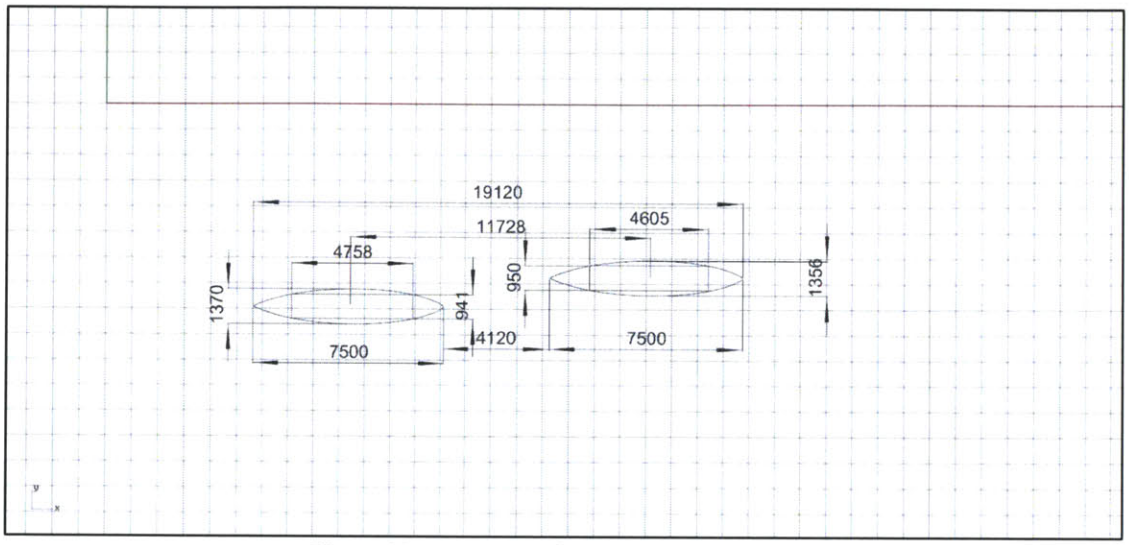

Figure 20: Lower strut dimensions 2-D drawing

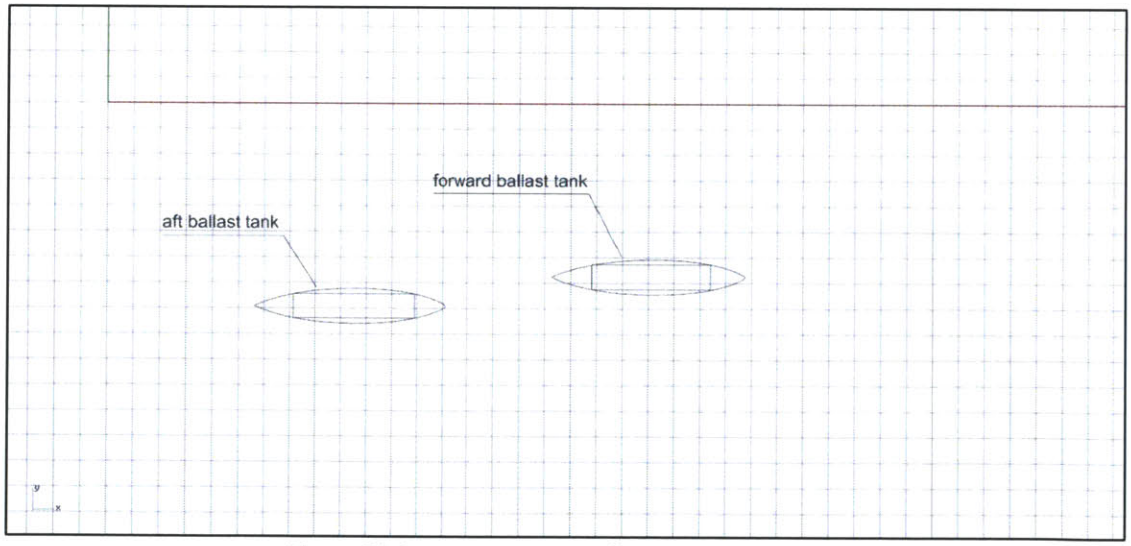

Figure 21: Lower strut space allocation 2-D drawing

Space is allocated in the aft upper struts to include a small high speed diesel engine with its accompanying generator. The front struts include space for electronics. This study did not focus on selecting particular electronics, but several electronics are a necessity for sea going vessels. Gyroscopic electronics, electricity converters, radar processing units are three examples of such necessary electronics.

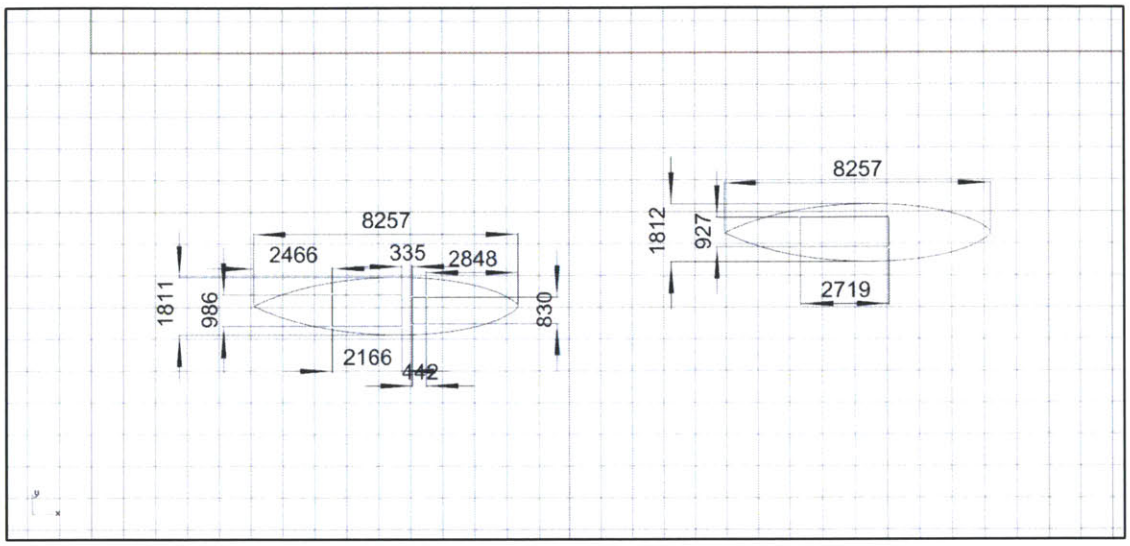

Figure 22: Upper strut dimensions 2-D drawing

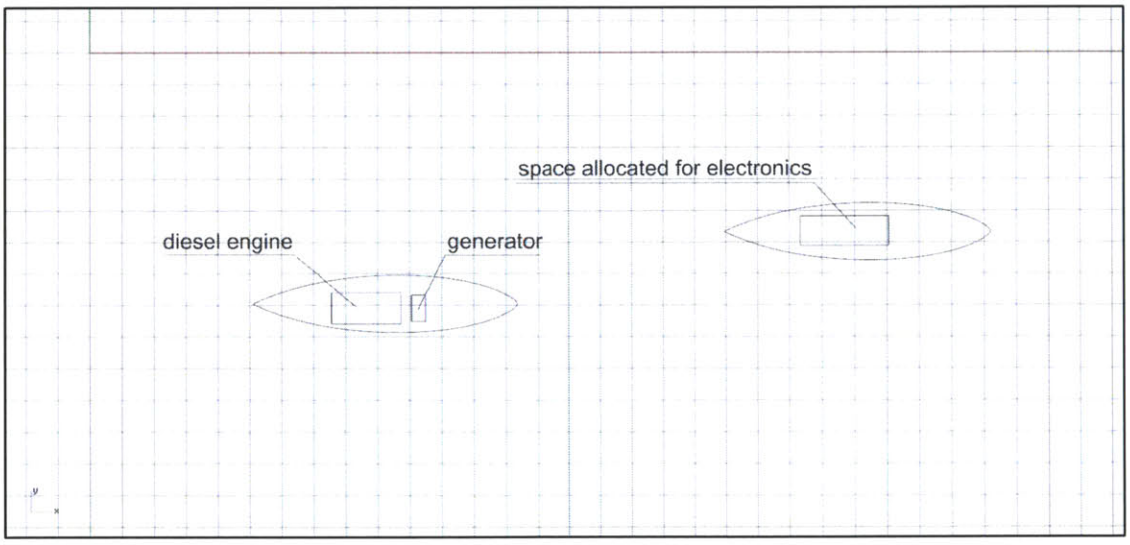

Figure 23: Upper strut space allocation 2-D drawing

The two figures below present the dimensions and space allocation for the wing and the wing deck.

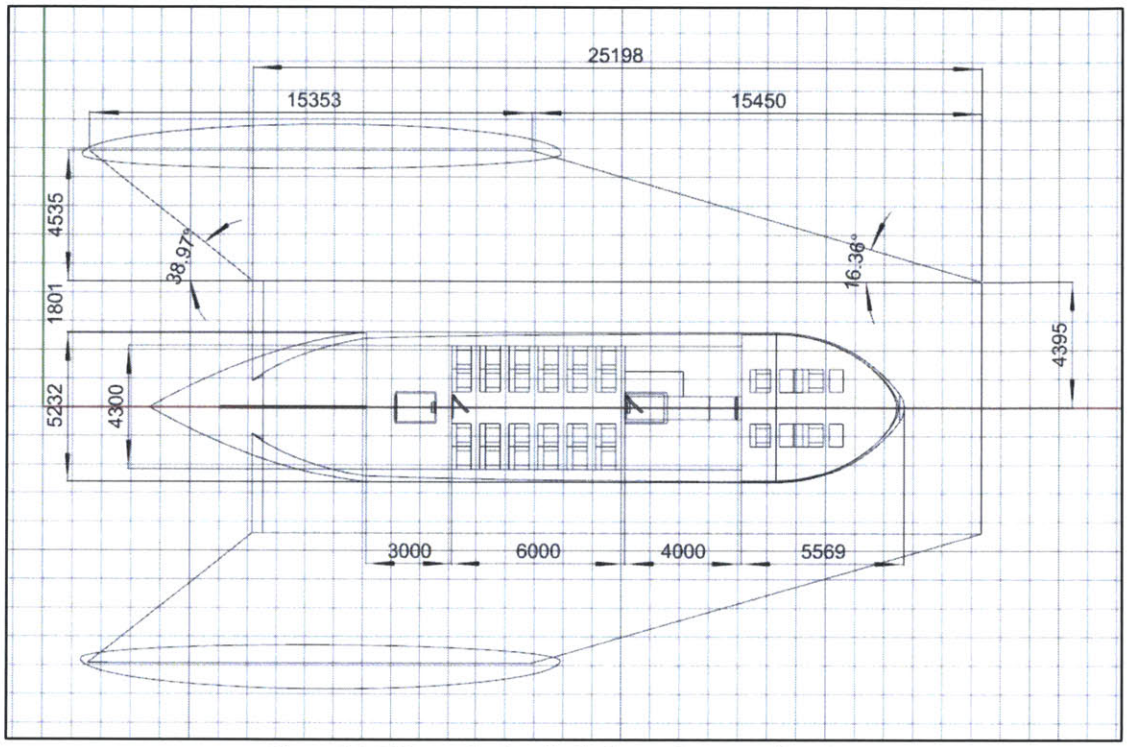

Figure 24: Wing and wing deck dimensions 2-D drawing

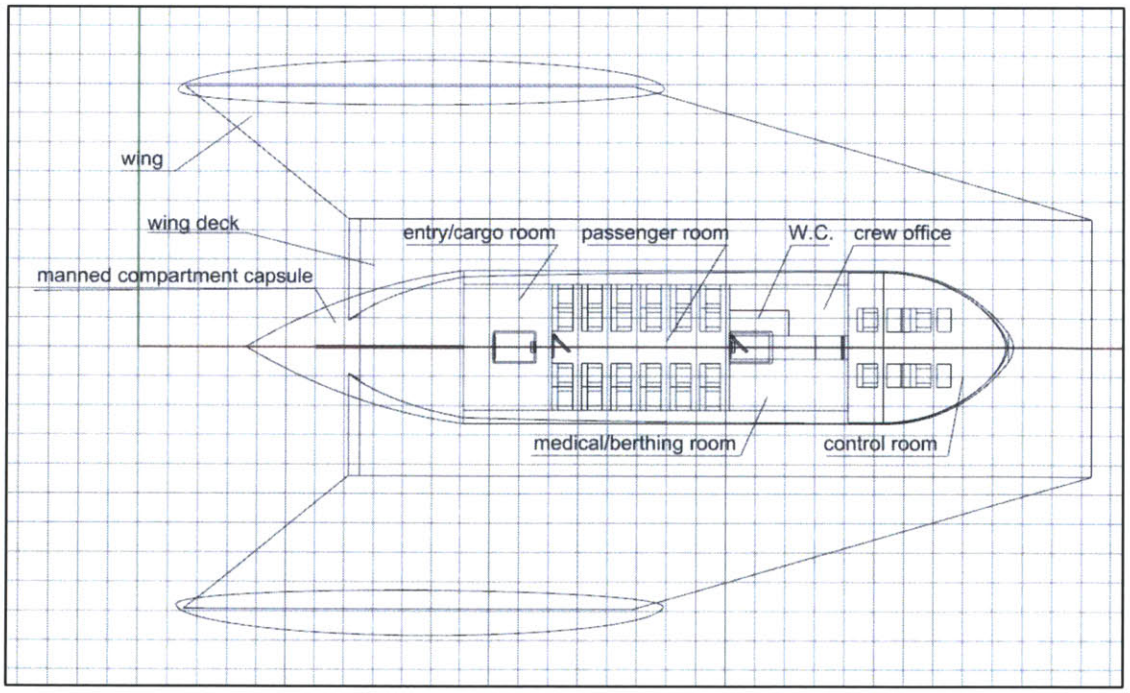

Figure 25: Wing and wing deck space allocation 2-D drawing

Manned compartment dimensions are presented in Figure 26. This figure shows the exact horizontal dimensions of seats and corridors, which were designed to be comfortable but frugal in space consumption. The hatches have been given some margin, because small cargo should be able to fit through them. Enough longitudinal distance is given between seats, to allow space for the human's feet. It can be seen that compartment configuration in this vessel reminds compartmentations in passengers airplanes. In fact, such compartmentations were used as an inspiration source in the concept design phase.

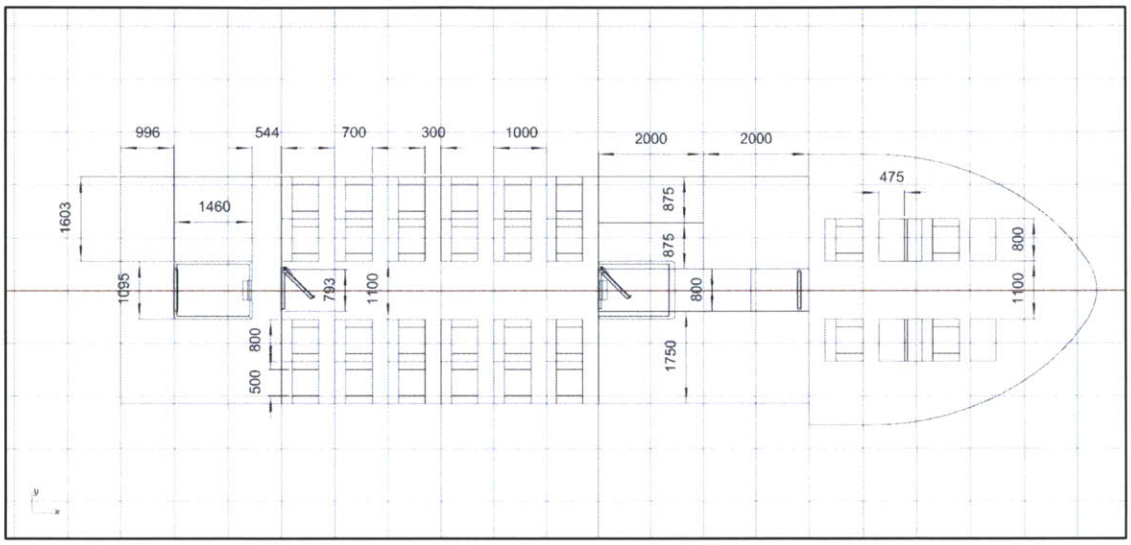

Figure 26: Manned compartments dimensions 2-D drawing

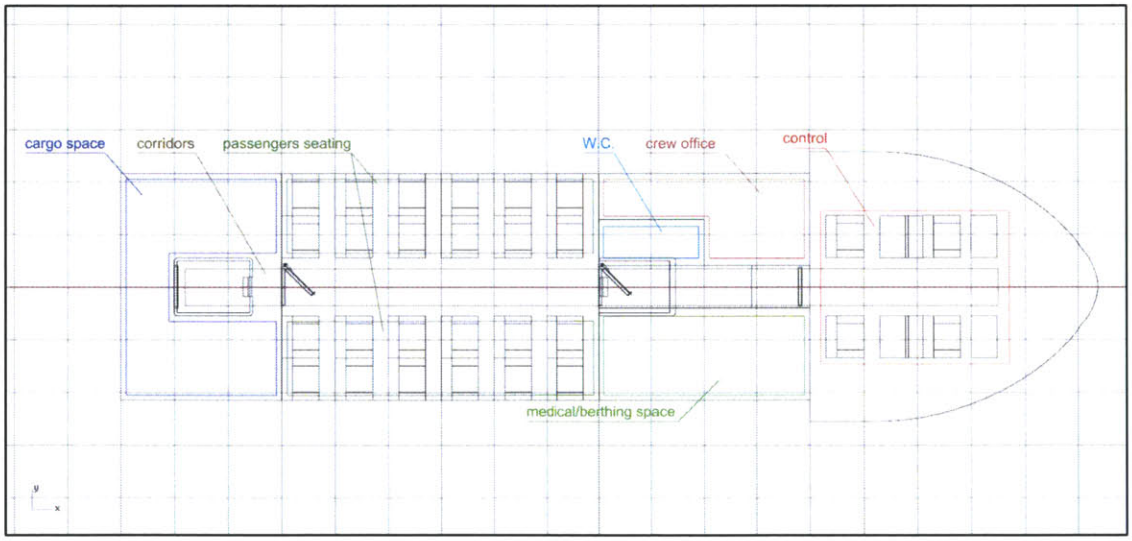

Figure 27: Manned compartments space allocation 2-D drawing

2.6 Evacuation plan

This sections describes a preliminary evacuation plan, in case of emergency. This evacuation plan is not inclusive of all the potential dangerous situations that may arise; it is a first approach on safety in case of emergency. The evacuation is shown in a series of steps throughout.

When an emergency situation occurs, it will find the crew and passengers in their normal positions, as showed in Figure 28. Two crew members will continue to navigate and monitor the vessel's machinery from the control room. One crew members will proceed to the passenger cabin and remain there to monitor passengers' safety. The remaining crew member will assess the situation and report any damage to the crew members that are navigating the vessel. After the situation is assessed, appropriate announcements will be made. In the announcements, it will be made clear which exit should be used for proceeding in the wing deck. The crew member that is assessing the situation should have first checked the condition of the emergency exit. If the emergency exit is blocked, the crew member should have checked the normal exit, located in the entry/cargo space. In this demonstration, exit from the emergency hatch has been assumed. It is a given that appropriate SOS signals will be transmitted immediately, when an emergency event occurs.

Passengers will be escorted in the wing deck. One crew member will remain in the passenger cabin, ensuring that passengers are exiting safely. Another crew members will remain on the deck ensuring that the passengers are arriving safely there. During this time the navigating crew members will prepare the vessel for evacuation, shutting down the propulsion system etc.

Navigating crew members will proceed to the deck and a fast count will be conducted, to ensure every passenger and crew member is on deck. Life rafts and escape ladders will be available in the front part of the wing deck, underneath the forward part of the control room. They would be activated remotely from the control room, before the last crew members proceed to the deck, or manually from the deck. The final step will be to board the life rafts and abandon the vessel. All the aforementioned steps are illustrated in Figures 28-33.

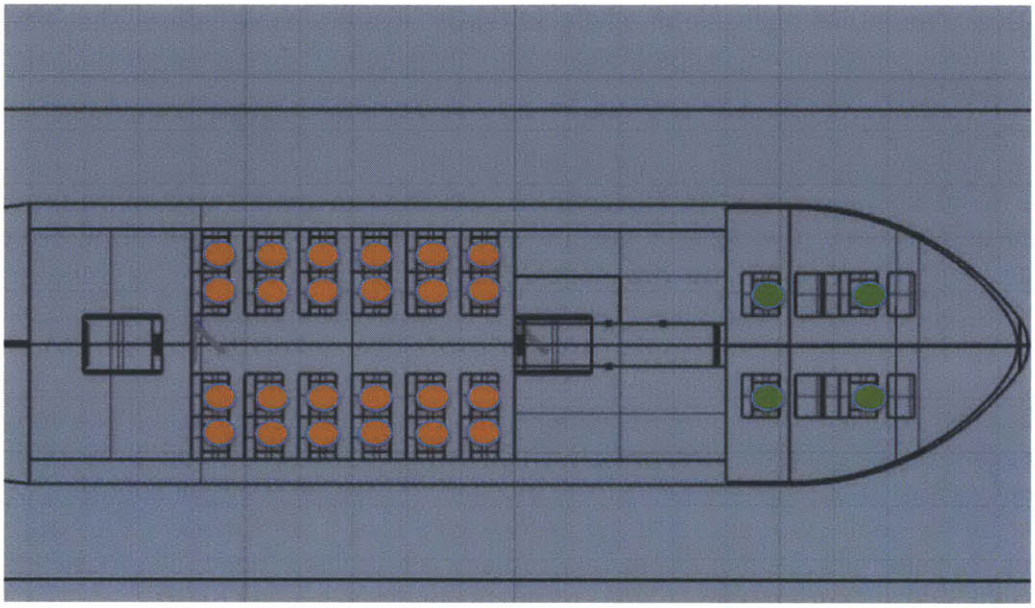

Figure 28: Evacuation plan step 1

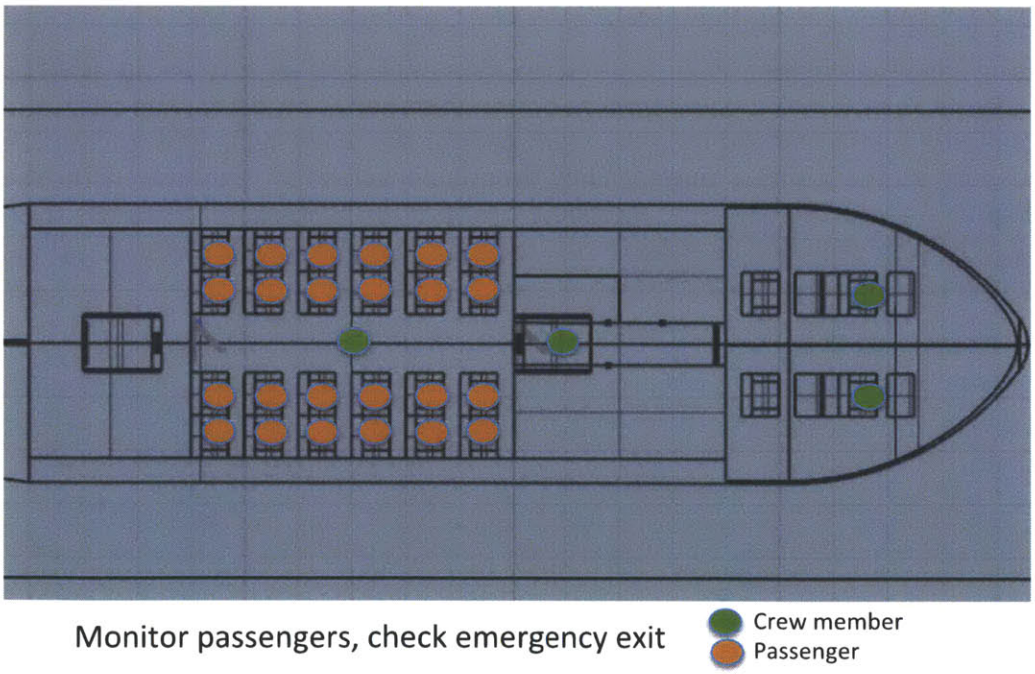

Figure 29: Evacuation plan step 2

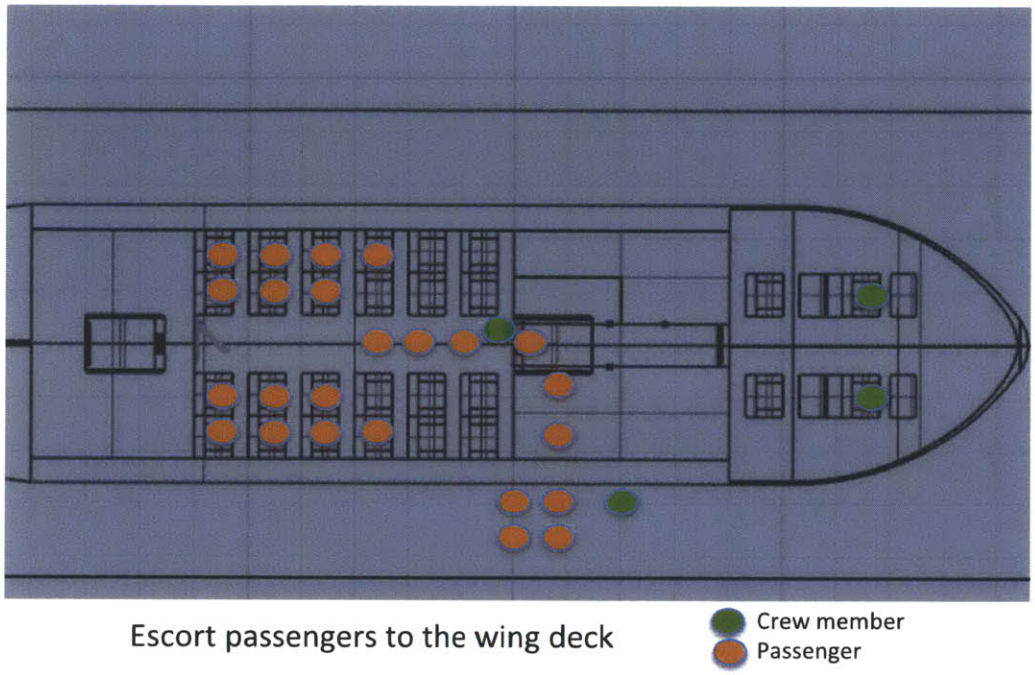

Figure 30: Evacuation plan step 3

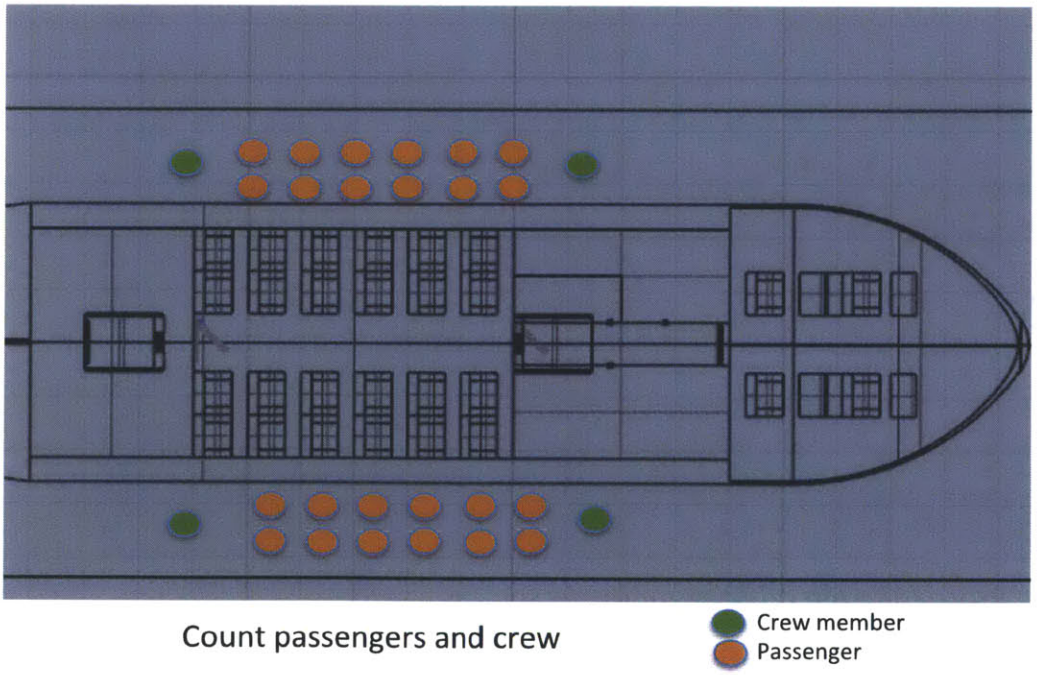

Figure 31: Evacuation plan step 4

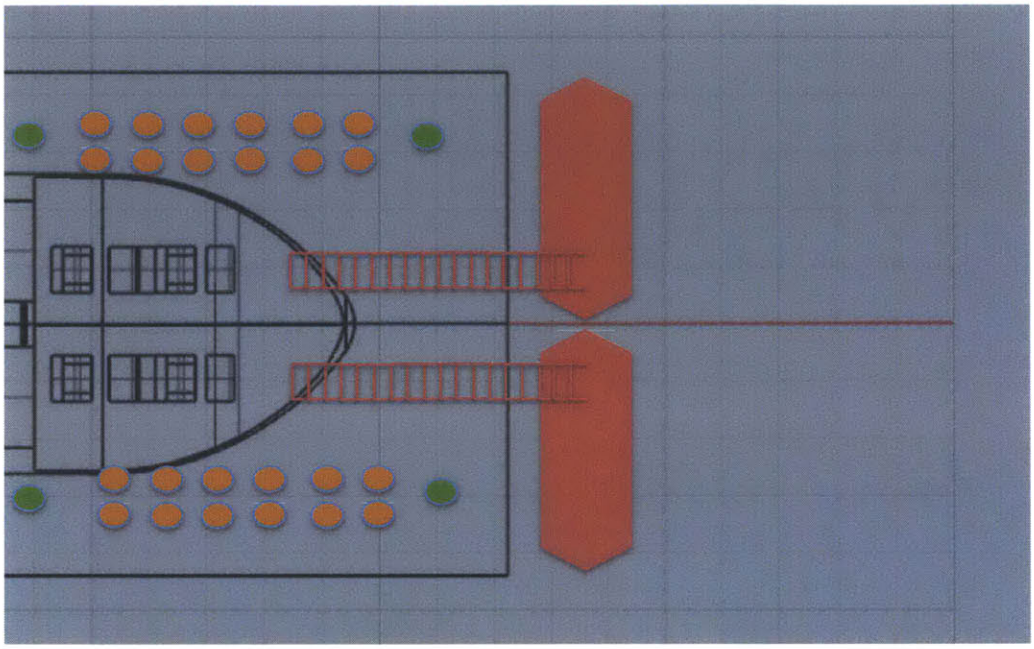

Figure 32: Evacuation plan step 5

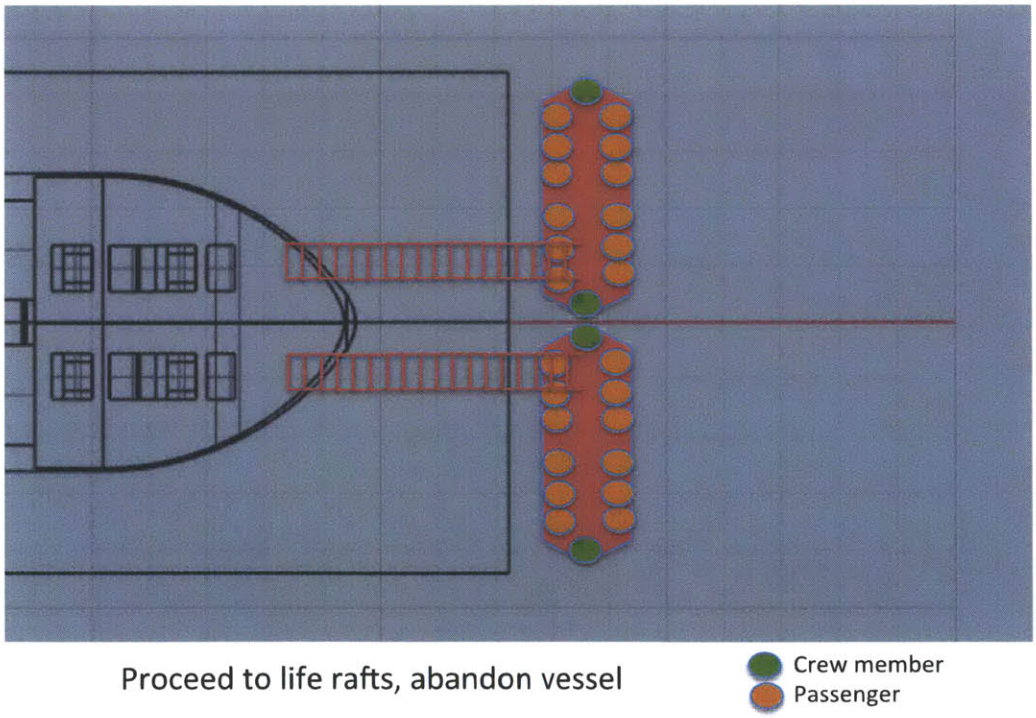

Figure 33: Evacuation plan step 6

3 Hydrofoil Design

The general design of the vessel is followed by the hydrofoil design, presented in this section. Foil type, profile and positioning are adopted from Brizzolara' s design (Brizzolara, 2010). Model experimental measurements are used to predict hydrofoil forces. Equilibrium condition at maximum speed reveals that the front foils need to be larger than the aft (see section 3.2.3 for exact dimensions), to counteract the 'bow-down' tendency of this vessel. This tendency is due to the high position of the turbo fans.

3.1 Foil type, configuration and profile selection

Surface piercing hydrofoils with negative dihedral angle were selected because they provide an inherent stability to the vessel, not requiring the use of control mechanisms, which is desired in this design. These features are adopted from the original design that the vessel is based upon (Brizzolara, 2010, pp. 43-57), as is the configuration of the foils. Thus, this vessel features four surface piercing, super-cavitating hydrofoils with a negative dihedral angle, positioned as shown in section 2.5.

The hydrofoil profile is adopted from S. Brizzolara's (Brizzolara, 2013). This particular version manages to retain steady ventilation under unsteady flow conditions. This can be seen in Figure 34, where the 2D section of the hydrofoil has been simulated in unsteady turbulent flow conditions. The blue area represents the ventilated part and the red area represents the non ventilated part of the fluid. The wedge on the lower surface of the foil serves to trigger cavitation on the back part, allowing the forward part to remain non cavitated. It is this exact capability of the hydrofoil that provides a solid basis for lift and drag prediction under unsteady conditions.

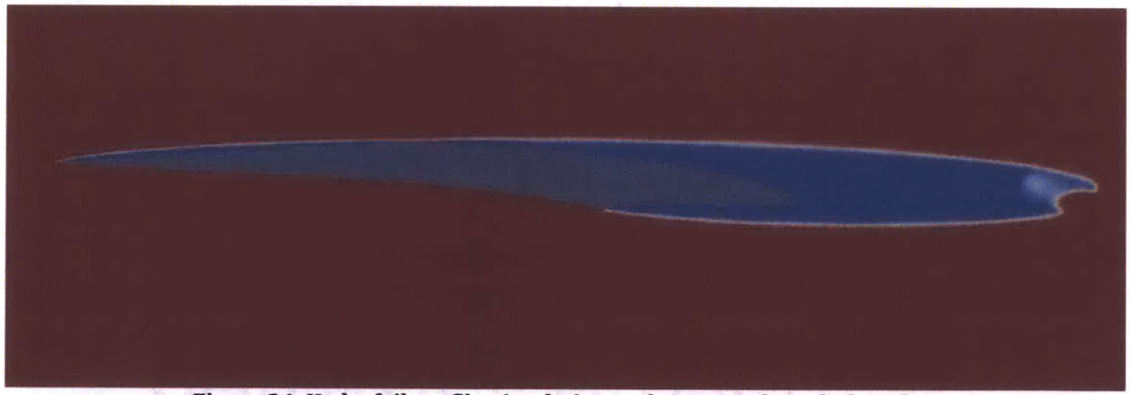

Figure 34: Hydrofoil profile-simulation under unsteady turbulent flow

Foil forces calculations are based on model experimental measurements, provided by Hochbaum & Eckl (Hochbaum & Eckl, 2012). The model has geometric similitude to the vessel's tapered part of the hydrofoils (model to actual foil ratio=1:9). The experimental foil is shown in Figure 35. It is a tapered and slightly swept profile (Hoerner & Borst, 1975, pp. 15-1). The lift-to-drag ratio achieved with this design

around super-cavitating speed is approximately 5-to-1. The model hydrofoil can be seen mounted in the cavitation tunnel in the figure below (right photo). Figure 36 shows a photo capture during the experiments. In this figure, the fully ventilated side is seen, which is the upper surface of the 2D foil of Figure 34.

Figure 35: Hydrofoil model used in experiments

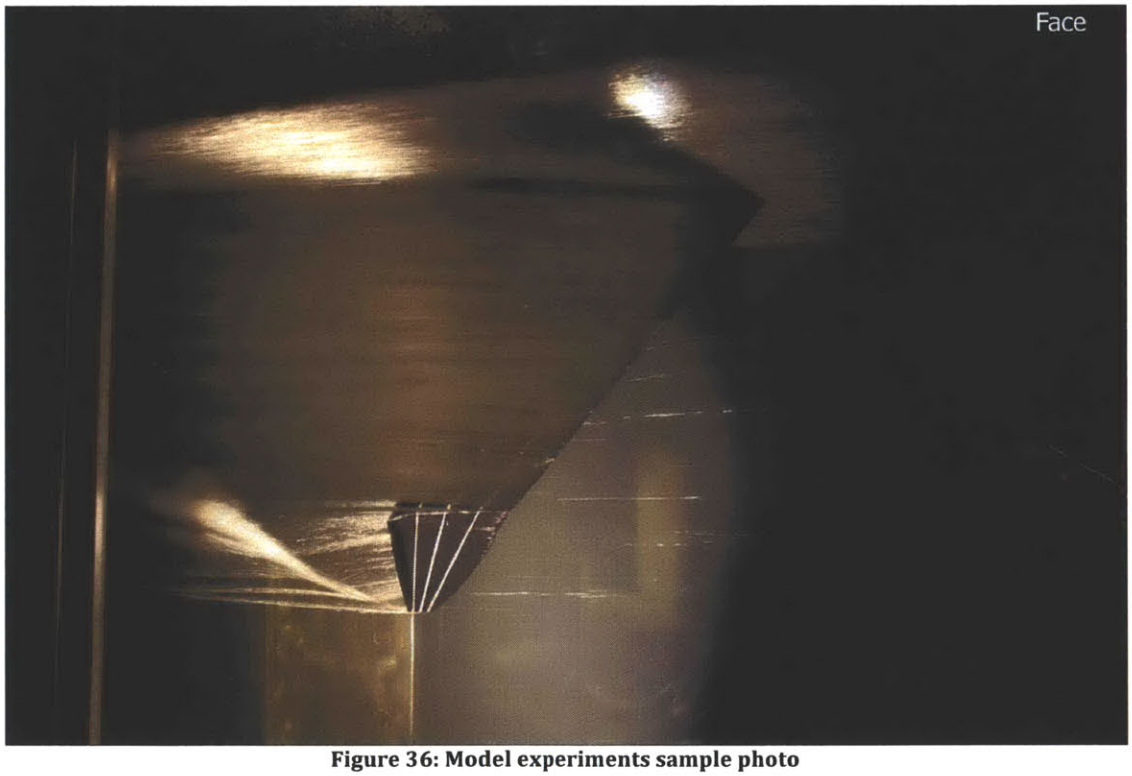

Figure 36: Model experiments sample photo

3.2 Hydrofoil sizing

The criteria for determining foil sizing were:

- Equilibrium and zero trim at maximum speed
- Sufficient clearance from SWATH hulls to avoid frequent slamming
- Folding mechanism size limitation

3.2.1 Equilibrium and zero trim at maximum speed

The three equations of equilibrium in the vertical plane (longitudinal) are:

$$\sum (F_i)_x = 0 \quad (1)$$

$$\sum (F_i)_z = 0 \quad (2)$$

$$\sum M_i = 0 \quad (3)$$

The forces, reference point for moments and the sign convention are seen in Figure 37. Equilibrium in the y direction is guaranteed by the fact that the vessel is symmetrical with respect to the vertical plane, so it is not examined.

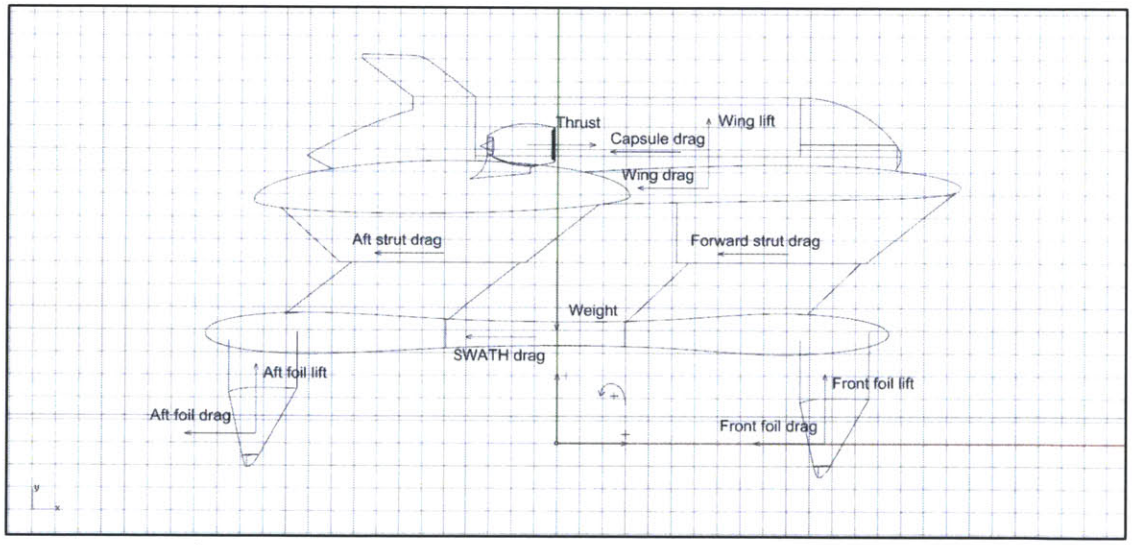

Figure 37: Forces 2-D drawing with reference point and sign convention

Five forces are unknown: front foils lift, aft foils lift, front foils drag, aft foils drag and thrust. Foil drag and lift are both dependent on submerged foil length and angle of attack through the experimental foil formulas (see appendix). Note that all assumptions that are made for the dynamic behavior analysis in section 4.2.1 are also made here.

Then

$$Lift = f(T, a)$$
$$Drag = f(T, a)$$

where

T: submerged foil length
a: angle of attack

However, the submerged foil length and angle of attack can be different for the front and aft foils. With that in mind the five unknowns of the equilibrium equations become:

1. Front foil submerged length
2. Aft foil submerged length
3. Front foil design angle of attack
4. Aft foil design angle of attack
5. Thrust

To obtain a unique solution to the system, two of the unknowns need to be defined prior to solving the equations. This is a design decision. Any two of these five factors can be defined to give a different unique solution to the system. It was decided to define the design angles of attack to be zero at equilibrium, at maximum speed. Zero angle of attack in this context means that the design angle of attack of the model hydrofoils is adopted, without change.

The choice of keeping the design angle of attack of the hydrofoils is made in order to avoid:

- extrapolating (predicting outside the bounds) of experimental data.
- large curvatures and values found in the force coefficients near large positive angles of attack.
- unstable ventilation phenomena at large negative angles of attack.

Thus the angles have been defined and a solution to the system can be obtained. The system has been solved using Matlab® environment, with all the relevant forces and moments being applied to the vessel. The unique* solution to the equilibrium equations has been found:

1. Front foil submerged length=3460.6 mm
2. Aft foil submerged length=2777.8 mm
3. Thrust=483.43 KN

We notice that the required submerged length of the front foils is larger than that of the aft foils by approximately 25%. This is due to the placement of the propulsion system high in the deck (shown in the 2D force sketch). The moment that the thrust force generates results in a tendency of the vessel to go 'bow down', and to counteract this tendency a great moment is required by the front foils. A similar phenomenon occurs in hydrofoil sailing race vessels that have similar hydrofoil configurations, where the propulsion force generated by the sails is much higher

* Because the experimental equations used to define foil lift and drag forces are non linear, many other solutions of the system exist. The one that has the minimum positive values for the three parameters has been selected, which is also the only solution that is physically feasible.

than the center of gravity. To counteract this moment in hydrofoil sailing vessels, the front hydrofoils are also made larger than the aft.

Figure 38 shows the moment distribution, at maximum speed in equilibrium condition with percentages. The weight lift distribution is shown in Figure 39. Indeed, it is noticed that the front foils are required to make a greater moment contribution, and as a result make a greater lift contribution as well.

In conclusion, applying equilibrium conditions at maximum speed for zero trim gives an indication of the foil size difference that is required. Specifically this difference is 682.8 mm, or approximately 700 mm.

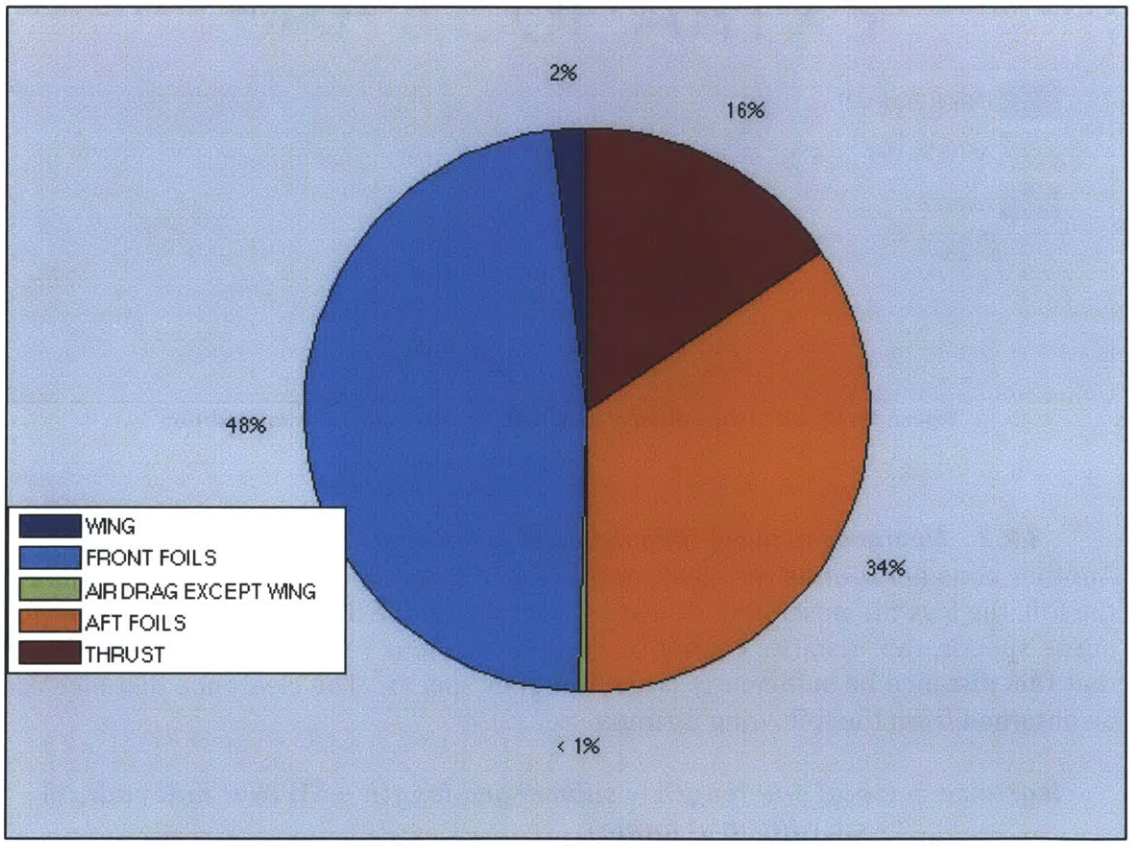

Figure 38: Moment distribution at maximum speed in equilibrium condition

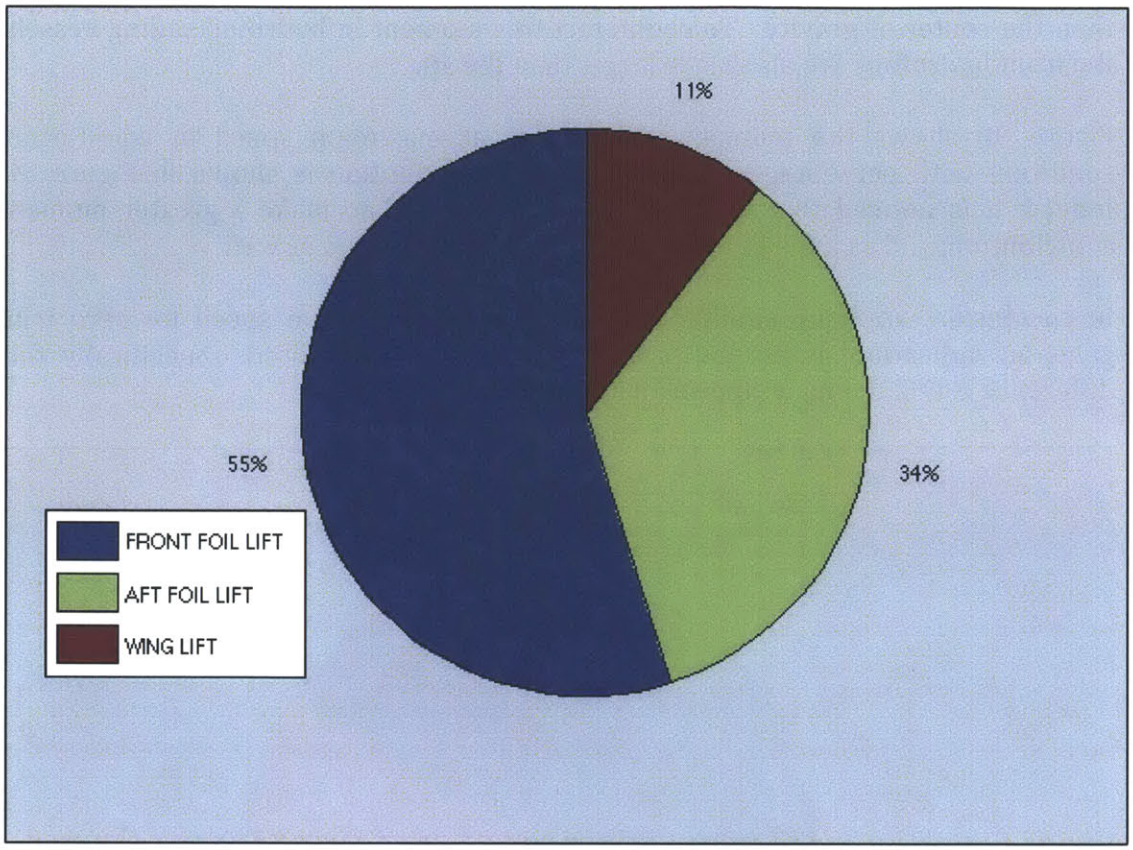

Figure 39: Weight distribution at maximum speed in equilibrium condition

3.2.2 Clearance to avoid slamming and foil folding mechanism limitations

Another consideration is the clearance distance from the SWATH hulls. The larger the foil, the less the possibility of water slamming to the SWATH hulls. At lower foil borne speeds, this distance cannot be large for obvious reasons. But it is important that this distance be sufficiently large at higher speeds. The clearance distance can be obtained from the following formula

$$clearance = (total\ foil\ length - submerged\ length - SWATH\ hull\ radius) * \sin(dihedral\ angle)$$

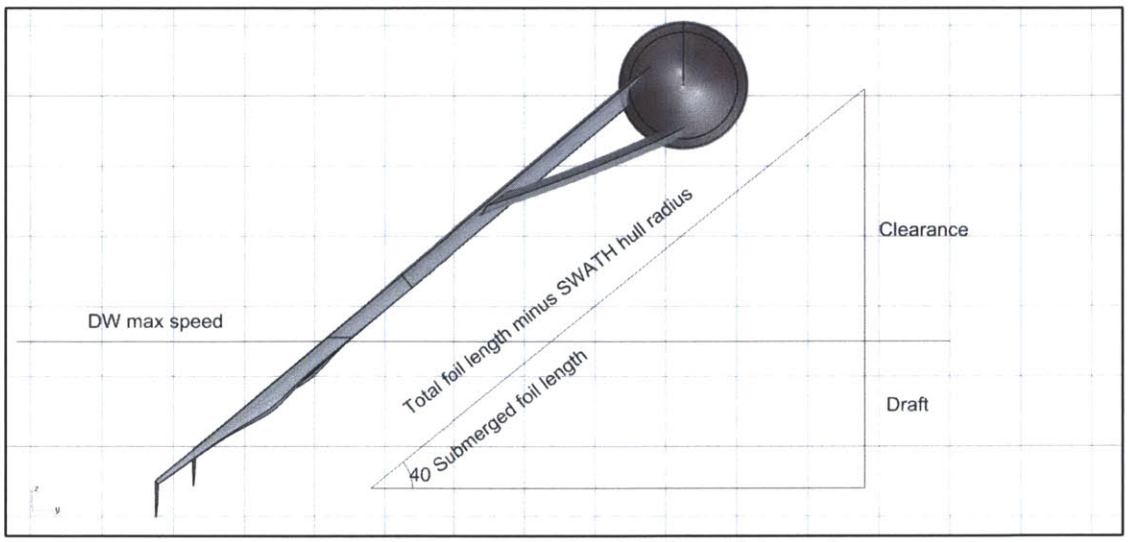

Figure 40: Clearance from SWATH hulls at high speeds

The upper threshold for the vessel's operational sea state, which has a significant wave height of 2.5 m, dictates the minimum acceptable total foil length for the vessel at the specified speed. With a wave height of 2.5 m and an allowance (+10%), a required clearance of 2.75 m (or ~2.8 m) is found. Using the required submergences at maximum speed from section 3.2.1, the minimum required total foil lengths can be found from the clearance formula above.

$$total\ foil\ length = \left(submerged\ length + SWATH\ hull\ radius + \frac{clearance}{\sin\left(dihedral\ angle\right)}\right)$$

The required front foil length for a clearance of 2.8 m is ~8.7 m for the front foil and ~8 m for the aft foils. At lower speeds clearance decreases and this increases slamming probability. This may impose an operational safety envelope for the vessel, and needs to be studied further at later stages of the design.

Another design constraint is dictated by the foil folding mechanism's longitudinal length limitation. This constraint limits the maximum foil span. The folding mechanism cannot be longer than 3 m, therefore the foil span cannot be longer than 3 m. This is why part of the foils are parallel and part of them are tapered.

3.2.3 Sizing conclusions

The decided sizing of the foils is shown in Figure 41. Each foil consists of two parts, the tapered and the parallel part. The tapered part is sized the same for the front

and aft foils, constrained by the folding mechanism length limit. The front foils are longer, to achieve zero trim at maximum speed.

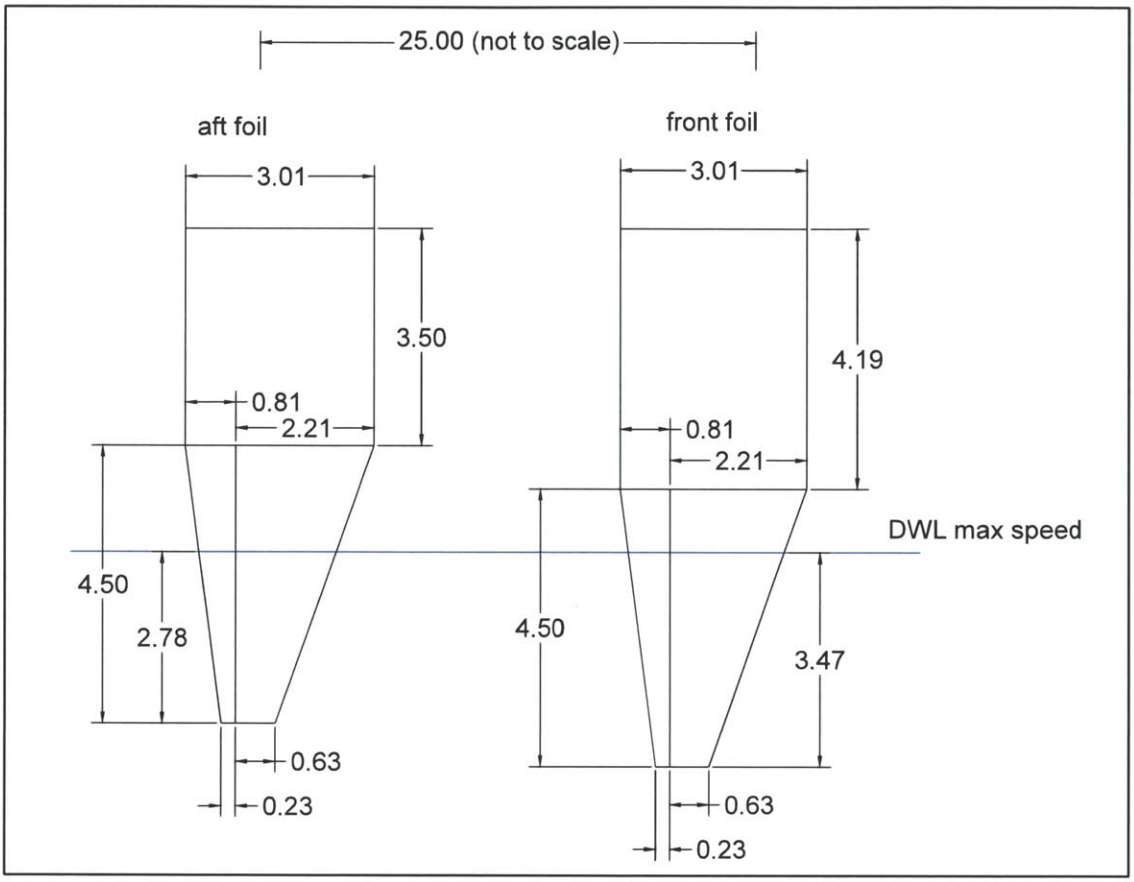

Figure 41: Foil sizing (all distances in m)

3.2.4 Consideration of trim at lower foil borne super-cavitating speeds

The vessel has been designed to have zero trim at maximum speed. With the chosen foil sizing, trim at lower speeds has also been examined and is presented in this section. The results indicate that at lower super-cavitating speeds, the vessel slightly trims forward (bow down). To adjust trim between various speeds, the dihedral angle of the front or aft foils can be changed. To adjust trim between different loading conditions, for example between full load and minimum operating condition, ballast tanks can be used. As previously mentioned, ballast tanks are located in the lower struts.

It is recognized that when the vessel trims, the angle of attack changes. Due to this, the lift/drag forces will change, and the equilibrium will be achieved at new submerged lengths. The static and dynamic simulations cover these effects in more detail, in the feasibility analysis (chapter 4). Nevertheless, Table 8 gives an understanding of the expected trim at lower super-cavitating speeds.

Table 8: Trims at lower super-cavitating speeds

Speed [knots]	Speed [m/s]	Front foil submerged length [mm]	Aft foil submerged length [mm]	Thrust [KN]	Trim [degrees]
85	43.73	3460.6	2777.8	483.43	0
80	41.15	3668.6	2971.7	475	-0.03
75	38.6	3888.4	3182.6	463.4	-0.05
70	36	4128.9	3420	447.7	-0.06
65	33.4	4388.8	3682.8	427.9	-0.05
60	30.9	4660.2	3963.3	404.5	-0.03

For non super-cavitating speeds, different formulas have to be used. This requires a separate analysis, which has not been performed in this study.

3.3 Hydrofoil preliminary strength analysis

The pie charts presented in section 3.2.1 indicate that, of all components of the vessel, the hydrofoils are subjected to the largest loading. A preliminary strength assessment of the hydrofoils has been performed and is presented in this section. The foil is treated as a fixed cantilever beam and its maximum stress (located at the root of foil) can be calculated from the formula:

$$\sigma_{max} = \frac{M_{max}}{I} * d_{max} + \frac{F_{ver}}{A}$$

$$M_{max} = F_{hor} * l$$

I: *area moment of inertia of the hydrofoil section at the root*
d_{max}: *maximum distance from neutral axis (line where total stress is zero)*
A: *area of the hydrofoil section at the root*
F_{ver}: *the component of the total force that is vertical to the section of the foil*
F_{hor}: *the component of the total force that is horizontal to the section of the foil*
l: *distance of force application center from the root section of the hydrofoil*

The maximum stresses for the aft and front hydrofoils is 1500 kg/cm^2 and 2334 kg/cm^2 respectively. With a safety factor of 3 these stresses become 4500 and 7002.

The materials considered for the hydrofoils are shown in Table 9. The most appropriate material for the hydrofoils is high tensile steel HY130.

Table 9: Materials considered for hydrofoils

Material	Yield stress [kg/cm^2]
CuNiAl	2500
Stainless Steel	2957
High Tensile Steel	9147
Pre-preg	13766
Aluminium Alloy Ergal 7075	4691

3.3.1 Other strength considerations

Dynamic behavior analysis (section 4.2.6) reveals that the loads imposed on the hydrofoils by incoming waves are cyclical with a high encounter frequency. This frequent periodic loading is very likely to lead to fatigue issues. In addition, due to the slender geometry of the foils, deformation under load requires a more in depth analysis. These issues hint that structural support of the hydrofoils will be a necessity for this vessel.

Research on this topic is a current work in progress. Two different options are being considered for adding structural support to the hydrofoils. The first is a strut, similar to what is shown in Figure 40. The second is the possibility of redesigning the upper portion of the parallel part of the hydrofoils, in order to make it have a larger sectional area and potentially a non cavitating foil profile. This portion of the hydrofoil only enters the water in low foil borne speeds, which are non cavitating speeds. Thus, it may be beneficial to design this portion to be more efficient in these speeds, and provide structural support to the whole hydrofoil at the same time. The aforementioned are being studied as part of a follow-up project that sprang from this preliminary design.

4 Feasibility assessment

This section describes the feasibility analysis phase of the thesis, which focuses on examining static stability and dynamic behavior of the vessel, in foil borne mode. To assess static stability, an 'inclining experiment' simulation has been performed and the righting moment graph is obtained. To assess dynamic stability, the ordinary differential equations of heave and pitch are defined and solved for different cases of external disturbances. Both the results from static stability and dynamic behavior indicate that the vessel is inherently stable and seaworthy. However, the high frequency of heave and pitch response motions may be an issue for crew/passengers, and requires further investigation. The seakeeping analysis of this study is limited to motion responses to head waves. Motion responses due to other external force sources should be studied in future work, such as high speed turning, various maneuvers and waves of incident angle other than the one of head waves.

4.1 Static stability

Longitudinal stability is of greater concern than transverse stability for this vessel. Transverse stability is more or less guaranteed from the large lateral distance of the surface piercing hydrofoils. Longitudinal stability is not as apparent and thus is a priority in this preliminary design study.

Positive static stability means that in a given pitch position, the reaction moment must tend to return the vessel to its upright position. A program has been developed in Matlab® environment simulating an 'inclining experiment' in the longitudinal/vertical plane. The output of the program is the righting arm moment generated at various consecutive pitch positions.

During a typical inclining experiment, weights are shifted inside the vessel. The result is a slow rotation and a heave position change. The latter occurs because vertical force equilibrium has to be satisfied. Assuming that a rotating mechanism is fixed at the rotation reference point of the vessel, the moment applied by this mechanism to pitch the vessel to a given position is the same as the static reaction moment that the vessel has at this position in the absence of the rotating mechanism.

When the vessel changes pitch position, several forces change direction (Figure 42), causing their moment with respect to the reference point to change. This effect has been considered in the calculation of the righting arm moment graphs (section 6.5).

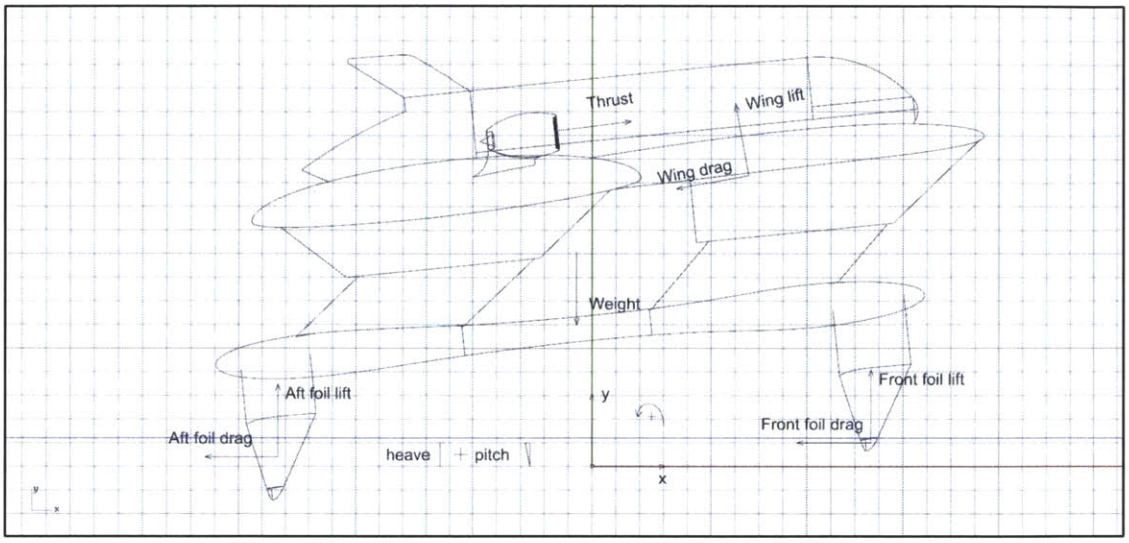

Figure 42: Inclining experiment simulation free body diagram

The simulation has been conducted at maximum speed (85 knots), foil borne mode. The resulting righting moment graph is seen in Figure 43. The moment is seen to be zero when pitch is zero, confirming that at zero pitch equilibrium occurs. This is a good validation that the program works properly, at least in the zero pitch condition. It can be seen that a negative reactive moment is produced in a positive pitch position. This indicates that the vessel has positive static stability. In later stages of the design (future work), this program can be adjusted to generate the high speed turning and wind righting moment curves.

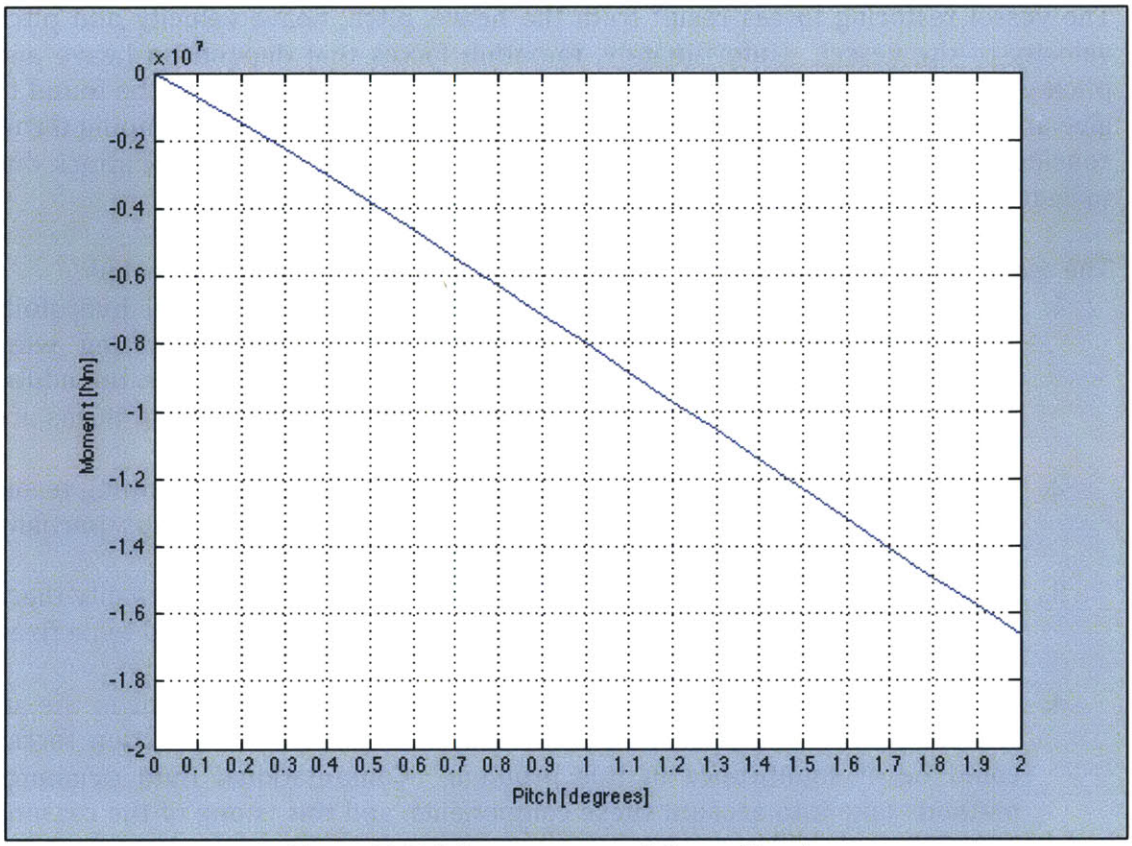

Figure 43: Righting moment graph for small angles

4.2 Dynamic behavior

To assess the vessel's dynamic behavior in the vertical plane, the differential equations of heave and pitch should be defined and solved. The approach and findings are presented in this section.

4.2.1 Methods and assumptions

In general, the dynamic responses of a vessel are an unsteady phenomenon, meaning that the parameters describing the phenomenon change with time, continuously. The simulations have been performed using a quasi-steady approach. This approach simplifies the study of an unsteady phenomenon by assuming that for discretized spans of time the phenomenon remains steady. The parameters change from one time span to the next, simulating the unsteadiness.

The seakeeping problem is simplified by superposing the wave exciting and the vessel restoring forces. To estimate the first, the vessel is assumed to be still in terms of heave and pitch, while the incoming waves imposed forces on the vessel. The exciting forces are a result of the wave imposing a different submerged length and angle of attack to the foils, while the vessel is traveling at maximum speed. To estimate vessel restoring forces the sea is assumed calm, and the vessel moving.

The vessel restoring forces result from the heave, pitch, heave velocity and pitch velocity of the vessel. Unfortunately, radiation forces that depend on heave and pitch velocities (damping forces) were not known, and no source could be found to give an estimation of them for super-cavitating hydrofoils. The only damping terms considered were the ones resulting from the imposed change in angle of attack due to heave velocity and pitch velocity, which are in fact highly dissipative.

The assumptions made to derive the equations of motion are described below.

1. Heave added mass and pitch added mass moment of inertia of the hydrofoils are approximated using empirical formulas for a non-cavitating wing accelerating in a fluid (Appendix section 6.4). All other terms in the added mass matrix are assumed zero. In addition added mass damping terms are neglected.
2. Free surfaces effects on added mass inertia and added mass damping terms are neglected for simplicity. In reality fully submerged versus partially submerged foils will have a difference in these terms.
3. Surge motion is considered uncoupled from heave and pitch. In reality there may be coupling involved with surge as well. Speed is considered to be fixed at 85 knots.
4. Foil interaction forces are neglected. The downwash of the front to the aft foil are ignored. However, the unsteady nature of foil interaction forces could be of significance in this problem. Computational fluid dynamics methods take into account these components, and this is one of the reasons why CFD analysis is one of the recommendations for future work.
5. The effect of the history of the motions is neglected, otherwise named memory effects. While memory effects are not a major concern in sub-cavitating bodies, they can be important for super-cavitating bodies, because the shape and extent of the cavity depends on the history of motion (Uhlman, Fine, & Kring, 2001, p. 1). Neglecting this effect is partially justified by the fact that the selected hydrofoil profile solves the unsteady ventilation problem that troubles many super-cavitating hydrofoil designs (Brizzolara, 2013).
6. Some nonlinear wave force effects are neglected in the calculation of the external forces. Specifically the vessel is considered fixed as the wave progressed, thus the submerged foil geometry below the wave contour only depends of the wave profile. In reality, as the vessel performs heave and pitch motions, the external forces change not only due to the wave profile, but also due to the change in the submerged part of the foil below the wave contour.
7. The only damping terms included are the ones caused by the change in the flow angle of attack to the foils due to heave and pitch velocity. As previously mentioned, other damping terms could not be determined for super-cavitating hydrofoils.
8. Wave exciting Froude-Krylov forces and diffraction forces are assumed negligible, due to the small volume of the hydrofoils.

The system of differential equations are solved with numerical methods, which is described in more detail in the Appendix section 6.6.

4.2.2 Equations of motions

The generic equations of motion are derived from Newton's second law.

$$(M_{33} + A_{33}) * \ddot{\eta}_3 + \sum F_{3res}(\eta_3, \eta_5, \dot{\eta}_3, \dot{\eta}_5) = \sum F_{3ex}(t) \quad \text{Heave equation}$$
$$(I_{55} + A_{55}) * \ddot{\eta}_5 + \sum F_{5res}(\eta_3, \eta_5, \dot{\eta}_3, \dot{\eta}_5) = \sum F_{5ex}(t) \quad \text{Pitch equation}$$

M_{33}: *vessel weight* $[kg]$
I_{55}: *vessel pitch mass moment of inetria* $[kg * m^2]$
A_{33}: *vessel heave added mass* $[kg]$
A_{55}: *vessel pitch added mass moment of inetria* $[kg * m^2]$
$\ddot{\eta}_3$: *heave acceleration* $[\frac{m}{s^2}]$
$\ddot{\eta}_5$: *pitch acceleration* $[\frac{rad}{s^2}]$
$\dot{\eta}_3$: *heave velocity* $[\frac{m}{s}]$
$\dot{\eta}_5$: *pitch velocity* $[\frac{rad}{s}]$
η_3: *heave position* $[m]$
η_5: *pitch position* $[rad]$
$\sum F_{3ext}$: *sum of all external forces* $[N]$
$\sum F_{5ext}$: *sum of all external moments* $[N * m]$
$\sum F_{3rad}$: *sum of all restoring forces* $[N]$
$\sum F_{5rad}$: *sum of all restoring moments* $[N * m]$

4.2.3 Inertia terms

The inertia terms can be calculated from the weight and the weight distribution of the vessel. The resulting mass and mass moment of inertia are:
$M_{33} = 2.5452 * 10^5 \ kg$
$I_{55} = 423.045 * 10^5 \ kg * m^2$

The added mass and added mass moment of inertia calculations are shown in the Appendix section 6.4. The results are:
$A_{33} = 8.3 * 10^3 \ kg$
$A_{55} = 207.74 * 10^4 \ kg * m^2$

The added mass components have been calculated for a sub-cavitating foil, because only formulas for sub-cavitating speeds could be found. It is noticed that the added mass components are only a small portion of the vessel's total inertia. Specifically:

$$\frac{A_{33}}{M_{33}} = 3.3\ \%$$

$$\frac{A_{55}}{I_{55}} = 4.9\ \%$$

Based on the above percentages, the added mass and added mass moment of inertia terms are not expected to play a significant role in determining the vessel's motion responses.

4.2.4 Restoring forces

Restoring forces can be found by assuming a random heave and pitch position and calculating the total force and moment at this position as a function of heave and pitch. The general process followed for conducting this is explained in more detail in the Appendix, section 6.5. This section focuses on describing how the hydrofoil forces change with heave and pitch position. Note that the reference coordinate system has been assumed to move in the longitudinal direction with the vessel, but not in the vertical and pitch direction. This can be noticed in Figure 42, where even though the vessel has heaved and pitched, the coordinate system has not. Restoring forces include damping terms, due to the change in angle of attack due to heave and pitch velocity. This change can be seen in the equations below, which show the submerged length and pitch-equivalent angle of attack due to a random heave and pitch position and velocity.

$$T_f = T_{f0} - \frac{\eta_3}{\sin(40)} - \frac{LBF}{2} * \frac{\tan(\eta_5)}{\sin(40)}, \qquad for\ small\ angles\ \tan(\eta_5) \cong \eta_5$$

$$T_a = T_{a0} - \frac{\eta_3}{\sin(40)} + \frac{LBF}{2} * \frac{\tan(\eta_5)}{\sin(40)}$$

$$p_f = p_{f0} + \eta_5 + tan^{-1}\left(\frac{\dot{\eta}_3 + \dot{\eta}_5 * \frac{LBF}{2} * \cos(\eta_5)}{V_{ship}}\right)$$

$$p_a = p_{a0} + \eta_5 + tan^{-1}\left(\frac{\dot{\eta}_3 - \dot{\eta}_5 * \frac{LBF}{2} * \cos(\eta_5)}{V_{ship}}\right)$$

T_{f0}: *front foil submerged length in equilibrium condition* [m]
T_{a0}: *aft foil submerged length in equilibrium condition* [m]
T_f: *front foil instant submerged length* [m]
T_a: *aft foil instant submerged length* [m]
p_{f0}: *front foil pitch – equivalent angle of attack in equilibrium condition* [rad]
p_{a0}: *aft foil spitch – equivalent angle of attack in equilibrium condition* [rad]

p_f: *front foil instant pitch – equivalent angle of attack* [*rad*]
p_a: *aft foil instant pitch – equivalent angle of attack* [*rad*]
LBF: *length between foils* [*m*]

The pitch-equivalent angle of attack is related to the angle of attack through the following geometric relationship.

$$p = a/\sin(dihedral\ angle)$$

p: *pitch – equivalent angle of attack*
a: *hydrofoil angle of attack*

Notice that the foil lift and drag in Figure 42 do not change direction. This is due to the fact that the experimental formulas already consider angle of attack influence in lift and drag, both in coefficient and due to direction change of the vectors. The resulting lift and drag of the experimental formulas give the lift and drag always facing these directions. However, the magnitude of the vectors changes with these formulas, and this is what creates a change in the vertical force and moment they impose. In the formulas below, the force and moment change due to lift and drag are shown. Lift and drag coefficients are functions of submerged length and pitch-equivalent angle of attack, and submerged areas are functions of submerged length.

$$F_{foils} = 2 * q * \left([CF_{zf} * A_f - CF_{zf0} * A_{f0}] + [CF_{za} * A_a - CF_{za0} * A_{a0}]\right)$$
$$M_{foils} = 2 * q * (\frac{LBF}{2}) * \left([CF_{zf} * A_f - CF_{zf0} * A_{f0}] - [CF_{za} * A_a - CF_{za0} * A_{a0}]\right)$$

F_{foils}: *hydrofoil force change due to a random heave and pitch position* [*N*]
M_{foils}: *hydrofoil moment change due to a random heave and pitch position* [*Nm*]
$CF_{zf} = f(T_f, p_f)$, *lift force coefficient front foil*
$CF_{za} = f(T_a, p_a)$, *lift force coefficient aft foil*
$A_f = f(T_f)$, *submerged area front foil* [m^2]
$A_a = f(T_a)$, *submerged area aft foil* [m^2]
$CF_{zf0} = f(T_{f0}, p_{f0})$, *lift force coefficient front foil in equilibrium condition*
$CF_{za0} = f(T_{a0}, p_{a0})$, *lift force coefficient aft foil in equilibrium condition*
$A_{f0} = f(T_{f0})$, *submerged area front foil in equilibrium condition* [m^2]
$A_{a0} = f(T_{a0})$, *submerged area aft foil in equilibrium condition* [m^2]
$q = \frac{1}{2} * \rho * Vship^2$, *coefficient* [$kg/(m^2 * s)$]
ρ: *water density* $\left[\frac{kg}{m^3}\right]$
Vship: *vessel speed* $[\frac{m}{s}]$

The final formulas of heave restoring force and pitch restoring moment are not presented here, because each is approximately 4 pages long. The formulas are highly non linear and both contain all terms of pitch, heave, pitch velocity and heave velocity.

4.2.5 External forces

External forces are caused by the environment of the vessel. Sinusoidal external forces are examined in this study, resulting from head waves. The wave height in both cases is taken as 0.5 m, which corresponds to the lower limit of sea state 3 per NATO standards (Figure 51). Two different cases of wave length are examined, which represent the worst potential situations.

The first is for a wave length of twice the length between front and aft hydrofoils (LBF). The second is for a wave length equal to the length between front and aft hydrofoils (LBF). These two cases are shown in the two figures below, where sketches of the vessel encountering the waves have been made. It is obvious that the first wave length is expected to generate the largest possible moment, while the second to generate the largest possible heave force.

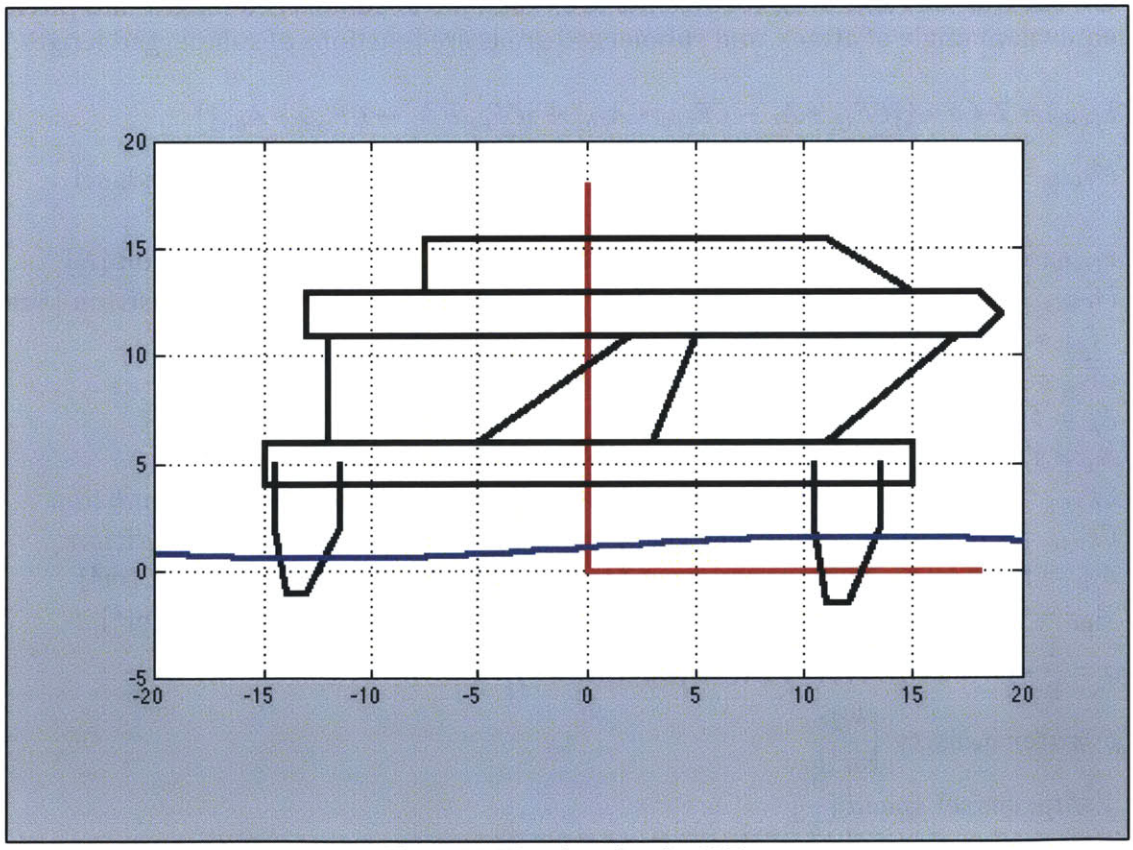

Figure 44: Wave length twice LBF

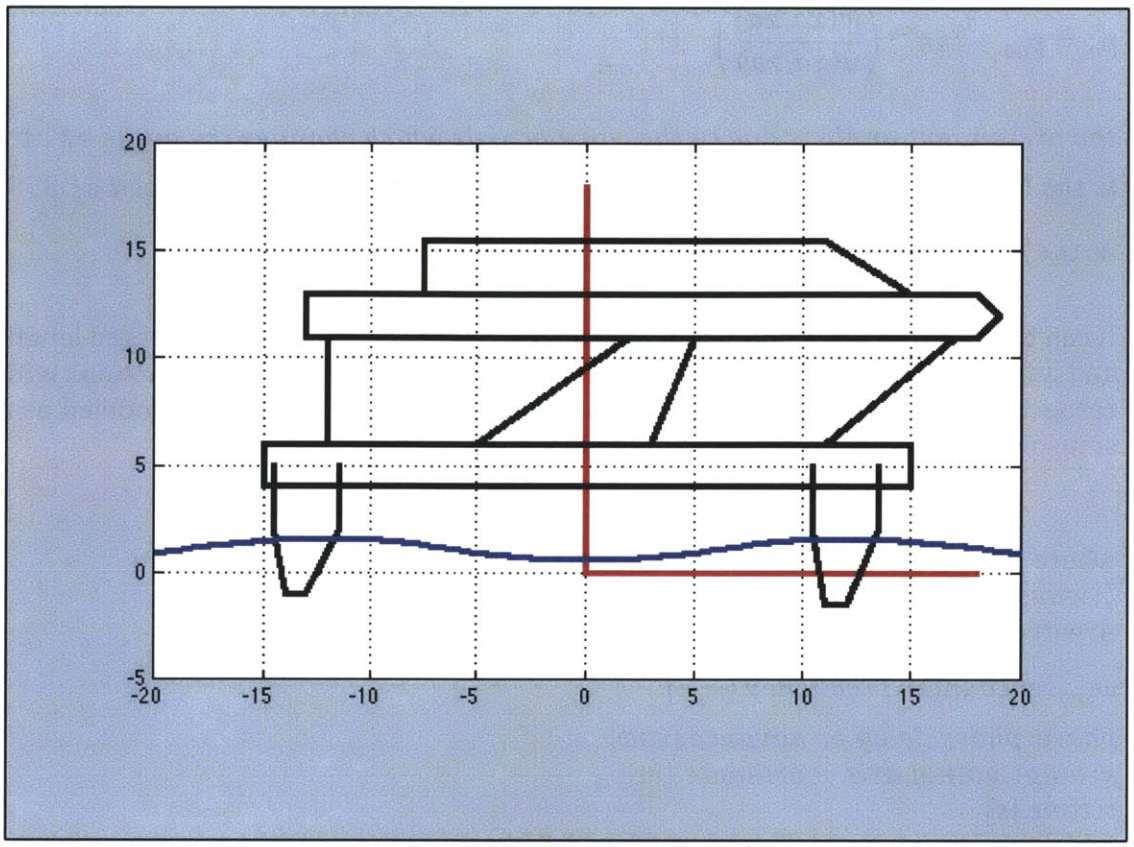

Figure 45: Wave length equals LBF

As mentioned in the assumptions (section 4.2.1), external forces resulting from the Froude-Krylov wave incident force and diffraction forces are considered negligible. Thus, the only forces significant to consider are the forces resulting by the imposed change in submerged length and angle of attack, by the wave to the hydrofoils.

Submerged length and angle of attack are calculated as follows. Note that the vessel is kept still in heave and pitch motion to calculate the wave excitation forces. The sine 40 degrees is added because of the dihedral angle of the foil.

$$T_f = T_{f0} + \frac{zeta\ (xf)}{\sin\ (40)}$$

$$T_\alpha = T_{\alpha 0} + \frac{zeta\ (xa)}{\sin\ (40)}$$

$zeta\ (xf)$: *wave elevation at front foil*
$zeta\ (xa)$: *wave elevation at aft foil*

$$p_f = p_{f0} + tan^{-1}\left(\frac{w(xf, zf)}{u(xf, zf)}\right)$$

$$p_a = p_{a0} + tan^{-1}\left(\frac{w(xa, za)}{u(xa, za)}\right)$$

the arctangent angle is due to the wave profile which changes the angle of attack
u: *the horizontal flow velocity* $[\frac{m}{s}]$ (*includes the vessel's forward speed of* 85 *knots*)
w: *the vertical flow velocity* $[\frac{m}{s}]$

It can be seen that force and moment changes, due to the imposed submerged length and angle of attack by the wave, can be represented using sinusoidal functions with respect to time. This is due to the fact that incoming wave has been modeled as a sinusoid. The elevation equation of the incoming head wave is

$$\zeta = Re\{A * e^{(i*(k*x+\omega_{enc}*t+phase))}\}$$

where
ζ: *wave elevation* $[m]$
A: *wave height* $[m]$
ω_{enc}: *encounter frequency* $[\frac{rad}{s}]$
phase: *phase delay or advance* $[rad]$
x: *longitudinal axis coordinate* $[m]$
t: *time* $[s]$

The derived wave exciting forces for the two cases are seen below.

Case 1: $\lambda = 2 * LBF,\ A = 0.5\ m$

$$F_3 = 3.3240 * 10^5 * \sin(6.7114 * t)$$
$$F_5 = 1.9920 * 10^7 * \sin(6.7114 * t)$$

Case 2: $\lambda = LBF,\ A = 0.5\ m$

$$F_3 = 1.7432 * 10^6 * \sin(12.7668 * t)$$
$$F_5 = 4.5931 * 10^6 * \sin(12.7668 * t)$$

The exciting wave forces for the two cases can be seen in the graph below. It is noticed that the total moment magnitude in the first case is almost four times as large than the magnitude in the second case, which is due to the front foil forces being 180^0 out of phase with the aft foil forces. On the contrary, the total force magnitude is much larger in the second case, because these forces are in phase. These differences hint that in the first case pitch motion responses may be of concern since they will be the largest encountered for the given wave height. In the second case, heave motions may be of concern since they will be encountered for the given wave height. The derived motion responses are seen in the next section.

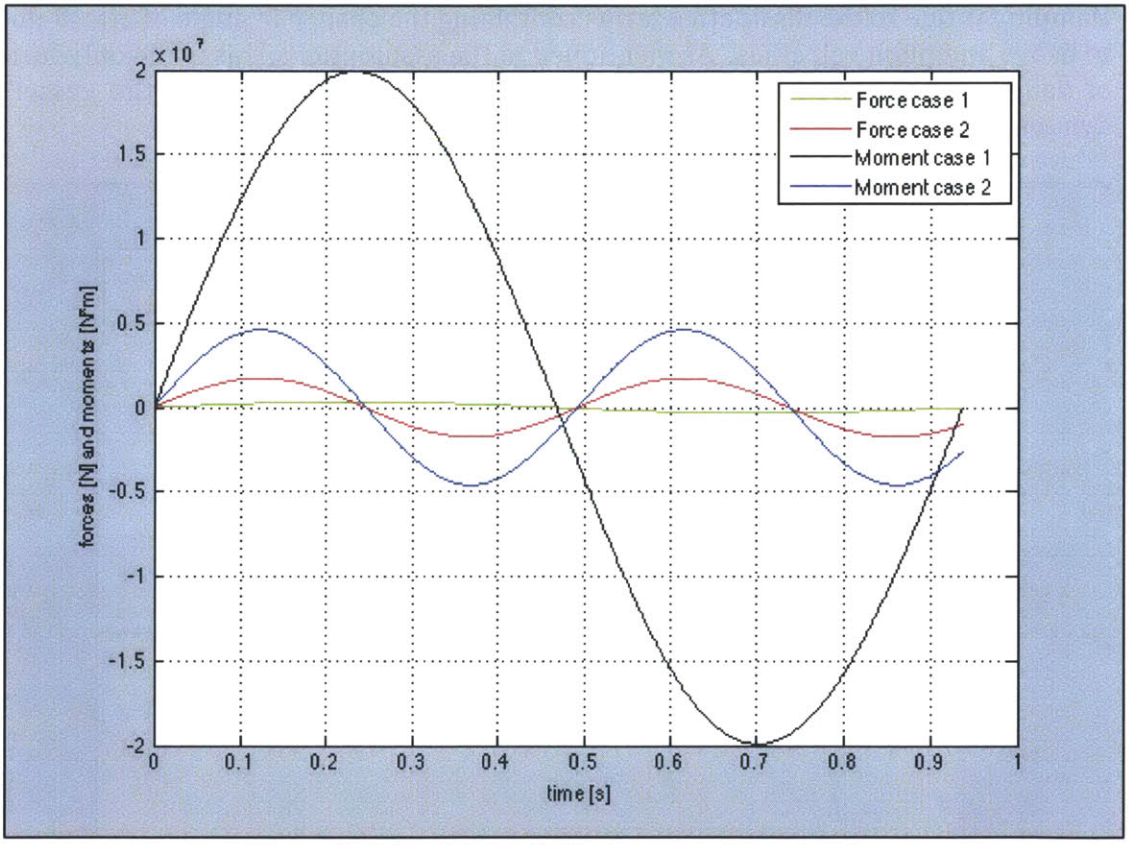

Figure 46: External forces for the two cases of wave length

4.2.6 Simulation results

Before imposing external forces to the system, a simulation has been performed with no external forces, but with initial conditions. This simulation serves to validate the results of the static stability analysis (4.1), as well as to observe the natural frequency of the system. The simulation has been performed at maximum speed (85 knots).

The initial conditions are a heave of 0.5 m and a pitch of 2^0. The results of simulation 1 are seen below. The vessel oscillates with its natural frequency. After approximately 4 natural periods, the vessel returns to its equilibrium position. Damping is due to the dissipative terms containing the change in angle of attack due to heave and pitch velocities. As mentioned in the assumptions, this is the only form of damping considered, but it seems to have a great contribution to the vessel's dynamic behavior.

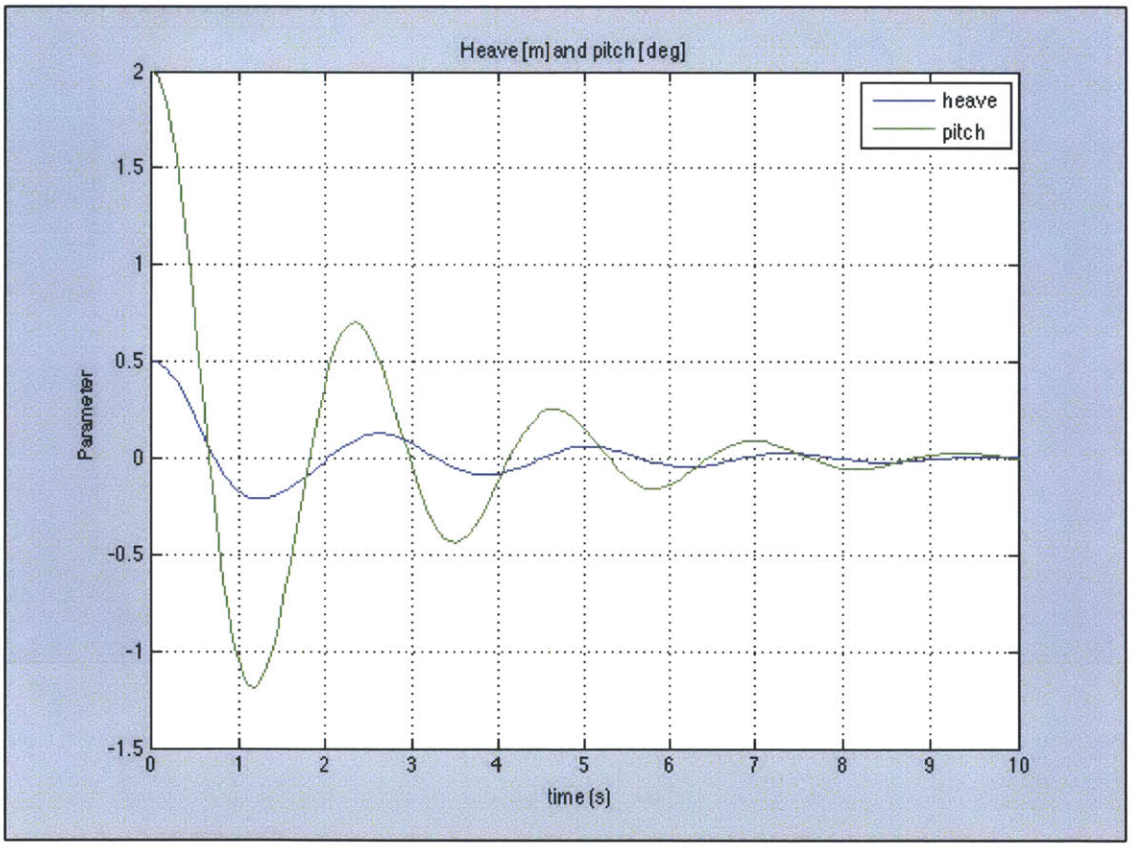

Figure 47: Dynamic behavior simulation 1-calm sea with initial conditions

The motion responses for the first case of external forces can be seen in Figure 48. The input to the system is essentially a combination of an impulse and a sinusoidal input, because the wave is encountered suddenly, without a gradual increase or initial conditions. It can be seen in the graph that there are initial peaks, before the system reaches stable oscillation. These peaks are due to the sudden encounter of the wave. The heave amplitude is not significant, compared to the wave height. As expected, the pitch amplitude is noticeable, because this wave length is the worst in terms of external moment. The period for both heave and pitch motion is seen ~0.9 s, which matches the encounter period of the wave. With this encounter frequency, issues regarding human safety and performance may arise, something which requires further consideration and study.

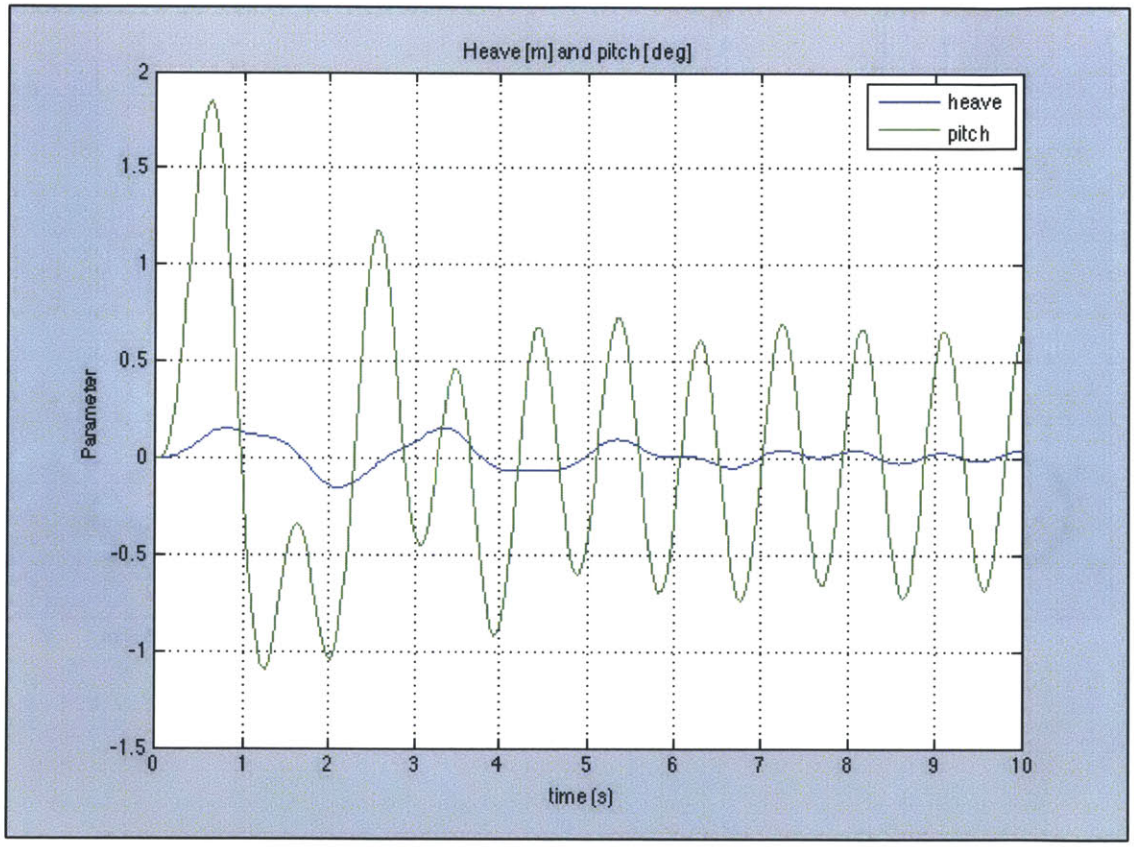

Figure 48: Dynamic behavior simulation 2-wave length twice LBF, wave height 0.5 m

The motion responses for the second case of wave length are seen in Figure 49. Again, initial peaks are noticed due to the sudden encounter of the wave. The encounter period is half of the first wave length case. None of the heave and pitch magnitudes are significantly large, but their frequencies are high. These frequencies may be too high for any crew/passenger to handle.

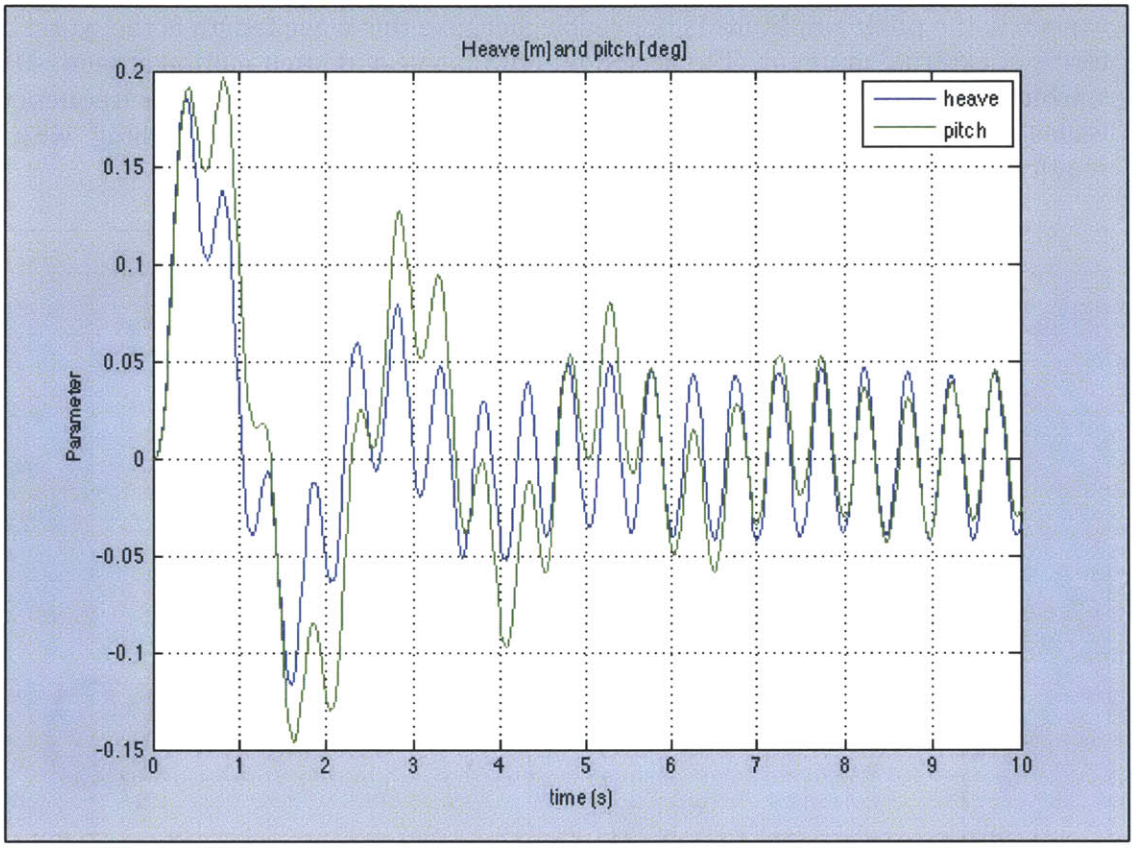

Figure 49: Dynamic behavior simulation 3-wave length equals LBF, wave height 0.5 m

5 Conclusions and recommendations

This study results in an innovative hybrid hydrofoil/SWATH high speed vessel, with the intended mission of rapid transportation of crew and cargo. The design builds on Brizzolara's unmanned high speed hybrid hydrofoil/SWATH vessel (Brizzolara, 2010). The design is expanding the borders of the family of unconventional SWATH vessels of Brizzolara and Chryssostomidis, by including manned vessel to this family (Brizzolara & Chryssostomidis, 2013). The general design phase focuses on the integration of the manned module, internal arrangements, weight estimation, speed profile determination and engine selection. The main characteristics of the vessel are seen below.

Table 10: Final design main characteristics

Weight [MT]	254.52
Maximum speed [knots]	85
Required power at maximum speed [KW]	21140
Passenger capacity [people]	24
Crew size [people]	4
Cargo capacity [MT]	15
Endurance [NM]	480

With the above capabilities, Wavecutter has been placed on the Gabrielli-von Karman graph of efficiency, shown in Figure 50. The following are noticed from this figure:

- Wavecutter achieves a higher speed than vessels with the same specific power. Thus it is more efficient than these vessels.
- Wavecutter achieves 85 knots, with a lower specific power than vessels of equal speed. Thus it is more efficient than these vessels as well.

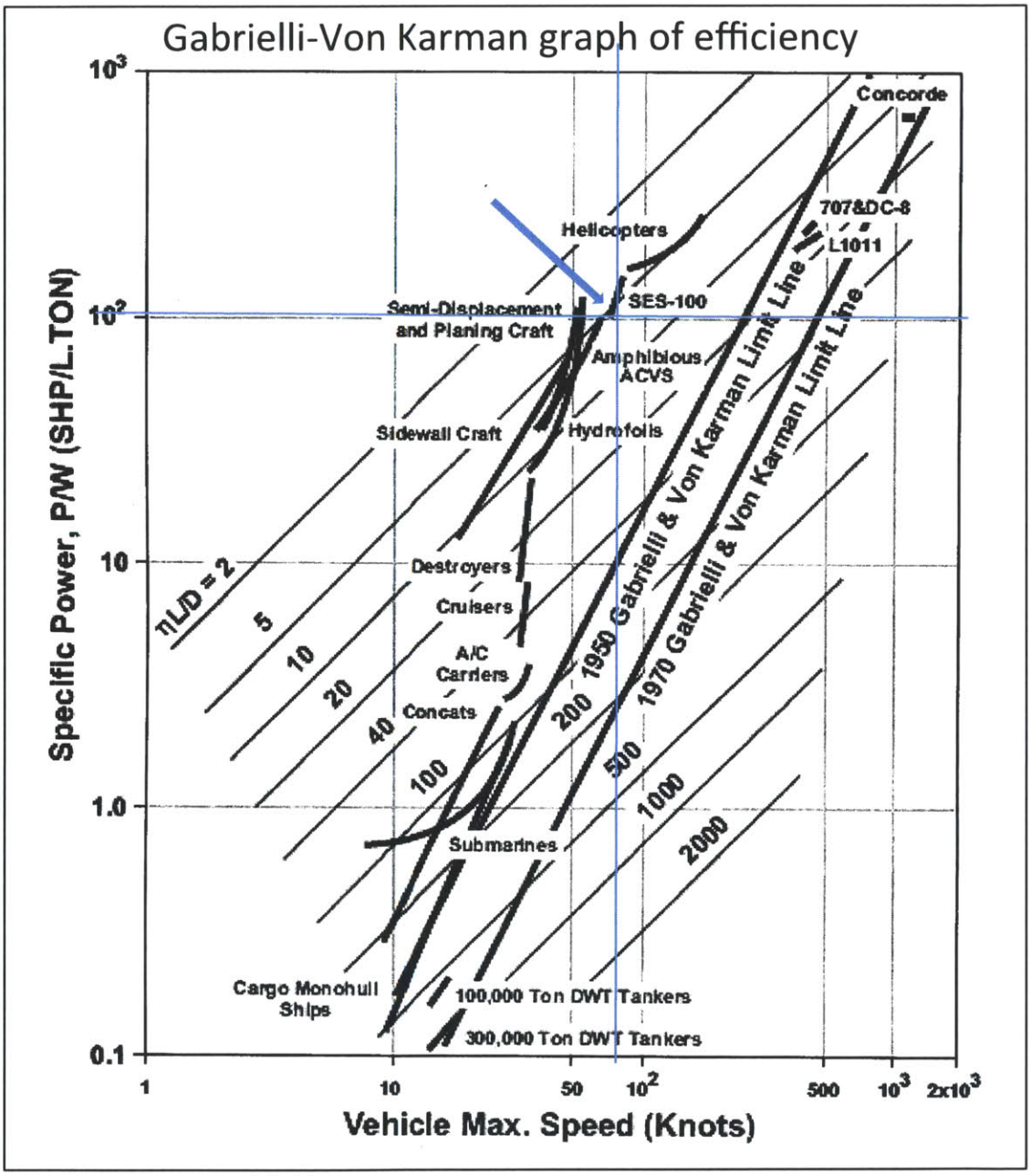

Figure 50: Gabrielli-von Karman graph of efficiency

The surface piercing configuration of the hydrofoils aims to make the vessel inherently stable, without the use of control mechanisms. Moreover, the distinct profile of the hydrofoils, created by S. Brizzolara, solves the unsteady ventilation problem of previous super-cavitating versions of the hydrofoil (Brizzolara, 2013). Prediction of lift and drag under unsteady condition are based on this capability of the hydrofoils. Model experiments provided force measurements which are used to estimate the hydrofoil forces on the vessel (Hochbaum & Eckl, 2012). The hydrofoil

design phase focuses on resizing the four surface-piercing super-cavitating hydrofoils to have zero trim at maximum speed. To have zero trim at maximum speed, the front foils need to be larger than the aft. This is due to the large moment produced by the thrust force, which is located on a high position on the vessel. A preliminary strength assessment of the hydrofoils has been made, and adding structural support to the hydrofoils is being considered as part of a follow-up project. It is recognized that this preliminary strength analysis has been carried out in calm seas and did not consider additional loads that may be imposed due to maneuvers of the vessel, encountering of regular waves or due to sudden impulse loads. A more in depth strength analysis is currently a work in progress within the scope of a follow-up project.

The final sizing of the hydrofoils is shown below. The exact dimensions of the foils are shown in Figure 41.

1. Front foil total length=8.7 m
2. Aft foil total length=8 m

The feasibility assessment phase focuses on predicting static stability and dynamic behavior of the vessel in foil borne mode. Static stability findings confirm the inherent stability of the hydrofoil configuration adopted (surface piercing foils with negative dihedral angle). Dynamic response findings indicate seaworthiness in foil borne mode, at least up to a sea state 3 (lower limit). However, issues regarding the human factor may be of concern, due to the high frequency of the response motions. The dynamic response findings of this study are not inclusive of all potential external disturbances that may occur. For example, motion responses due to high speed turning, various maneuvers and waves of incident angle other than the one of head waves are very important and should become the focus of future work. The results of the seakeeping analysis are shown in the table below. The magnitudes of heave and pitch response motions are for the steady state phase of the response.

Table 11: Seakeeping analysis results summary

Wave height [m]	Wave length [m]	Time to reach steady state phase [s]	Heave magnitude in steady state [m]	Pitch magnitude in steady state [deg]
0.5	49.14	~8	0.06	0.65
0.5	24.57	~9	0.04	0.045

It is recommended that future work be conducted simulating unsteady flow in Computation Fluid Dynamics (CFD) programs. CFD simulations will provide a more accurate understanding of the vessel's dynamic behavior. In addition a global structural design of the vessel is necessary in later stages of design, which was not in the scope of this study. Finally, wing and nacelle form optimization for minimizing resistance in air is another area for future work.

6 Appendix

6.1 Operational sea state requirement (R6) derivation

This vessel is intended to operate in the Gulf of Mexico or similar environments. The Gulf of Mexico has been chosen because numerous offshore oil platforms exist there. The sea keeping requirement corresponds directly to ocean statistics data of the Gulf of Mexico, which were estimated using collections of observations of wave heights and periods (Lumb & Hogben, 1967, p. 7). The observations have been transformed into percentages, shown in Table 12. The column on the very right shows the percentage of data that is below a certain wave height. The last row shows equivalent information for the wave period.

The chosen operational profile is highlighted in green. Operational profile in this context means the percentage of time that the vessel is expected to operate. This is a design choice. One can always design a vessel to withstand higher sea states, but at what cost? The chosen values are a rational choice for the mission of this vehicle. Significant wave height is more definitive, being the lower of the two. The chosen value means that the vessel will be able to operate safely approximately 85% during a given year.

Table 12: Ocean statistics for Gulf of Mexico

	Zero crossing period [s] (where there are two numbers it is a range of periods)											
			4.58	6.04	7.48	8.91	10.33	11.74	13.15	14.55		
Significant wave height [m]	Calm sea or undetermined	3.84	5.31	6.76	8.20	9.62	11.04	12.45	13.85	15.25	Total	Percent of data that is below x wave height
0.59	6.13%	8.45%	0.49%	0.19%				0.11%	0.19%	0.15%	15.71%	15.71%
1.00	0.04%	18.47%	1.42%	0.26%	0.07%	0.04%				0.56%	20.87%	36.57%
1.68	0.11%	22.77%	6.10%	1.42%	0.34%	0.04%	0.04%		0.11%	0.26%	31.19%	67.76%
2.28	0.04%	7.78%	8.34%	2.24%	0.41%	0.11%			0.04%		18.96%	86.72%
2.83	0.04%	1.08%	3.55%	1.94%	0.45%	0.04%					7.11%	93.83%
3.34	0.04%	0.45%	1.80%	0.79%	0.45%	0.30%	0.04%	0.04%			3.89%	97.72%
3.83		0.11%	0.34%	0.52%	0.15%	0.11%					1.23%	98.95%
4.30		0.07%	0.22%	0.26%	0.07%	0.07%					0.71%	99.66%
4.75			0.07%	0.07%							0.15%	99.81%
5.19							0.04%				0.04%	99.85%
5.62					0.04%						0.04%	99.89%
6.03					0.04%						0.04%	99.93%
7.61					0.07%						0.07%	100.00%
Total	6.39%	59.20%	22.33%	7.70%	2.09%	0.71%	0.11%	0.15%	0.34%	0.97%	100.00%	
Percent of data that is below x period	6.39%	65.59%	87.92%	95.62%	97.72%	98.43%	98.54%	98.69%	99.03%	100.00%		

According to NATO standards (Figure 51), the sea state that corresponds more closely to this significant wave height is sea state 4. Sea state 4 has an upper significant wave height of 2.5 [m] and period of 15.2 [s]. This is why this sea state has been chosen as the goal for the operational sea state requirement (R6).

Sea State No.	Significant Wave Height (m)		Modal Wave Period (sec)	
	Range	Mean	Range	Most Probable
0 – 1	0 – 0.1	0.05	–	–
2	0.1 – 0.5	0.3	3.3 – 12.8	7.5
3	0.5 – 1.25	0.88	5.0 – 14.8	7.5
4	1.25 – 2.5	1.88	6.1 – 15.2	8.8
5	2.5 – 4	3.25	8.3 – 15.5	9.7
6	4 – 6	5	9.8 – 16.2	12.4
7	6 – 9	7.5	11.8 – 18.5	15.0
8	9 – 14	11.5	14.2 – 18.6	16.4
>8	>14	>14	15.7 – 23.7	20.0

Figure 51: NATO Sea State numeral table

6.2 Data analysis of model experiments

Hydrofoil force estimations are made through data analysis of experimental measurements (Hochbaum & Eckl, 2012) performed on a second generation super-cavitating hydrofoil model (Brizzolara, 2013). To accomplish this the following assumptions are made:

- Geometric similitude is sufficient to allow equating the coefficients of force to be equal, model to full size hydrofoil, in the same normalized submerged length and angle of attack.
- In addition, it is assumed that scaling up the model hydrofoil will retain its capability to ventilate steadily even under unsteady conditions. The distinct hydrofoil sectional profile created by S. Brizzolara (Brizzolara, 2013) resolves the unsteady ventilation problem under unsteady flow conditions. Without this basis, prediction of hydrofoil forces under such conditions would be meaningless, and the seakeeping analysis performed here nullified.
- It is assumed that cavitation number does not play a significant role in the full scale hydrofoil for angles of attack† between -3 and 8. This was evident in the model experiments' results and the same is assumed for the full scale hydrofoils. (F.Campana, 2011)
- It is recognized that Froude and Reynolds number similitude was not achieved between the model and full scale foil. Doing so would not allow the

† Wherever angle of attack is mentioned in this section, pitch equivalent angle of attack is meant. Pitch equivalent angle of attack is equal to the angle of attack divided by the sinusoid of the dihedral angle of the foil.

distinct geometrical features of the design to be transferred to the model (the model would be too small). Froude number and/or Reynolds number do have an effect, but the extent of this effect could not be quantified from the model test campaign which concentrated on the angle, submergence and cavitation number effects. The effect of Froude number on the dynamic forces of surface piercing hydrofoil due to wave generation on the free surface is very important up to Fn=1 (relative to chord). For Fn>1 the Froude number effect is related to ventilation, but for this specific hydrofoil design its influence is very limited. Reynolds scale effects are expected to influence the viscous drag part which is a small portion of the total for super-cavitating hydrofoils and even less significant for the lift force. This partially justifies the assumption to neglect Reynolds and Froude scaling effects on the experimental measurements.

For reference purposes, the Froude numbers of the model and full scale hydrofoils are presented in Table 13 and Table 14, at three submerged lengths. The speed for the model is 9 knots (4.63 m/s) and the speed for the full scale foil is 85 knots (43.73 m/s). The submerged lengths are 175 mm, 250 mm and 350 mm for the model and 1750 mm, 2500 mm and 3500 mm for the full scale. The normalized percentage difference was found 66.52%, for both chord and length Froude numbers.

$$\frac{Fr_{full\ scale} - Fr_{model}}{Fr_{full\ scale}} = 66.52\%$$

Table 13: Chord Froude number comparison

	Model	Full Scale
Length 1	3.592644594	10.72977642
Length 2	3.264869335	9.750844284
Length 3	2.941210192	8.784205323

Table 14: Submerged length Froude number comparison

	Model	Full Scale
Length 1	0.003533651	0.010553588
Length 2	0.002956465	0.008829765
Length 3	0.002498669	0.007462513

The model experimental data contained several measurements of forces and moments, relative to various angles of attack, for three (3) different drafts (Hochbaum & Eckl, 2012). A sample graph of the experimental measurements is shown in Figure 52. It is evident from this figure that for pitch angles under -3 degrees, different cavitation numbers affect the results significantly. For this reason only data above -3 degrees are used to estimate equations, and this means that

when conditions impose negative angles below this value, the results from this study do not apply.

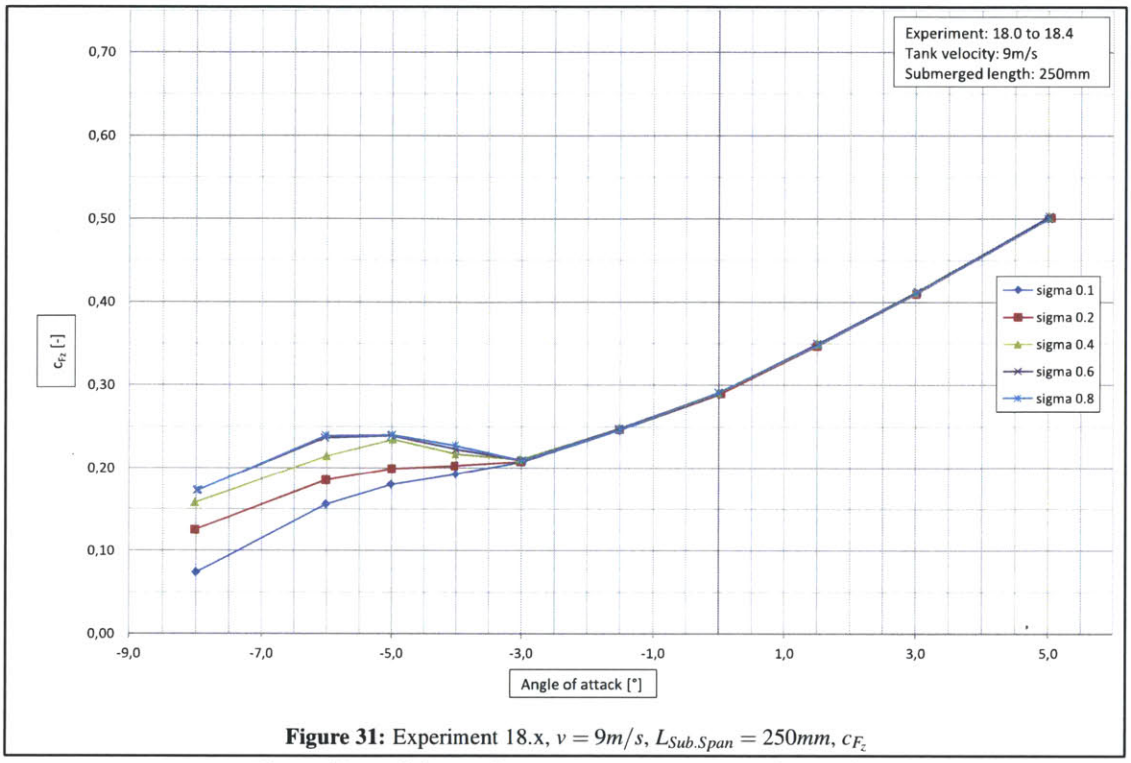

Figure 31: Experiment 18.x, $v = 9m/s$, $L_{Sub.Span} = 250mm$, c_{F_z}

Figure 52: Model experiments measurement graph sample

The experimental study provided numerous force measurements for each data point (angle of attack and submerged length). The mean values were calculated and used for this study. Standard deviations were not found large; there were all below the mean in value, for the data that was used.

Moment coefficients were also provided from the experimental data. It was determined that moment magnitudes were insignificant, compared to the moments imposed by the forces, relative to the reference point used in this study.

The mass center of the submerged part of the foil is used as the force center of application. The error that this simplifying assumption introduces is insignificant; the distance between the assumed center of application and the actual is very small compared with the distance between the foils and the moment reference point. The reference point for the moments can be seen in Figure 37.

6.2.1 Calculation of force coefficients

The force coefficients were calculated using the formula below.

$$C_{F_i} = \frac{F_i}{\frac{1}{2} * \rho_{water} * u^2 * A_{foil}}, i = 1,2,3$$

The water density ρ_{water} did not change during the experiments. Also the flow speed u was equal to 9 [m/s], and remained constant. The submerged hydrofoil area A_{foil} changed in every different set of experiments, because the submerged length changed. The submerged length took the values 175mm, 250mm and 350mm for each set respectively. The formula used to calculate the submerged area is seen below.

$$A_{foil} = 0.1768 * (L_{sub})^2 + 0.0613 * L_{sub}$$

where
L_{sub}: *submerged length in m*
A_{foil}: *submerged area in* m^2

In the three figures below, the force coefficient curves are a polynomial interpolation between the three different sets of experiments. Every set of experiments was performed at a specific submerged length, and the angles of attack varied. Each of the three experiment sets is represented by a black colored curve in the graphs below.

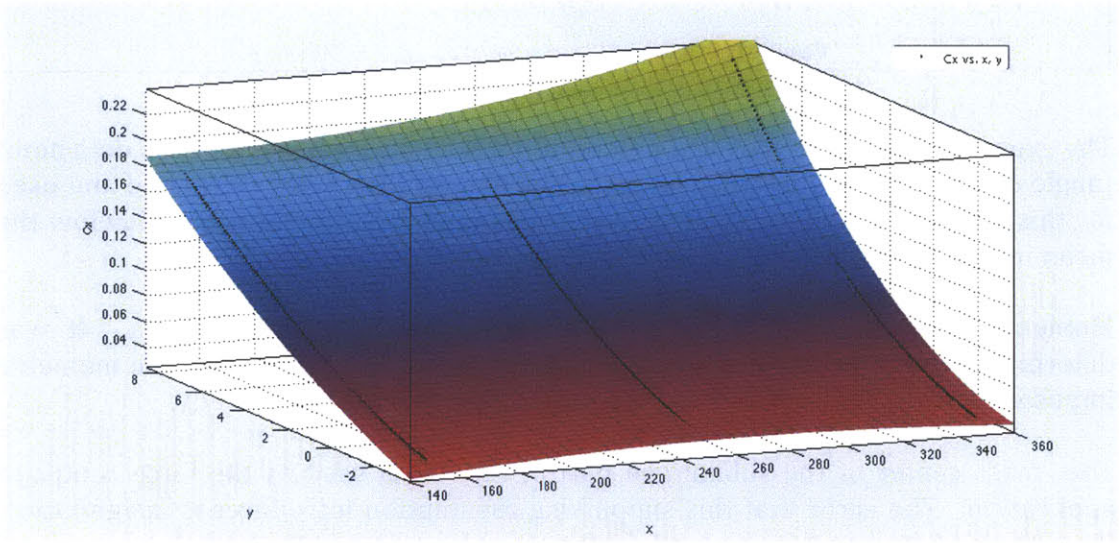

Figure 53: Foil drag force coefficient plot based on experimental data

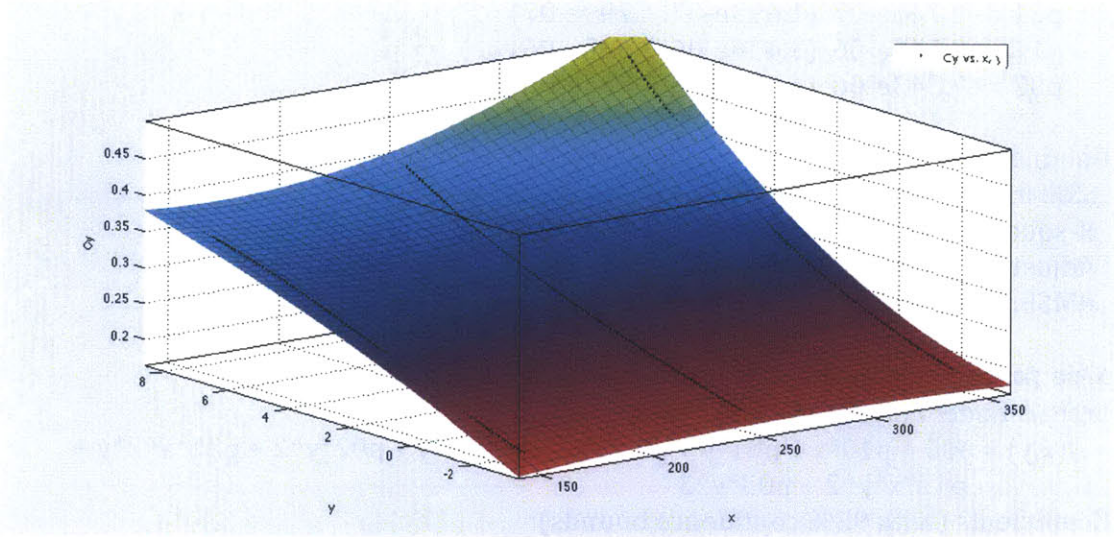

Figure 54: Foil side force coefficient plot based on experimental data

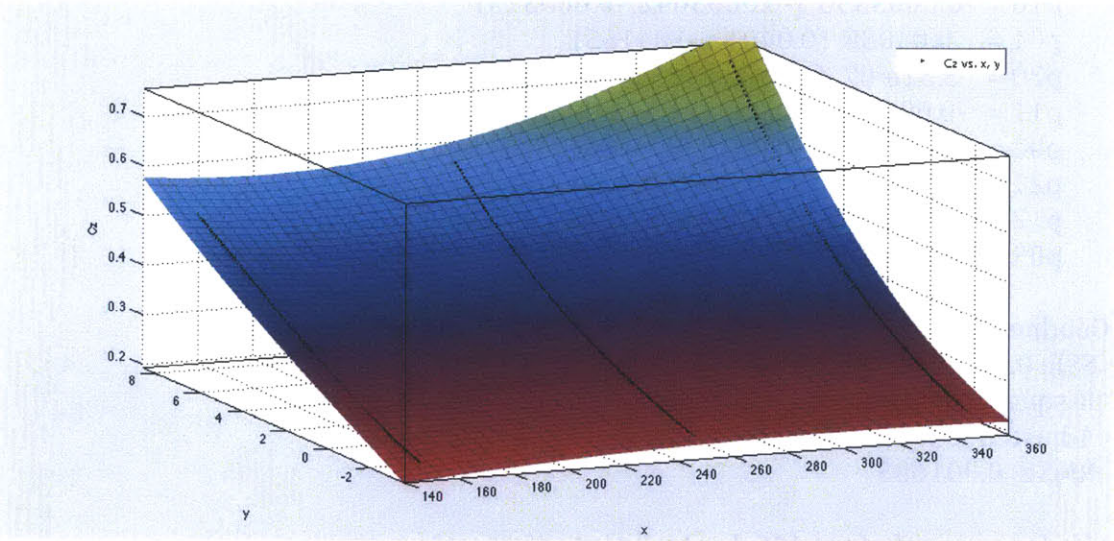

Figure 55: Foil lift force coefficient plot based on experimental data

Drag force coefficient (CFx) interpolated equations

Linear model Poly23:

f(x,y) = p00 + p10*x + p01*y + p20*x^2 + p11*x*y + p02*y^2 + p21*x^2*y + p12*x*y^2 + p03*y^3

Coefficients (with 95% confidence bounds):

p00 = 0.05818 (0.05693, 0.05943)
p10 = 4.581e-05 (3.501e-05, 5.661e-05)
p01 = 0.01901 (0.01868, 0.01935)
p20 = -1.143e-07 (-1.357e-07, -9.283e-08)
p11 = -8.285e-05 (-8.555e-05, -8.014e-05)
p02 = -0.0001188 (-0.0001551, -8.254e-05)

p21 = 1.746e-07 (1.693e-07, 1.799e-07)
p12 = 3.542e-06 (3.436e-06, 3.649e-06)
p03 = 7.343e-06 (4.258e-06, 1.043e-05)

Goodness of fit:
SSE: 0.0001771
R-square: 0.9998
Adjusted R-square: 0.9998
RMSE: 0.0007393

Side force coefficient (CFy) interpolated equations

Linear model Poly23:

f(x,y) = p00 + p10*x + p01*y + p20*x^2 + p11*x*y + p02*y^2 + p21*x^2*y + p12*x*y^2 + p03*y^3

Coefficients (with 95% confidence bounds):

p00 = 0.2789 (0.276, 0.2817)
p10 = -0.0003396 (-0.0003642, -0.000315)
p01 = 0.04088 (0.04012, 0.04165)
p20 = 5.32e-07 (4.832e-07, 5.808e-07)
p11 = -0.000215 (-0.0002212, -0.0002088)
p02 = -0.001856 (-0.001938, -0.001773)
p21 = 4.353e-07 (4.233e-07, 4.473e-07)
p12 = 9.727e-06 (9.485e-06, 9.969e-06)
p03 = 1.002e-05 (2.995e-06, 1.705e-05)

Goodness of fit:
SSE: 0.0009182
R-square: 0.9994
Adjusted R-square: 0.9994
RMSE: 0.001683

Lift force coefficient (CFz) interpolated equations

(note that here we consider z axis upwards-opposite to the convention that the experimental report uses)

Linear model Poly23:

f(x,y) = p00 + p10*x + p01*y + p20*x^2 + p11*x*y + p02*y^2 + p21*x^2*y + p12*x*y^2 + p03*y^3

Coefficients (with 95% confidence bounds):

p00 = 0.343 (0.3397, 0.3464)
p10 = -0.0005382 (-0.0005671, -0.0005094)
p01 = 0.06212 (0.06122, 0.06301)
p20 = 1.2e-06 (1.143e-06, 1.257e-06)
p11 = -0.0003446 (-0.0003518, -0.0003373)
p02 = -0.001203 (-0.0013, -0.001106)
p21 = 7.274e-07 (7.133e-07, 7.415e-07)

p12 = 1.05e-05 (1.022e-05, 1.079e-05)
p03 = 3.685e-05 (2.861e-05, 4.509e-05)

Goodness of fit:
SSE: 0.001264
R-square: 0.9997
Adjusted R-square: 0.9997
RMSE: 0.001975

6.3 Estimation of drag and lift in air

At foil borne mode, air drag and lift forces result from the vessel's components that are above the water surface. The contribution of these forces has been considered and the approach for calculating them is described in this section.

First, there is the main deck, which is composed of the side wings and the middle body. Then, there are the struts and the hulls. All these components impose resistance due to drag in air. In addition, the wings contribute to lift. Air drag estimation of all these components are made using semi-empirical formulas available from Hoerner's references. In drag calculations frictional, pressure and lift-induced drag (for the side wings) are all included in Hoerner's formulas.

The upper part of the vessel is composed of the wings and the middle body. The middle body contains the manned compartments, and roughly has a cylindrical shape. The middle body only imposes drag, while the wings imposes drag but also contributes to lift.

The aspect ratio of a wing is

$$AR = \frac{b^2}{S}$$

This ratio equals 0.27 for the side wings. The top view geometry of the wing can be seen in the figure below. Though this wing has the shape of a swept wing, it falls more into the category of small aspect ratio wings. To calculate the wing's drag and lift, practical formulas described by Hoerner is used (Hoerner, 1992, pp. 7-16) and (Hoerner & Borst, 1975, pp. 17-1).

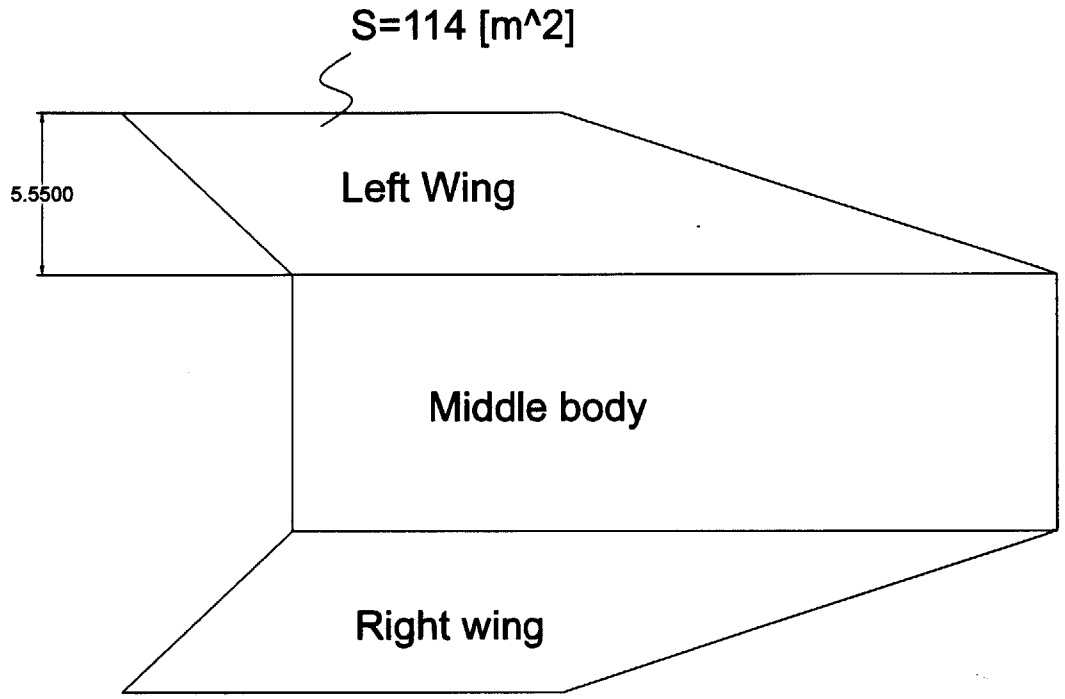

Figure 56: Wing top view geometry

The middle body, struts and hulls can be treated as streamlined bodies. Their Reynolds number is

$$Re = \frac{Vh * mc}{v} = 6.2 * 10^7$$

where

$Vh = 43.73 \left[\frac{m}{s}\right], maximum\ speed$

$mc = \frac{s}{span}\ [m], mid\ chord\ (found\ from\ dividing\ Area\ with\ wing\ span)$

$v = 0.145 * 10^{-4} \left[\frac{m^2}{s}\right], kinematic\ viscosity\ of\ air\ at\ 300\ Kelvins$

and their drag is found as a function of their individual thickness ratio (Hoerner, 1992, pp. 6-6).

6.4 Added mass approximations

Added mass calculations are based only on the non cavitating part, as seen in Figure 57. Only a few references can be found on the added mass of foils, and all refer to non cavitating speeds. Using the best of the few available references, the added mass of the foil can be approximated with Korotkin's formulas for a subsonic airfoil (Korotkin, 2007, p. 90). It should be noted that these formulas are for a fully submerged foil.

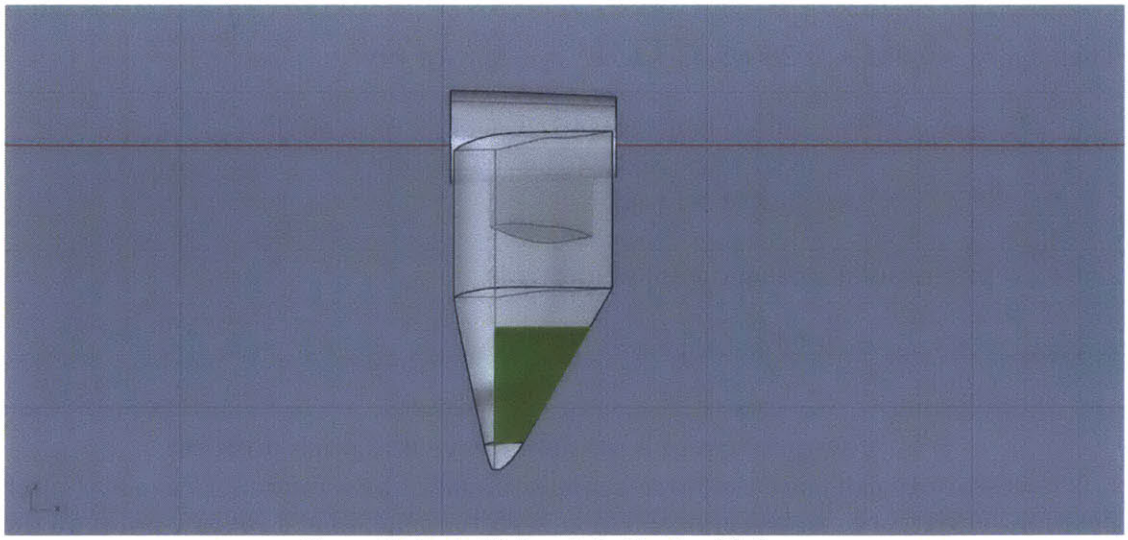

Figure 57: Part of foil contributing to added mass

According to Korotkin, the added mass of a flat airfoil shaped like the hydrofoil of interest, has the following added mass with respect to the axis vertical to its flat surface.

$$a_{33} = k_{33} * \rho * S * b$$

where
k_{33}: *added mass coefficient*
ρ: *salt water density*
S: *foil surface area*
b: *foil root chord*

The added mass coefficient depends on the root-to-tip-chord ratio and the front edge wing sweep angle and is 0.5.

Then $a_{33} = 0.5 * 1025 * 3.87 * 1.78 = 3530\ kg$

Transformation formulas can be applied to find the added mass with respect to the reference axis (Korotkin, 2007, p. 7).

$$a'_{33} = a_{33} * (\cos(40))^2 = 2071\ kg$$

The total heave added mass of the foils is

$A_{33\,total} = 4 * a'_{33} \cong 8300\ kg$

Then, the added mass moment of inertia is

$$a_{55} = k_{55} * \rho * S * b^3$$

The added mass coefficient here is -0.025

Then $a_{55} = -0.025 * 1025 * 3.87 * 1.78^3 = -560\ kg * m^2$

$$a'_{55} = a_{33} * (\xi * \cos(40) + \eta * \sin(40))^2 + a_{55} * (\cos(40))^2$$
$$= 3530 * (15 * \cos(40) + 1 * \sin(40))^2 - 560 * (\cos(40))^2$$
$$= 519360\ kg * m^2$$

The total pitch added mass moment of inertia is

$A_{55\,total} = 4 * a'_{55} \cong 2077441\ kg * m^2$

6.5 Vessel forces at a random heave and pitch position

It is necessary to calculate the force changes imposed by a random heave and pitch position. Each force can be represented as a vector, applied at a specific point on the vessel. A rotational matrix is defined to incorporate the change in the point of application of the force vectors, as the vessel changes pitch position. Another matrix incorporates the change in heave position.

Let $\vec{r}$ be the point of application of the the force $\vec{F}$ on the vessel.

$$\vec{r} = [r_x, r_z]$$
$$\vec{F} = [F_x, F_z]$$

$$Rot = \begin{bmatrix} \cos(pitch) & \sin(pitch) \\ -\sin(pitch) & \cos(pitch) \end{bmatrix}$$

$$Heave = [0, heave]$$

$$\vec{r}_{new} = \vec{r} * Rot + Heave$$

Some of the force vectors rotate with pitch and some do not. Hydrofoil forces already include the rotation element in the formulas, so they do not change direction with pitch motion. Weight vector also does not alter its direction with pitch. Air drag force components, thrust and wing lift do alter their direction with pitch. Apart from vector direction, all forces except weight also change in magnitude, in a different heave and pitch position. For each force, the resulting moment change from a random heave and pitch position is shown below.

$$\overrightarrow{\Delta M} = \vec{r}_{new} \times \vec{F}_{new} - \vec{r} \times \vec{F}$$

6.6 Differential equations solver using numerical methods

Numerical methods are a common time domain method to solve differential equations, nowadays with the use of computers. These methods can be used to

solve almost any type of differential equation, after transforming the equations to their state space form.

6.6.1 Transformation of differential equations into state space form

The differential equations of heave and pitch motion are shown below. The terms of the equations are explained in section 4.2.1.

$$(M_{33} + A_{33}) * \ddot{\eta}_3 + \sum F_{3res}(\eta_3, \eta_5, \dot{\eta}_3, \dot{\eta}_5) = \sum F_{3ex}(t) \quad \text{Heave equation}$$
$$(I_{55} + A_{55}) * \ddot{\eta}_5 + \sum F_{5res}(\eta_3, \eta_5, \dot{\eta}_3, \dot{\eta}_5) = \sum F_{5ex}(t) \quad \text{Pitch equation}$$

The differential equations should be written in the form of a first order ordinary differential equation:

$$\begin{cases} M_{33} * \ddot{\eta}_3 = \sum F_{3ex}(t) - \sum F_{3res}(\eta_3, \eta_5, \dot{\eta}_3, \dot{\eta}_5) \\ I_{55} * \ddot{\eta}_5 = \sum F_{5ex}(t) - \sum F_{5res}(\eta_3, \eta_5, \dot{\eta}_3, \dot{\eta}_5) \end{cases} \Rightarrow$$

$$\begin{cases} \ddot{\eta}_3 = \dfrac{(\sum F_{3ex}(t) - \sum F_{3res}(\eta_3, \eta_5, \dot{\eta}_3, \dot{\eta}_5))}{M_{33}} \\ \ddot{\eta}_5 = \dfrac{(\sum F_{5ex}(t) - \sum F_{5res}(\eta_3, \eta_5, \dot{\eta}_3, \dot{\eta}_5))}{I_{55}} \end{cases}$$

The vector of auxiliary variables are defined:

$$z = \begin{bmatrix} z_1 \\ z_2 \\ z_3 \\ z_4 \end{bmatrix} = \begin{bmatrix} \eta_3 \\ \dot{\eta}_3 \\ \eta_5 \\ \dot{\eta}_5 \end{bmatrix}$$
$$\dot{z} = \begin{bmatrix} \dot{z}_1 \\ \dot{z}_2 \\ \dot{z}_3 \\ \dot{z}_4 \end{bmatrix} = \begin{bmatrix} \dot{\eta}_3 \\ \ddot{\eta}_3 \\ \dot{\eta}_5 \\ \ddot{\eta}_5 \end{bmatrix}$$

Using this notation, the system of equations is written in state space form:

$$\begin{cases} \dot{z}_1 = z_2 \\ \dot{z}_2 = \dfrac{1}{M_{33}} * \left(\sum F_{3ex}(t) - \sum F_{3res}(\eta_3, \eta_5, \dot{\eta}_3, \dot{\eta}_5)\right) \\ \dot{z}_3 = z_4 \\ \dot{z}_4 = \dfrac{1}{I_{55}}\left(\sum F_{5ex}(t) - \sum F_{5res}(\eta_3, \eta_5, \dot{\eta}_3, \dot{\eta}_5)\right) \end{cases}$$

Before using the numerical model to obtain any responses of the vessel, the model is validated with a simple system of known response, shown in the next section.

6.6.2 Numerical model validation

To validate the numerical model, the simple problem of a spacecraft landing on a planet is solved, and the known solutions are found the same as the ones generated by the model. The known solutions can be obtained from the official website of Matlab® (Tearle, 2011), which is the platform used to solve the differential equations numerically. The particular Matlab® differential equation solver that is used (ODE45) uses a Runge-Kutta variable step method to calculate solutions. The spacecraft landing problem is described in Figure 58.

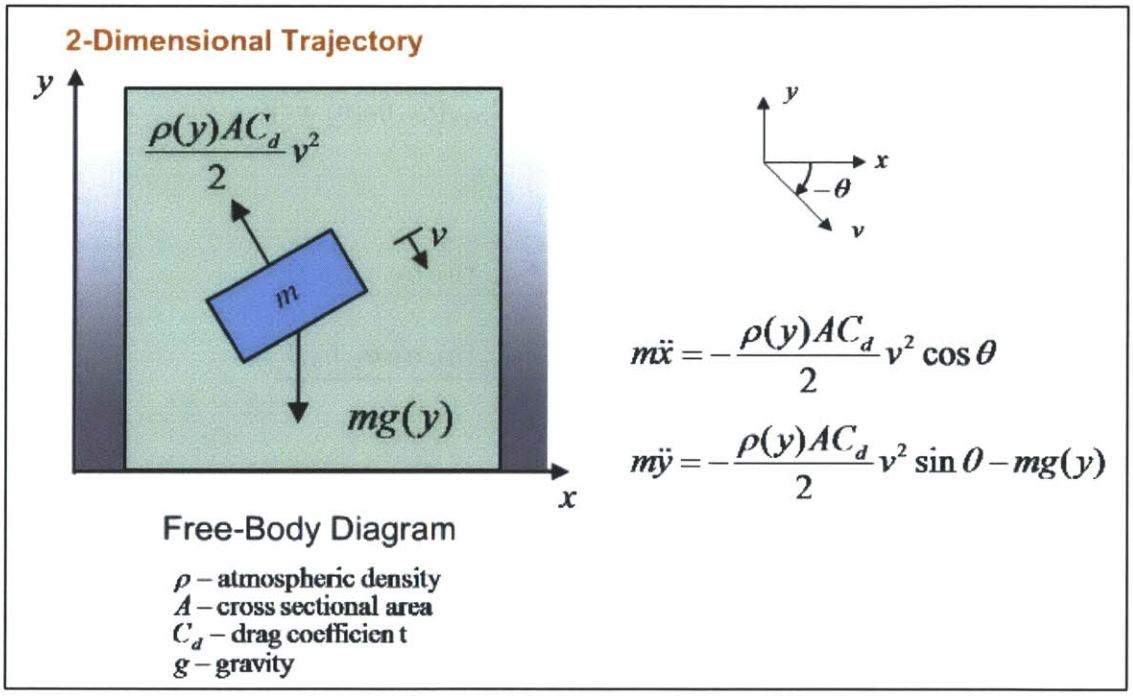

Figure 58: Spacecraft landing on a planet problem

From the problem equations the following derivations are made:

$$\ddot{x} = -D(y) * \dot{x} * \sqrt{\dot{x}^2 + \dot{y}^2}$$
$$\ddot{y} = -D(y) * \dot{y} * \sqrt{\dot{x}^2 + \dot{y}^2} - g(y)$$

where

$$\dot{x} = v * \cos(\theta)$$
$$\dot{y} = v * \sin(\theta)$$
$$v = \sqrt{\dot{x}^2 + \dot{y}^2}$$

$$D(y) = \frac{\rho(y) * A * C_d}{2 * m}$$

Next, the equations are written in state space form:

$$z = \begin{bmatrix} z_1 \\ z_2 \\ z_3 \\ z_4 \end{bmatrix} = \begin{bmatrix} x \\ \dot{x} \\ y \\ \dot{y} \end{bmatrix}$$

$$\dot{z} = \begin{bmatrix} \dot{z}_1 \\ \dot{z}_2 \\ \dot{z}_3 \\ \dot{z}_4 \end{bmatrix} = \begin{bmatrix} \dot{x} \\ \ddot{y} \\ \dot{x} \\ \ddot{y} \end{bmatrix}$$

$$\begin{cases} \dot{z}_1 = z_2 \\ \dot{z}_2 = -D(z_3) * z_2 * \sqrt{{z_2}^2 + {z_4}^2} \\ \dot{z}_3 = z_4 \\ \dot{z}_4 = -D(z_3) * z_4 * \sqrt{{z_2}^2 + {z_4}^2} - g(z_3) \end{cases}$$

where

$$D(z_3) = \frac{\rho(z_3) * A * C_d}{2 * m}$$

The model solutions are presented below, and the known solutions follow. It can be seen that they are the same; the scaling is different but the solutions are the same. This validates the model used for obtaining seakeeping responses of the vessel, because the model has been proved to generate accurate solutions, as compared to known solutions of a simple two order ordinary differential equation system.

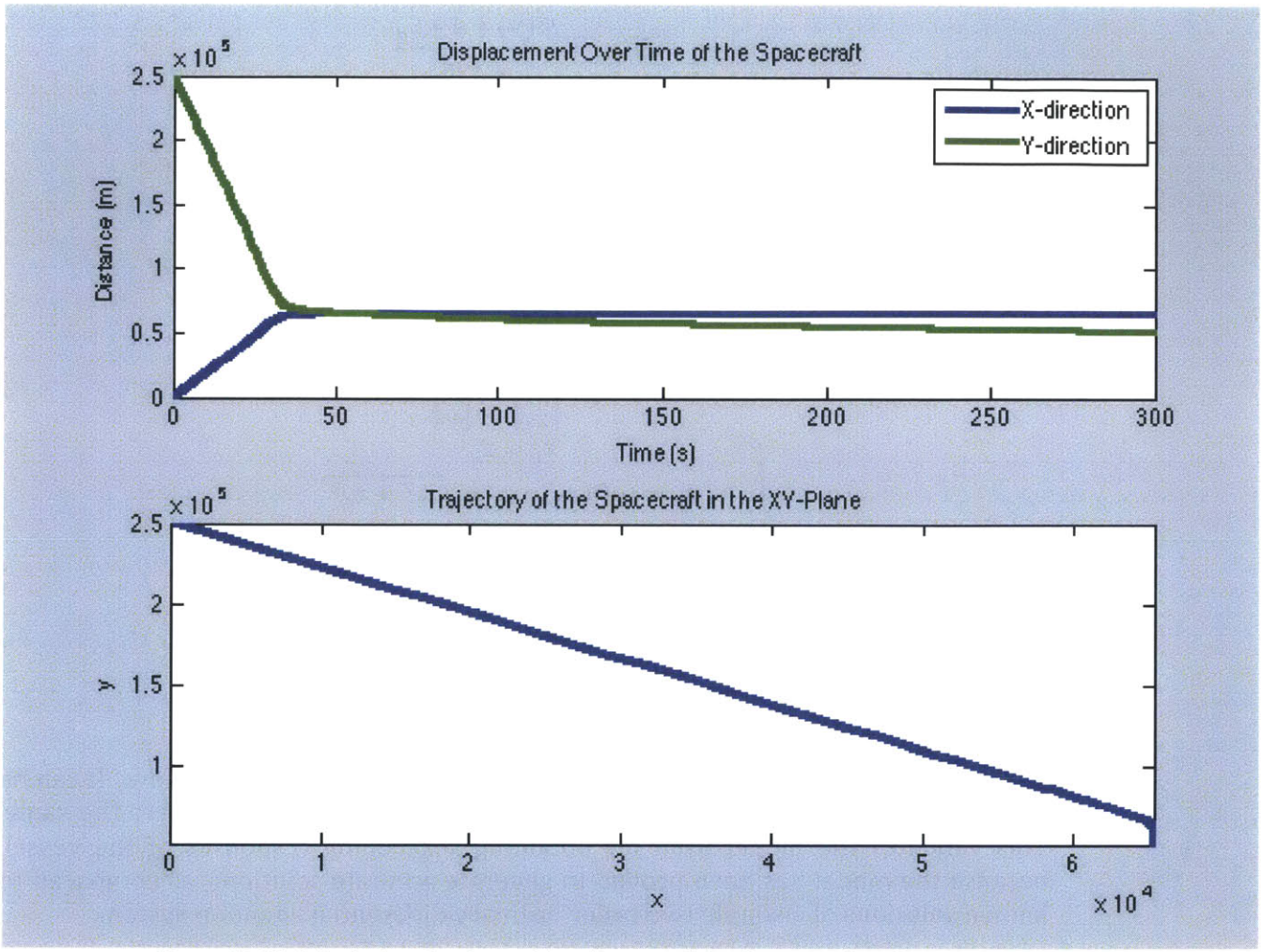

Figure 59: Model solutions for the problem 'Spacecraft landing on a planet'

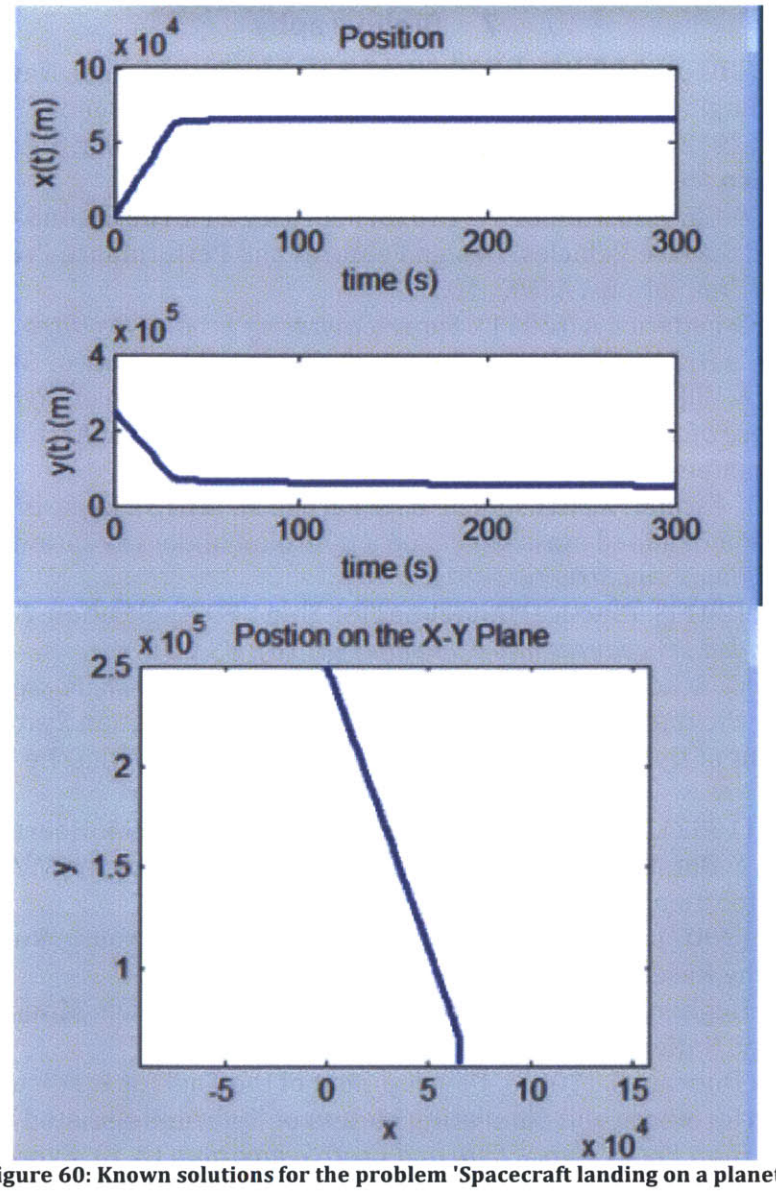

Figure 60: Known solutions for the problem 'Spacecraft landing on a planet'

7 Bibliography

Brizzolara, S. (2010). *ONR USV HYGE-SWATH.* University of Genoa, Naval and Electrical Engineering Department. Genova: University of Genoa.

Brizzolara, S. (2013). *Super-cavitating Surface-Piercing Hydrofoils: Design and Optimization Methods.* Boston: US Navy.

Brizzolara, S., & Chryssostomidis, C. (2013, February 21). The Second Generation of Unmanned Surface Vehicles: Design Features and Performance Predictions by Numerical Simulations. *ASNE* , 10.

Brizzolara, S., & Federici, A. (2011). *Super-Cavitating Profiles for Ultra High Speed Hydrofoils: a Hybrid CFD Design Approach.* Genova: University of Genova.

Brizzolara, S., & Villa, D. (2010). *Numerical and Experimental Hydrodynamic Performance of Slice Hull Forms.* University of Genova, Naval Architecture and Marine Engineering DINAV. Genoa: University of Genova.

De La Torre, O., Escaler, X., Egusquiza, E., & Farhat, M. (2013). Experimental investigation of added mass effects on a hydrofoil under cavitation conditions . *Journal of Fluids and Structures* , 15.

F.Campana, E. (2011). Practical Guidelines for Ship CFD Application. *ITTC Recommended Procedures and Guidelines* (p. 18). USA: ITTC.

Hochbaum, A. C., & Eckl, C. (2012). *Technische Universitat Berlin, Forces on a Super-Cavitating Hydrofoil.* Institute of Land and Sea Transportation Systems, Department of Dynamics of Maritime Systems. Berlin: Technische Universitat Berlin.

Hoerner, S. F. (1992). *Fluid-Dynamic Drag.* Bakersfield, CA, USA: Hoerner, Sighard F.;.

Hoerner, S. F., & Borst, H. V. (1975). *Fluid-Dynamic Lift.* Vancouver, WA, USA: Liselotte Hoerner.

Korotkin, A. I. (2007). *Added mass of ship structures.* St. Petersburg, Russia: Krylov Shipbuilding Research Institute.

Lumb, F. E., & Hogben, N. (1967). *Ocean Wave Statistics.* London: Ministry of Technology, National Physical Laboratory.

Matveev, K., & Duncan, R. (2005). Development of the Tool for Predicting Hydrofoil System Performance and Simulating Motion of Hydrofoil-Assisted Boats. *High Speed and High Performance Ship and Craft Symposium* (p. 8). Everett, WA: ASNE.

Raymer, D. P. (2012). *Aircraft Design: A Conceptual Approach.* Blacksburg, Virginia, USA: American Institute of Aeronautics and Astronautics, Inc.

Tearle, M. (2011, 01 01). *Solving Ordinary Differential Equations.* Retrieved 03 27, 2014, from Mathworks: http://www.mathworks.com/academia/student_center/tutorials/computational-math/solving-ordinary-diff-equations/player.html

The Society of Naval Architects and Marine Engineers. (1989). *Principles of Naval Architecture, Volume III, Motions in Waves and Controllability* (Vol. 3). (E. V. Lewis, Ed.) Jersey City, NJ, USA: The Society of Naval Architects and Marine Engineers.

Uhlman, J., Fine, N., & Kring, D. (2001). Calculation of the Added Mass and Damping Forces on Supercavitating Bodies. *Fourth International Sumposium on Cavitation* (p. 23). Pasadena, CA USA: California Institute of Technology.